

Quarterly Research Performance Progress Report

| | |
|--|---|
| Federal Agency and Organization Element to Which Report is Submitted | U.S. Department of Energy Office of Fossil Energy |
| FOA Name | Advanced Technology Solutions for Unconventional Oil & Gas Development |
| FOA Number | DE-FOA-0001722 |
| Nature of the Report | Research Performance Progress Report (RPPR) |
| Award Number | DE-FE0031606 |
| Award Type | Cooperative Agreement |
| Name, Title, Email Address, and Phone Number for the Prime Recipient | <p>Technical Contact (Principal Investigator): Abhijit Dandekar, Professor, adandekar@alaska.edu 907-474-6427</p> <p>Business Contact: Rosemary Madnick Executive Director UAF Office of Grants and Contracts Administration rmadnick@alaska.edu, 907-474-6446</p> |
| Name of Submitting Official, Title, Email Address, and Phone Number | Same as PI |
| Prime Recipient Name and Address | University of Alaska Fairbanks Grants and Contracts Administration PO Box 757880, Fairbanks AK 99775 |
| Prime Recipient Type | Not for profit organization |
| Project Title | <u>FIRST EVER FIELD PILOT ON ALASKA'S NORTH SLOPE TO VALIDATE THE USE OF POLYMER FLOODS FOR HEAVY OIL EOR a.k.a ALASKA NORTH SLOPE FIELD LABORATORY (ANSFL)</u> |


| | |
|--------------------------------------|--|
| Principal Investigator(s) | PI: Abhijit Dandekar, <i>University of Alaska Fairbanks</i> Co-PIs: Yin Zhang, <i>University of Alaska Fairbanks</i> John Barnes and Samson Ning, Hilcorp Alaska LLC Randy Seright, <i>New Mexico Institute of Mining & Technology</i> Baojun Bai, <i>Missouri University of Science and Technology</i> Dongmei Wang, <i>University of North Dakota</i> |
| Prime Recipient's DUNS number | 615245164 |
| Date of the Report | September 27, 2019 |
| Period Covered by the Report | June 1 2019-August 31 2019 |
| Reporting Frequency | Quarterly |
| Signature of Principal Investigator: |  Abhijit Dandekar |

TABLE OF CONTENTS

| | |
|--|----|
| 1. ACCOMPLISHMENTS | 7 |
| a. Project Goals | 7 |
| b. Accomplishments | 7 |
| c. Opportunities for Training and Professional Development | 74 |
| d. Dissemination of Results to Communities of Interest | 74 |
| e. Plan for Next Quarter | 74 |
| 2. PRODUCTS | 77 |
| 3. PARTICIPANTS & OTHER COLLABORATING ORGANIZATIONS | 77 |
| 4. IMPACT | 77 |
| 5. CHANGES/PROBLEMS | 77 |
| 6. SPECIAL REPORTING REQUIREMENTS | 77 |
| 7. BUDGETARY INFORMATION | 78 |
| 8. PROJECT OUTCOMES | 79 |

LIST OF FIGURES

| | |
|--|----|
| Figure 2.1: Results when injecting 2000-ppm 3430 HPAM into 673-md NB sand. | 10 |
| Figure 2.2: Grain-size distributions for the NB and OA sands. | 11 |
| Figure 2.3: Analysis of polymer produced from Wells J-27 and J-28. | 13 |
| Figure 2.4: Comparison of 3630 and 3430 powder-particle size distributions. | 14 |
| Figure 2.5: Injection of hypochlorite after 12-PV of 2000-ppm 3430 polymer. | 15 |
| Figure 2.6: No precipitation noted when bleach was added to polymer solutions. | 15 |
| Figure 3.1: The oil recovery and water cut results | 17 |
| Figure 3.2: The oil saturation (fraction) vs. PV (dimensionless) results | 17 |
| Figure 3.3: The impact of polymer injection sequence on oil recovery performance | 18 |
| Figure 3.4: The impact of initial wettability of sandpack cores on oil recovery performance | 20 |
| Figure 3.5: 1D Lab scale model illustration - Hypothesis 1 | 21 |
| Figure 3.6: Production and pressure history matching result – Hypothesis 1 | 22 |
| Figure 3.7: Fitting result of relative permeability curve – Hypothesis 1 | 23 |
| Figure 3.8: 1D Lab scale model illustration – Hypothesis 2 | 23 |
| Figure 3.9: Production and pressure history matching result – Hypothesis 2 | 25 |
| Figure 3.10: Fitting result of relative permeability curve – Hypothesis 2 | 25 |
| Figure 3.11: Production result of optimal case with fitting the shear thinning coefficient | 26 |
| Figure 3.12: Pressure result of optimal case with fitting the shear thinning coefficient | 26 |
| Figure 3.13: Production and pressure history matching result – Hypothesis 3 | 28 |
| Figure 3.14: Fitting result of relative permeability curve – Hypothesis 3 | 29 |
| Figure 3.15: Production result of optimal case with fitting the shear thinning coefficient | 30 |
| Figure 3.16: Pressure result of optimal case with fitting the shear thinning coefficient | 30 |
| Figure 4.1: Relative water permeabilities (dimensionless) used for core flooding simulations of NB-1, NB-2, and OA-1 | 33 |
| Figure 4.2: Solid volume changes for the core flooding simulations of NB-1, NB-2, and OA-1 | 34 |
| Figure 4.3: Water cut history match of Well J27 | 35 |

| | |
|---|----|
| Figure 4.4: Water cut history match of Well J28 | 36 |
| Figure 4.5: Oil rate history match of Well J27 | 37 |
| Figure 4.6: Oil rate cut history match of Well J28 | 37 |
| Figure 4.7: Permeability heterogeneity of block/stripe type in the simulation model | 38 |
| Figure 4.8: History matching results of (a) water cut (b) oil production rate for producer J27 and (c) water cut (d) oil production rate for producer J28 | 41 |
| Figure 4.9: History matching results of (a) T140A concentration (b) T140C concentration in producer J27 and (c) T140A concentration (d) T140C concentration in producer J28 | 43 |
| Figure 4.10: Permeability distribution of (a) layer #1, (b) layer #2, (c) layer #3, (d) layer #4, (e) layer #5, (f) layer #6, (g) layer #7 and (h) layer #8 in the reservoir simulation model | 45 |
| Figure 4.11: Porosity distribution of (a) layer #1, (b) layer #2, (c) layer #3, (d) layer #4, (e) layer #5, (f) layer #6, (g) layer #7 and (h) layer #8 in the reservoir simulation model | 46 |
| Figure 4.12: The relative permeability curves of (a) oil/water and (b) gas/oil | 47 |
| Figure 5.1: J-23A step rate test | 50 |
| Figure 5.2: J-24A step rate test | 51 |
| Figure 5.3: Polymer concentration | 52 |
| Figure 5.4: Injection rate and pressure for J-23A and viscosity | 53 |
| Figure 5.5: Injection rate and pressure for J-24A | 53 |
| Figure 5.6: Hall plot for J-23A and J-24A | 54 |
| Figure 5.7: Pore volume of polymer injected | 55 |
| Figure 5.8: J-27 Production performance | 56 |
| Figure 5.9: J-28 Production performance | 56 |
| Figure 5.10: Water/Oil ratio versus oil recovery factor trend | 57 |
| Figure 5.11: Pre-polymer tracer concentration in produced water samples | 58 |
| Figure 6.1: Typical transmission light profile for demulsifier. | 59 |
| Figure 6.2: The performance of four emulsion breakers for oilfield emulsion. | 60 |
| Figure 6.3: The transmission light intensity of the oilfield emulsion with four demulsifiers | 61 |
| Figure 6.4: Demulsification performance comparison for three oil-soluble demulsifiers | 61 |
| Figure 6.5: The effect of polymer on emulsion stability at 50% WC | 62 |
| Figure 6.6: The oil content in the separated water at varying polymer concentration | 62 |
| Figure 6.7: Volume of phases in the presence of polymer | 63 |
| Figure 6.8: The performance of four demulsifiers for emulsions without polymer at 50% WC | 63 |
| Figure 6.9: The performance of four demulsifiers at different residence time | 64 |
| Figure 6.10: The effect of dosage on the performance of E12085A | 64 |
| Figure 6.11: The effect of dosage on the performance of E18276A | 65 |
| Figure 6.12: The effect of dosage on the performance of R01319 | 65 |
| Figure 6.13: The performance of compound emulsion breaker for emulsions at 50% WC | 66 |
| Figure 6.14: The performance of E12+E18 at two different dosages | 66 |
| Figure 6.15: The performance of E12+N16 at two different dosages | 67 |
| Figure 6.16: Performance comparison for all qualified demulsifiers | 68 |
| Figure 6.17: The performance of four emulsion breakers at presence of 800ppm polymer | 69 |
| Figure 6.18: The performance of R01319 at varying polymer concentration | 69 |
| Figure 6.19: The performance of compound emulsion breaker at 800ppm polymer | 70 |

| | |
|--|----|
| Figure 6.20: Performance comparison for all qualified demulsifiers at presence of polymer | 70 |
| Figure 6.21: Copper Tubes after Experiment at 350 °F | 71 |
| Figure 6.22: Comparison of deposit amount on Stainless-Steel and Copper | 72 |
| Figure 6.23: SEM images of deposit at different polymer concentrations at 350 °F at 3000 magnification on copper tubes | 73 |

LIST OF TABLES

| | |
|--|----|
| Table 2.1: Summary of Polymer Retention Values. | 9 |
| Table 2.2: Elemental analysis of sands (expressed in parts per million for the first 3 rows). | 10 |
| Table 3.1: Model specification – Hypothesis 1 | 21 |
| Table 3.2: Model specification – Hypothesis 2 | 23 |
| Table 4.1: Parameters used for polymer retention simulation by core flooding | 31 |
| Table 6.1: Deposit rates on copper tube at 800ppm polymer concentration | 72 |
| Table 6.2: Comparison of heating times for Stainless-Steel and Copper at 165 °F and 800ppm polymer concentration | 73 |
| Table A: Summary of milestone status. | 74 |
| Table B: Budgetary information for Budget Period 2, Q1. | 79 |

NOMENCLATURE

| | |
|----------|---|
| ANS | Alaska North Slope |
| BS&W | Basic Sediment and Water |
| bpd | Barrel Per Day |
| BHP | Bottomhole Pressure |
| BS | Backscattering |
| CMG | Computer Modeling Group |
| cp or cP | Centipoise |
| DMP | Data Management Plan |
| EB | Emulsion Breaker |
| EOR | Enhanced Oil Recovery |
| FR | Filter Ratio |
| Fr | Resistance Factor |
| Frr | Residual Resistance Factor |
| f_w | Fractional Flow of Water |
| HPAM | Hydrolyzed Polyacrylamide |
| HM | History Matching |
| HSPF | High Salinity Polymerflood |
| HSWF | High Salinity Waterflood |
| ICD | Inflow Control Device |
| IMEX | Implicit Pressure Explicit Saturation Simulator |
| I PROF | Injection Profile |
| KI | Potassium Iodide |
| k or K | Permeability (generally absolute) |
| Kro | Relative Permeability to Oil |
| Krw | Relative Permeability to Water |

University of Alaska Fairbanks

| | |
|------------------------------------|--|
| LSWF | Low Salinity Waterflood |
| LSPF | Low salinity Polymerflood |
| md or mD | MilliDarcy |
| mg | Milligram |
| nm | Nanometer |
| No | Corey Exponent for Oil |
| Nw | Corey Exponent for Water |
| OIW | Oil in Water |
| OOIP | Original Oil in Place |
| PF | Polymerflood |
| PFO | Pressure Falloff |
| PMP | Project Management Plan |
| PPB | Parts Per Billion |
| PPM | Parts Per Million |
| PRV | Pressure Release Valve |
| PSU | Polymer Skid Unit |
| PV | Pore Volume |
| QC | Quality Control |
| RF | Recovery Factor |
| RPM | Rotation Per Minute |
| SC | Standard Conditions |
| SCTR | Abbreviation of Sector as used in CMG |
| SEM | Scanning Electron Microscopy |
| S _{or} | Residual Oil Saturation |
| SPE | Society of Petroleum Engineers |
| STB | Stock Tank Barrel |
| STOOIP | Stock Tank Original Oil in Place |
| S _{wc} or S _{wi} | Connate/Irreducible Water Saturation |
| T _o | Oil Content in the Water Sample (Equation 2) |
| TPV | Total Pore Volume |
| μ | Viscosity |
| μg | Microgram |
| ULSPF | Ultra Low Salinity Polymerflood |
| URTeC | Unconventional Resources Technology |
| USBM | United State Bureau of Mines |
| UV | Ultraviolet |
| VRR | Voidage Replacement Ratio |
| VRV | Vacuum Release Valve |
| WC | Water Cur |
| WF | Waterflood |
| WOR | Water Oil Ratio |
| XRD | X-ray Diffraction |
| XRF | X-ray Fluorescence |

1. ACCOMPLISHMENTS

a. Project Goals

The overall objective of this project is to perform a research field experiment to validate the use of polymer floods for heavy oil Enhanced Oil Recovery (EOR) on Alaska North Slope.

The main scientific/technical objectives of the proposed project are:

1. Determine the synergy effect of the integrated EOR technology of polymer, low salinity water, horizontal wells, and conformance treatments (e.g., gels), and its potential to economically enhance heavy oil recovery.
2. Assess polymer injectivity into the Schrader Bluff formations for various polymers at various concentrations.
3. Assess and improve injection conformance along horizontal wellbore and reservoir sweep between horizontal injectors and producers.
4. Evaluate the water salinity effect on the performance of polymer flooding and gel treatments.
5. Optimize pump schedule of low-salinity water and polymer.
6. Establish timing of polymer breakthrough in Schrader Bluff N-sands.
7. Screen an optimized method to control the conformance of polymer flooding at the various stages of the polymer flooding project.
8. Estimate polymer retention from field data and compare with laboratory and simulation results.
9. Assess incremental oil recovery vs. polymer injected.
10. Assess effect of polymer production on surface facilities and remediation methods.

The technical tasks proposed in these studies focus on the following: (1) optimization of injected polymer viscosity/concentration and quantification of polymer retention via laboratory scale experiments; (2) optimization of injection water salinity and identification of contingencies for premature polymer breakthrough via laboratory scale experiments and numerical analyses; (3) reservoir simulation studies for optimization of polymer injection strategy; (4) design and implementation of a field pilot test at Milne Point on ANS; (5) identification of effective ways to treat produced water that contains polymer (including polymer fouling of heater tubes), and finally (6) the feasibility of commercial application of the piloted method in ANS heavy oil reservoirs. The project milestones, and current milestone status are shown toward the end in **Table A**.

b. Accomplishments

The primary focus of the research program, since the start of the polymer injection in August 2018, has been monitoring the performance of the pilot in the injection wells J-23A and J-24A, and production wells J-27 and J-28 respectively. In order to complement the polymer injection, focus of other supporting tasks has been advancing reservoir simulation, tackling flow assurance challenges and laboratory corefloods. The accomplishments to date are summarized in the following bullet points:

University of Alaska Fairbanks

- Finalized manuscripts of the SPE and URTeC conferences have been uploaded in the US DOE's E-link system.
- The URTeC paper presentation was well received with lots of questions from the audience. Several people from the industry and academia appreciated seeing actual field test data.
- The project was successfully presented at the CSONG2019 DOE review meeting on August 26th, 2019.
- The project has successfully entered BP2.
- Field pilot has demonstrated that polymer can be handled and hydrated effectively on Alaska North Slope and injected at reasonable concentration and injection rate into the Schrader Bluff heavy oil reservoir via horizontal injectors.
- No polymer production or breakthrough observed one year after start of polymer injection, which has been confirmed with both the clay flocculation and water composition tests. Although clay flocculation test just started to show positive results, water composition analysis could not detect presence of polymer.

Since the official project start date of June 1, 2018, the entire project team has continued the practice of working meetings every other Friday for two hours to discuss the various tasks and the project as a whole. A summary of these bi-weekly meetings is provided to the project manager. Additionally, separate meetings, as needed, between the sub-groups also take place.

The following summarizes the team's progress to date in relation to the various tasks and sub-tasks outlined in the Project Management Plan (PMP):

- Task 1.0 - Project Management and Planning

Revised PMP and DMP are on file with DOE, which were submitted on April 30th 2019.

- Task 2.0 - Laboratory Experiments for Optimization of Injected Polymer Viscosity/Concentration and Quantification of Polymer Retention

Polymer Retention. During the present quarter, our efforts focused on determining polymer retention in cores and sand packs with permeabilities that are representative of the field (i.e., 200-700 md). **Table 2.1** summarizes our most recent results for polymer retention in Milne NB and OA sands. For all listings in **Table 2.1** beyond the first listing, the desired permeability (absolute permeability to brine) was achieved by applying an overburden pressure between 500 and 1700 psi. As can be seen from **Table 2.1**, most of the retention values were quite high—i.e., generally, greater than 200 µg/g. For reference, a retention value of 200 µg/g means that roughly twice as much 1800-ppm HPAM solution must be injected to achieve a desired oil recovery (than if retention was zero). This would be very economically unattractive for our field project, so we have a high interest in determining (1) whether these results are a laboratory artifact or are valid to our field application, (2) what causes these high values, and (3) if these high values can be avoided in the field application.

Table 2.1: Summary of Polymer Retention Values.

| Sand | Polymer | k_w abs, md | k_w at S_{or} , md | Overburden pressure, psi | Polymer retention, $\mu\text{g/g}$ | |
|--------------------|---------|---------------|------------------------|--------------------------|------------------------------------|-----------------|
| | | | | | N ₂ -based | Viscosity-based |
| 1 st NB | 3630 | 10900 | 7000 | 0 | 28 | 45 |
| 1 st NB | 3630 | 548 | 50 | 1000 | 372 | 931 |
| 2 nd NB | 3630 | 625 | 73 | 1700 | 533 | 844 |
| 2 nd NB | 3430 | 673 | 116 | 1700 | 236 | 389 |
| OA | 3630 | 233 | 19 | 800 | 126 | 593 |
| OA | 3630 | 158 | No oil | 500 | 87 | 246 |
| OA | 3430 | 328 | No oil | 1000 | 0 | 33 |

As indicated in **Table 2.1**, several variables have been tested, including sand type (NB vs OA), presence/absence of residual oil, permeability, and polymer molecular weight (3630 or 3430). Some insight into our current thoughts can be appreciated by viewing the results from the fourth listing in **Table 2.1** (2nd NB sand with 3430 HPAM). Details of that experiment are shown in **Figure 2.1**. Note that the effluent viscosity and nitrogen concentration reaches 50% of the injected value at ~2 pore volume (PV)—indicating a significant polymer retention. After ~2.3 PV, both effluent nitrogen and viscosity values slowly increase over the next 6-8 PV to finally reach the injected values. This behavior suggests that a low-Mw part of the HPAM distribution propagates reasonably quickly through the core (bringing the effluent polymer concentration up to ~50% of injected), and then the high-end of the Mw distribution propagates more slowly—resulting in the high calculated polymer retention values. In other words, mechanical entrapment of the polymer is suspected of causing the high retention values.

One could question whether our polymer was fully dissolved before injection. This possibility can be discounted since (1) no polymer accumulation has ever been observed on the inlet face of our cores (at the end of the experiment), (2) prior to injection, no signs of any polymer lumps were seen when slowly pouring the solution from one beaker to another (using a thin solution film), and (3) injection pressures did not continually increase after 2 PV of injection (grey curve in **Figure 2.1**).

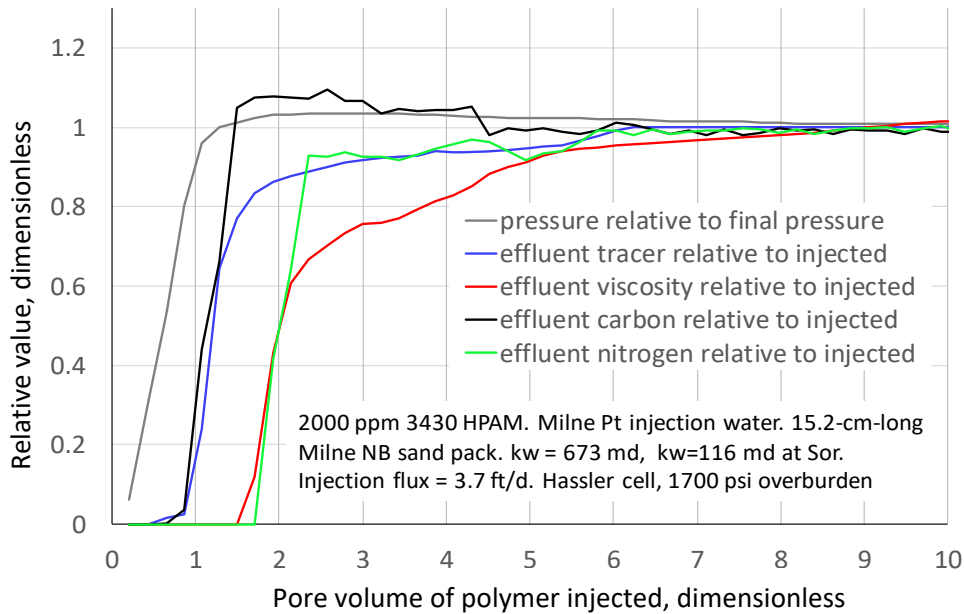


Figure 2.1: Results when injecting 2000-ppm 3430 HPAM into 673-md NB sand.

Table 2.1 and **Figure 2.1** give several hints about what might be happening. First, retention was generally lower in the OA sand than the NB sand, even though the NB sand was 2-4 times more permeable than the OA sand. Thus, sand composition probably plays an important role in determining polymer retention. **Table 2.2** compares elemental compositions of the sands (as determined by x-ray fluorescence analysis with a Bruker Tracer 5g instrument with helium purge). The sands are fairly similar in elemental composition, except the OA sand contains about seven times as much calcium, 30-60% more iron, and 30-80% more magnesium than the NB sands.

Table 2.2: Elemental analysis of sands (expressed in parts per million for the first 3 rows).

| Element | Si | Al | Fe | K | Mg | Ti | Na | Ca | S | Ba | Mn | P | Zr | Zn | Sr | V |
|---------------|--------|-------|-------|------|------|------|------|-------|-----|-----|-----|-----|-----|-----|-----|-----|
| 1st NB | 168582 | 19537 | 18351 | 6043 | 2807 | 1914 | 1906 | 1756 | 804 | 542 | 257 | 140 | 89 | 59 | 54 | 48 |
| 2nd NB | 175986 | 16167 | 15829 | 5548 | 2082 | 1720 | 1921 | 1924 | 712 | 517 | 186 | 104 | 82 | 61 | 59 | 68 |
| OA | 150396 | 18509 | 24720 | 6754 | 3714 | 2045 | 2357 | 12651 | 263 | 385 | 211 | 267 | 260 | 79 | 98 | 150 |
| 1st NB/2nd NB | 1.0 | 1.2 | 1.2 | 1.1 | 1.3 | 1.1 | 1.0 | 0.9 | 1.1 | 1.0 | 1.4 | 1.3 | 1.1 | 1.0 | 0.9 | 0.7 |
| OA/ 1st NB | 0.9 | 0.9 | 1.3 | 1.1 | 1.3 | 1.1 | 1.2 | 7.2 | 0.3 | 0.7 | 0.8 | 1.9 | 2.9 | 1.3 | 1.8 | 3.1 |
| OA/2nd NB | 0.9 | 1.1 | 1.6 | 1.2 | 1.8 | 1.2 | 1.2 | 6.6 | 0.4 | 0.7 | 1.1 | 2.6 | 3.2 | 1.3 | 1.7 | 2.2 |

Second, the grain sizes for the NB sands were almost twice those for the OA sands. **Figure 2.2** compares the grain-size distributions for the two sands. These distributions were obtained using a laser-diffraction method (Malvern Mastersizer 3000 with Hydro EV dispersing unit), which provides volume-based measurements. Note that the median grain size ranges from 166 to 179 μm for the NB sands and was 96.6

μm for the OA sand. The Malvern instrument provided estimates of average surface area of the sands, which did not indicate a definitive difference—possibly because the NB sands contained a greater fraction of very fine material that compensated for its larger average grain size. The greater fraction of very fine material might account for retention being higher in NB sands.

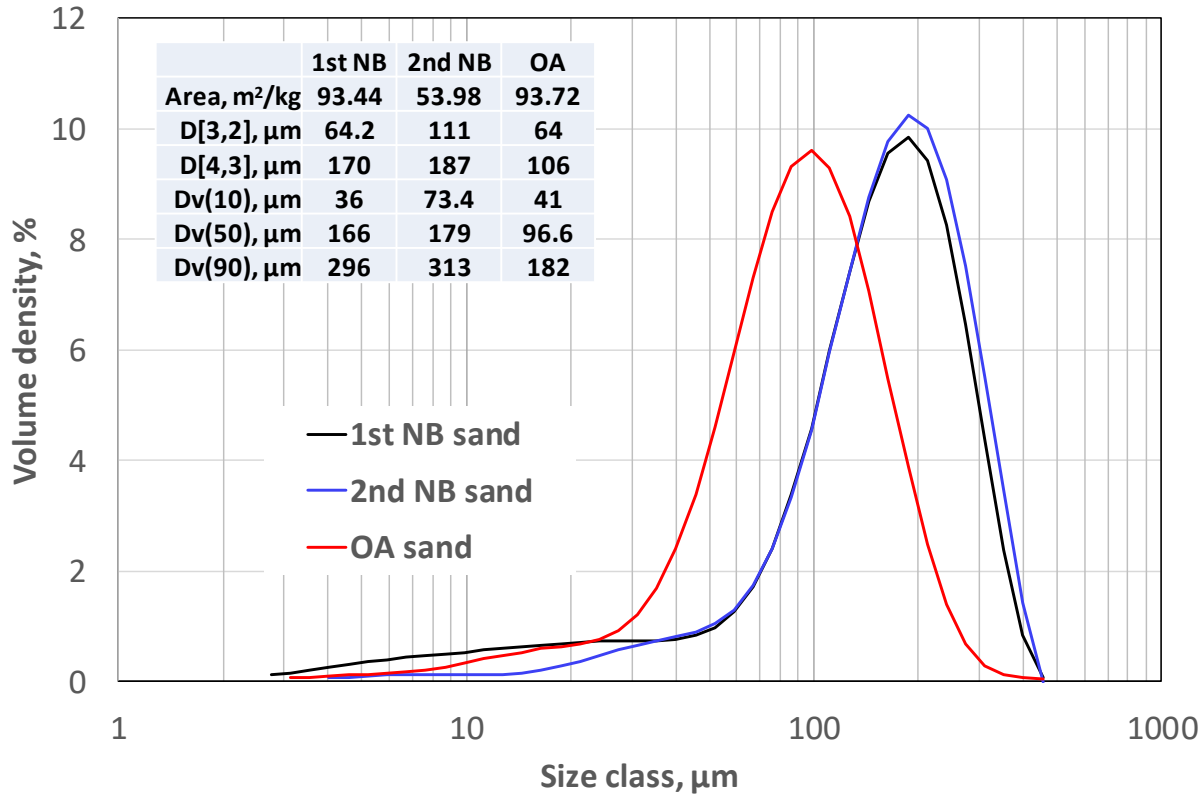


Figure 2.2: Grain-size distributions for the NB and OA sands.

Table 2.1 also reveals that polymer retention on the OA sands was much greater with a residual oil saturation present than without. Since oil should coat the sand grains and reduce polymer retention, it seems that the observed differences are tied to the lower permeability that exists when a trapped oil saturation is present. In other words, mechanical entrapment of the HPAM may play an important role in determining polymer retention. This thought is consistent with the tailing of effluent viscosity and nitrogen analysis mentioned earlier in **Figure 2.1**. Also consistent with this logic, retention for the highest Mw polymer (SNF Flopaam 3630, 18-million Daltons) was greater than for the lower Mw polymer (SNF Flopaam 3430, 13-million Daltons).

Concerning future work on this topic, our next studies will focus on elucidating the role of mechanical entrapment during polymer retention. Experiments will be conducted (1) with longer cores, (2) with internal pressure taps in the cores, (3) with polymers of other molecular weights, and (4) with sands where the finest sand particles have been removed.

Analysis of Polymer Produced from Production Wells. Produced water samples from Wells J-27 and J-28 have been monitored weekly for signs of polymer breakthrough and salinity changes. Total organic carbon and nitrogen chemiluminescence were used to detect the presence of polymer, while atomic absorbance spectroscopy was used to monitor common cations (Na, K, Mg, Ca, Fe, Sr). To date, no polymer was detected and no change in produced water composition occurred. **Figure 2.3** details results of analysis of produced fluids (using a Shimizu TOC-L/TNM-L chemiluminescence instrument) for total nitrogen. (Recall that HPAM contains nitrogen.) Since November 2018, the produced fluids have contained the same amount of nitrogen—about 20 ppm. This is a baseline amount which may be due to nitrogen compounds in the oil or to some other oilfield chemical that Hilcorp adds (perhaps corrosion inhibitor, biocide, scale inhibitor). It is not polymer, since it was present at the start of the project. If one wanted to argue that this concentration was due to HPAM, it would be equivalent to 1% of the injected HPAM concentration (as indicated in **Figure 2.3**).

Within the past two months, Hilcorp noted that clay-flocculation tests showed positive for produced polymer. However, **Figure 2.3** reveals that these clay-flocculation results are false positives. The clay-flocculation test is an easy, qualitative test that is convenient for field application, but it can give false positives due to interferences in the produced fluids. Any positive indication from the clay-flocculation test should be re-tested using a more reliable laboratory method—such as our chemiluminescence test, which has a normal limit of detection of 50 parts per billion (ppb) of nitrogen.

If one attempted to argue that 20-ppm HPAM was actually being produced, a credible explanation must be found to justify that. Since ~1800-ppm HPAM is injected, with a viscosity of 40-50 cp, that polymer solution should efficiently displace resident water in its path. So, when the polymer arrives at a production well, it might show a low concentration for a short time, but the concentration should rapidly rise to a value consistent with the flow contribution from the offset polymer injection well—i.e., at least, hundreds of ppm. A sustained produced polymer concentration of only 20 ppm is not credible based on any reasonable reservoir-engineering-based judgement. This further supports the fact that the clay-flocculation tests gave false positives.

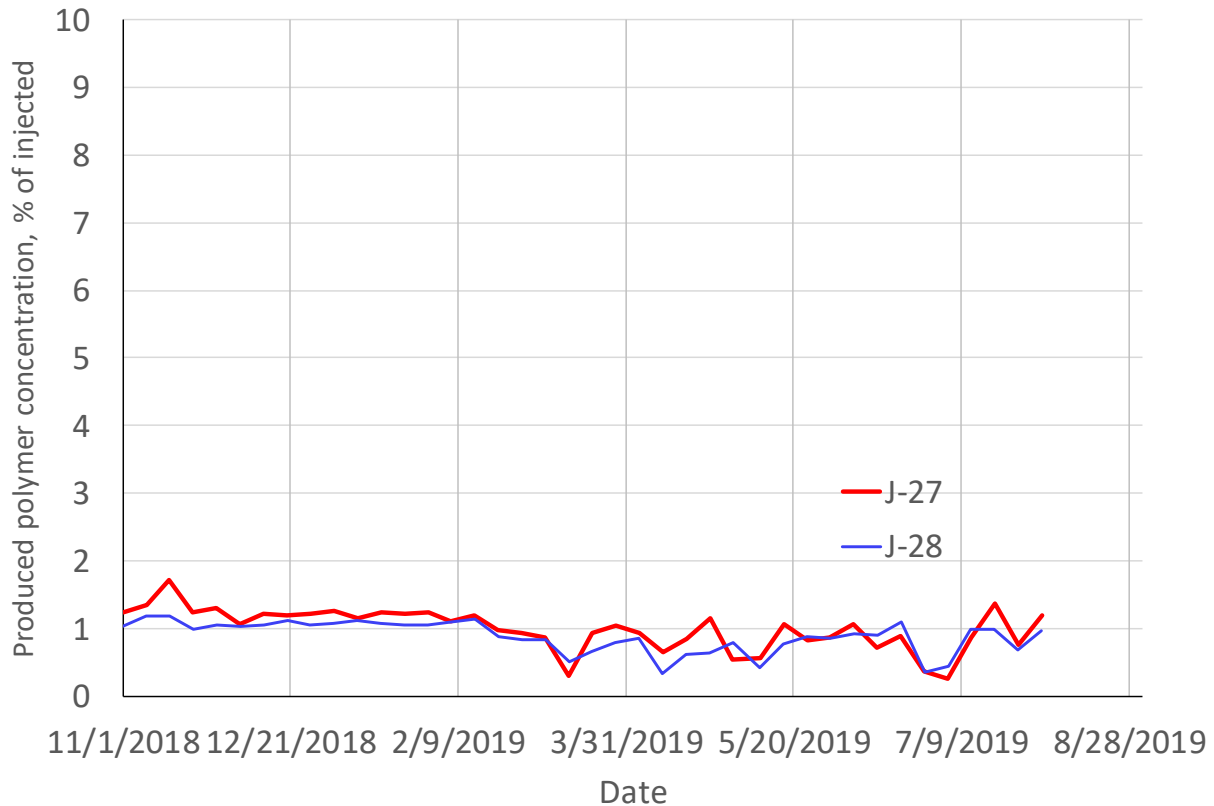


Figure 2.3: Analysis of polymer produced from Wells J-27 and J-28.

Effect of Hypochlorite on HPAM Solutions and NB sand.

Because of an upset in the polymer-injection-flow stream, undissolved polymer was apparently injected a few months ago at the field project.

At one point, the question was raised whether HPAM powder provided from SNF was too large (in particle size) around the time of the upset. So, we determined polymer powder particle size distributions for the field sample of Flopaam 3630 that was provided to our lab, September 26, 2018. The measurements were performed using a Malvern Mastersizer 3000 with Areo-S dispersion unit. **Figure 2.4** shows the volume-based polymer-powder size distribution for Flopaam 3630, along with that associated with our laboratory sample of SNF Flopaam 3430. Based on this and other information (associated with the field polymer-dissolution equipment), Hilcorp assessed that the powder-particle size distribution was not the source of the upset.

Malvern Mastersizer 3000 Aero S. Flopaam 3430S Lot 3460. October 9, 2009.
 Flopaam 3630 from Milne Point Lot GJ1201 September 26, 2018.

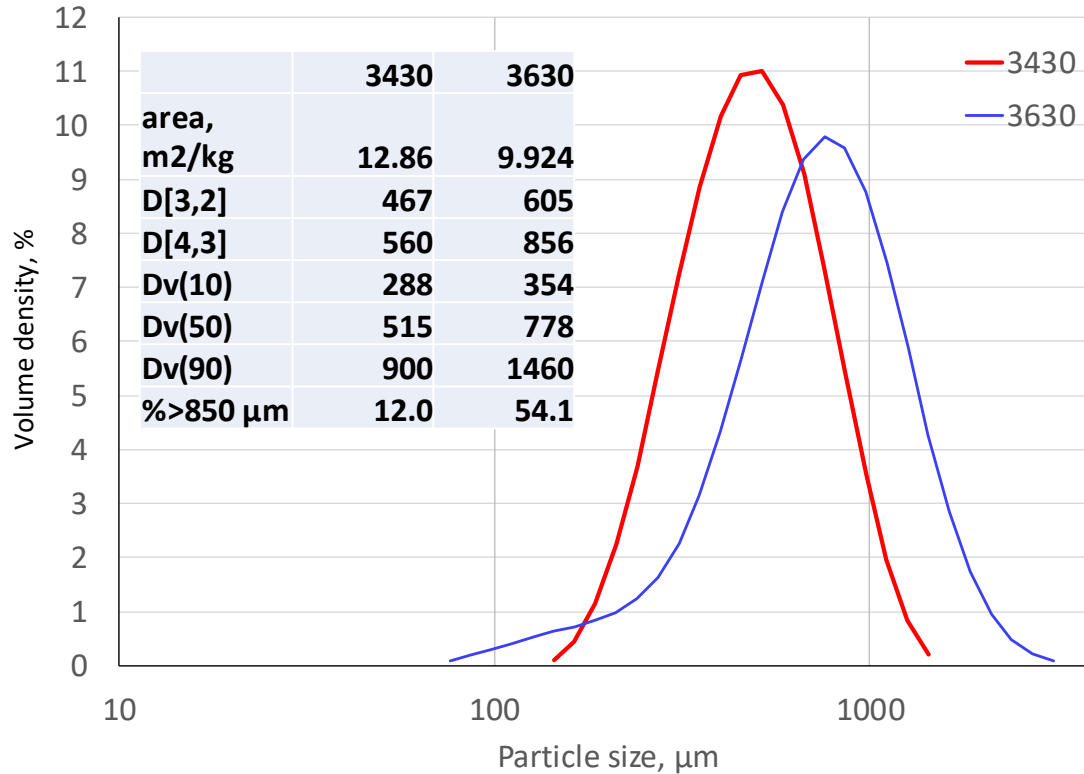


Figure 2.4: Comparison of 3630 and 3430 powder-particle size distributions.

Hilcorp considered using hypochlorite (bleach) to destroy undissolved polymer that accumulated in the injection wells. They expressed an interest in assessing whether a hypochlorite treatment would have adverse effects on the project—other than destroying polymer/gel in the wellbore. In response, we added a bleach treatment to the end of a polymer retention experiment—specifically the fourth listing in **Table 2.1** (2nd NB sand, Flopaam 3430 polymer). After completion of the retention study, we injected 100 cm³ (~5.5 PV) each of 1000-ppm, 2000-ppm, 3000-ppm, 4000-ppm, and 5000-ppm hypochlorite (in Milne brine) at 15.24 ft/d (about 1 hour for each slug). Followed by 100 cm³ of Milne brine. **Figure 2.5** plots resistance factors during this process. (The bleach was household HDX bleach with 8.25% active hypochlorite.) Small amounts of fine gray buoyant particles were produced during hypochlorite injection, but no significant brine discoloration was noted. Also, no plugging or incompatibility with the core or polymer was noted. Further, no precipitates were noted when hypochlorite was added to the polymer (see **Figure 2.6**).

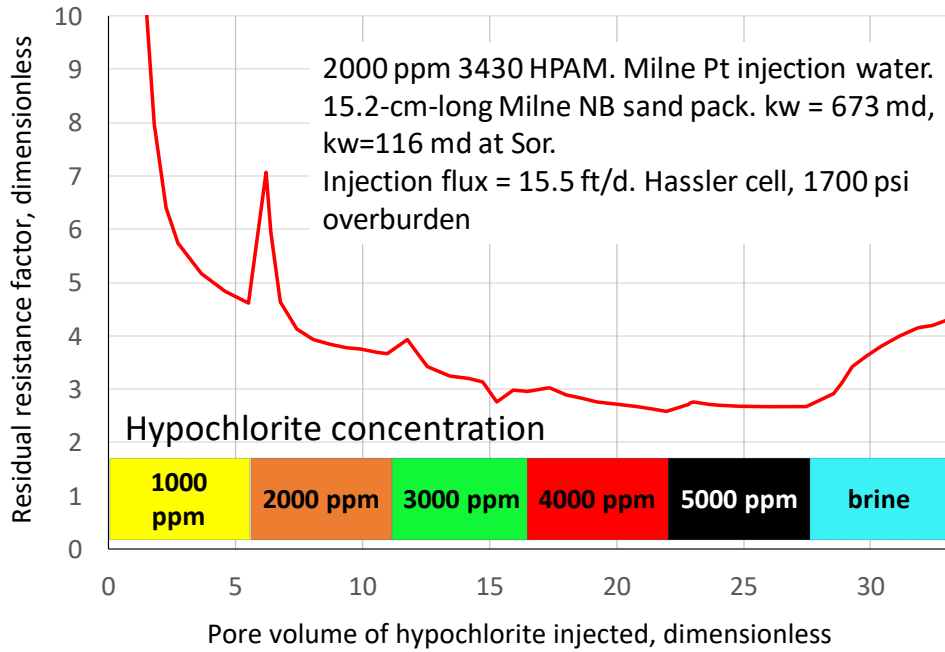


Figure 2.5: Injection of hypochlorite after 12-PV of 2000-ppm 3430 polymer.

Left: polymer only.
 Middle: 50%
 polymer+50% 5000-
 ppm hypochlorite.
 Right: 50% polymer
 +50% straight bleach.
 NO INCOMPATIBILITY



Figure 2.6: No precipitation noted when bleach was added to polymer solutions.

Activity is ongoing.

- Task 3.0 - Laboratory Experiments for Optimization of Injection Water Salinity and Identification of Contingencies in Premature Polymer Breakthrough in the Field

Core flooding experiments and lab-scale simulation work were carried out in this quarter. Comparative study was done based on the experiments done during this quarter and previous experiment work.

Experimental Study

Sandpack coreflooding experiments were conducted using clean NB sand. The sand was provided by Hilcorp LLC. The sand was cleaned with toluene and ethanol to remove oil covered on the sand. The purpose of the experiment includes: (1) To confirm the reproducibility of positive performance of low salinity waterflood and low salinity polymerflood observed in the previous experiments; (2) To investigate the effect of original wettability of sand on oil recovery performance; (3) To investigate and optimize the injection sequence of polymer solutions.

The diameter of the sandpack core was 2.54 cm with a length of 20.4 cm. The porosity was 0.316 and the permeability 478 was mD. The flood process is: (1) normal salinity water flood (salinity=formation brine); (2) Low salinity water flood (salinity=injection source water used in the pilot injection wells); (3) Low salinity polymer flood (salinity=low salinity water, viscosity \approx 45cp, filtered); (4) High salinity polymer (salinity=formation brine, viscosity \approx 45cp, filtered). The injection flowrate was set at 0.1 mL/min, which made the flow velocity in the porous media to be approximately 1 ft/d, typically representing the flow velocity in matrix of an oil reservoir in the field.

Oil Recovery Performance of Low Salinity Water Flood and Low Salinity Polymer Flood. Figure 3.1 and Figure 3.2 show the experiment results. Positive effect of low salinity water and low salinity polymer on oil recovery was observed in this experiment. The incremental oil recovery was 6.55% from low salinity water flooding (LSWF). The oil saturation was reduced from 0.409 to 0.354. The incremental oil recovery was 12.37% from low salinity polymer flooding (LSPF). The oil saturation was further reduced to 0.251. Almost no incremental oil recovery was obtained during the following high salinity polymer flood.

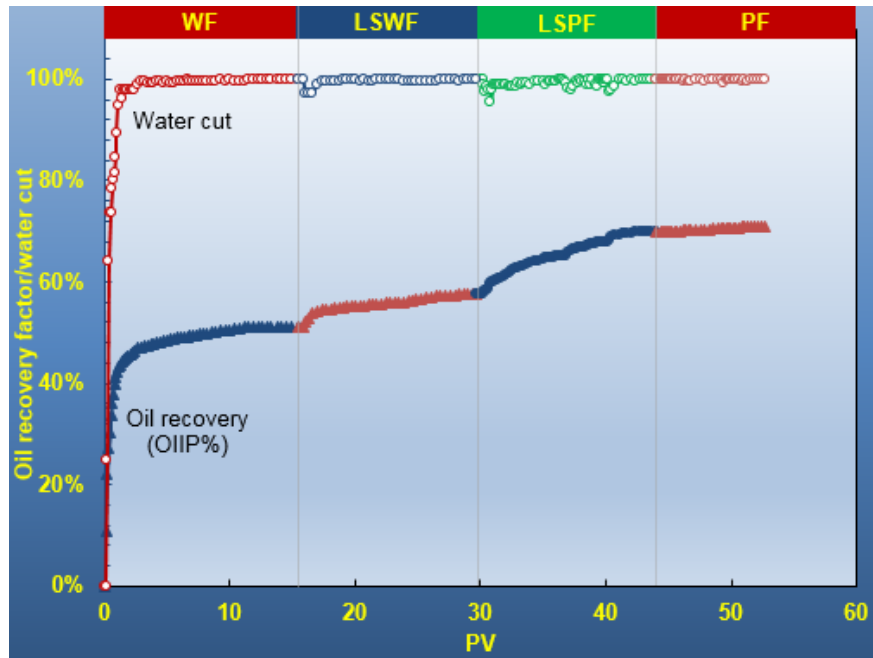


Figure 3.1: The oil recovery and water cut results

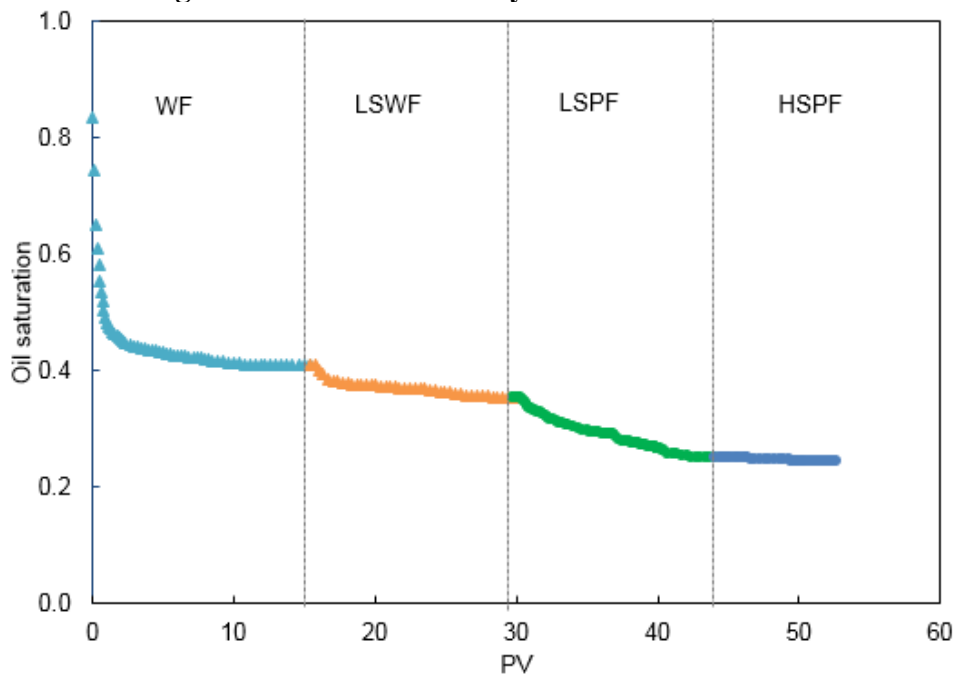
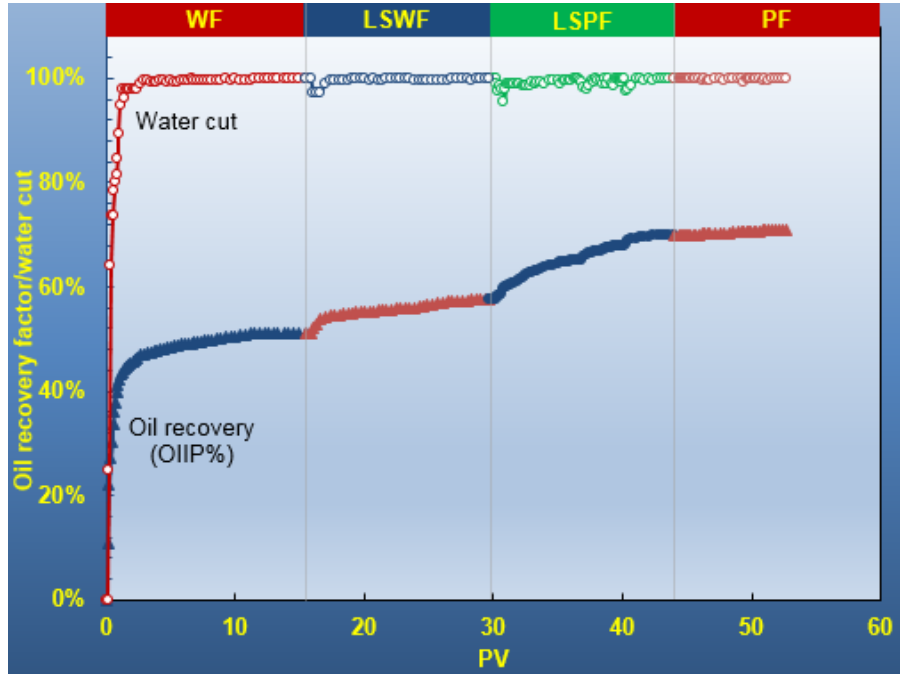


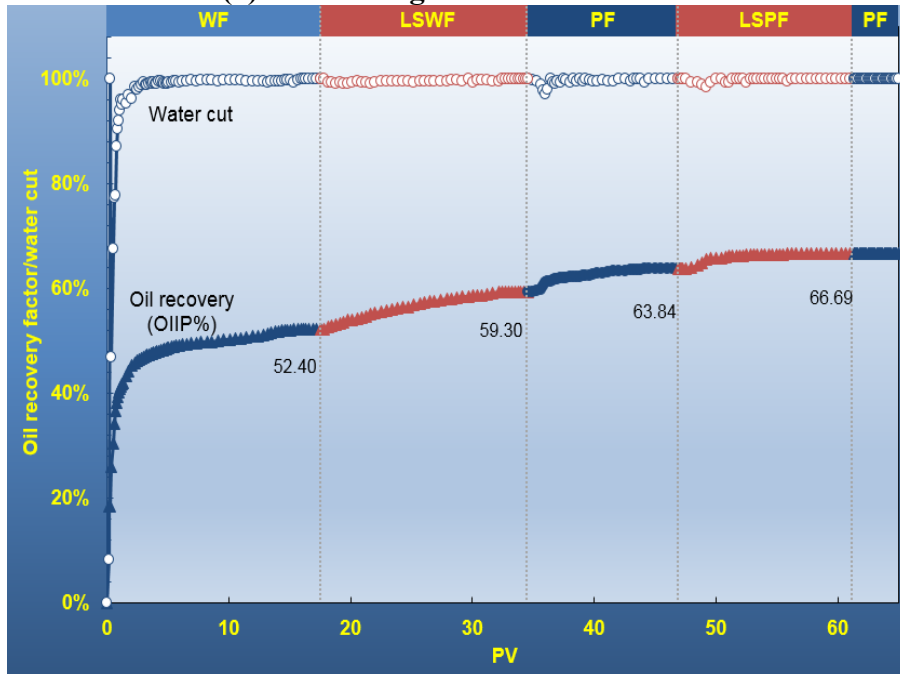
Figure 3.2: The oil saturation (fraction) vs. PV (dimensionless) results

The Impact of Injection Sequence on Oil Recovery Performance. The injection sequence of polymer flood can influence the oil recovery performance. The influence was shown by comparing the two sandpack experiment results in **Figure 3.3**. The oil recovery performance of water flooding and low salinity water flooding was comparably similar, indicating the repeatability of the experiment. A higher

overall recovery efficiency was achieved when the low salinity polymer flood was performed before high salinity polymer flood (70.9% versus 66.7%).



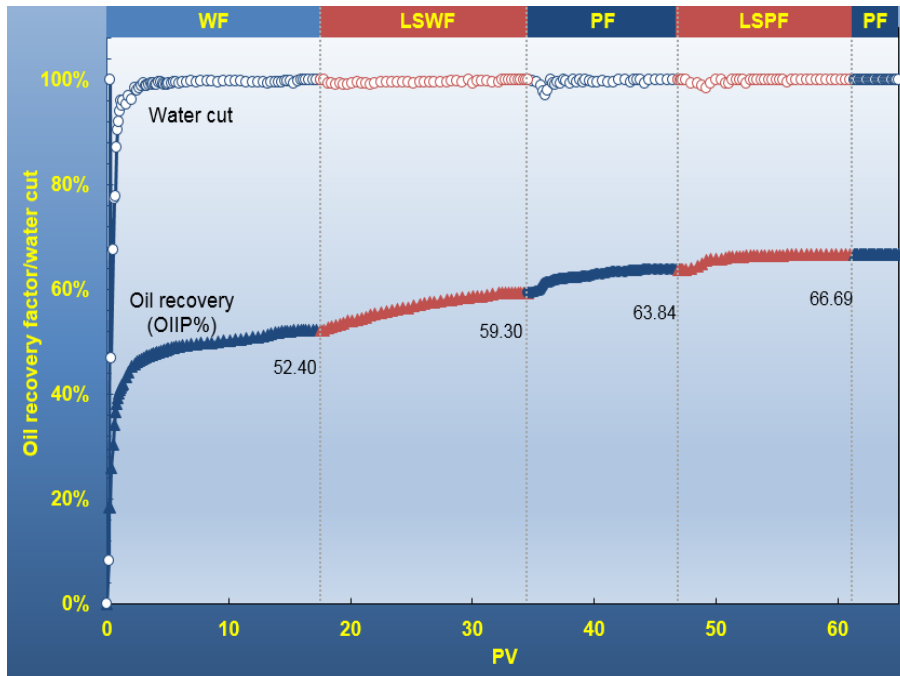
(a) Performing LSPF before HSPF



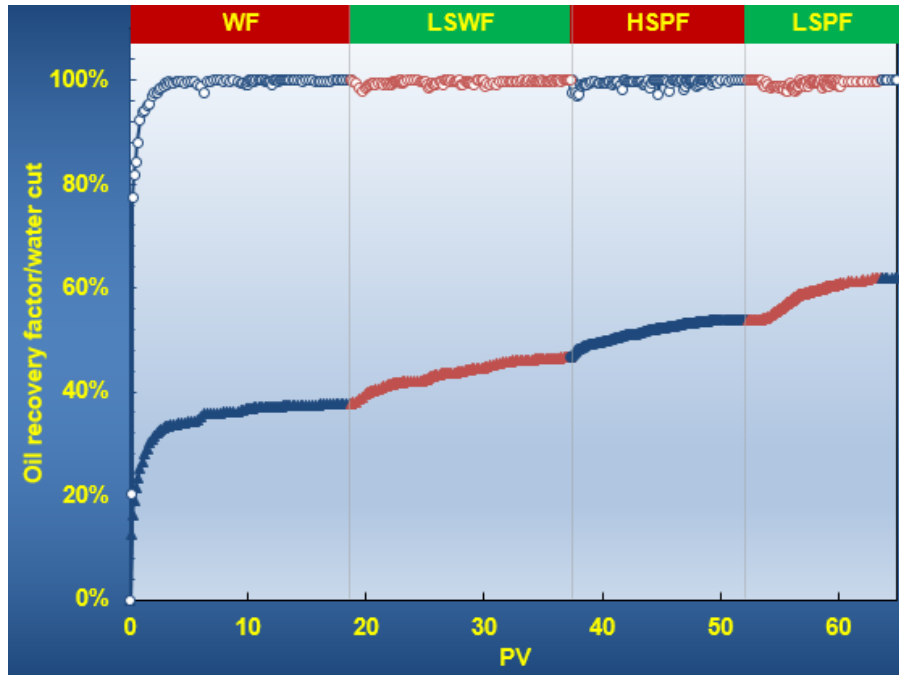
(b) Performing LSPF after HSPF

Figure 3.3: The impact of polymer injection sequence on oil recovery performance

The Impact of initial wettability of sand surface on Oil Recovery Performance. The impact of initial wettability of the sandpack cores on oil recovery performance was analyzed based on the comparison of the experimental results shown in **Figure 3.4**. The water flooding oil recovery efficiency is much lower when the porous media is originally more oil-wet, while a higher oil recovery can be achieved if the porous media is originally more water-wet. The oil recovery by normal salinity water flood was 37.8% and 52.4% for initially oil-wet and water-wet sandpack cores respectively. The oil recovery factor was 47.6% and 59.3%, respectively. The final oil recovery after water flood (including normal salinity water flood and low salinity water flood) and polymer flood (including normal salinity polymer flood and low salinity polymer flood) was lower if the porous media is originally more oil-wet (61.88% versus 66.69%); Nevertheless, the oil recovery improvement by low salinity water flood and low salinity polymer flood is more significant if the porous media is originally more oil-wet (8.71% versus 6.90% for LSWF, 7.94% versus 2.85% for LSPF).



(a) Initially water-wet sandpack core



(b) Initially oil-wet sandpack core

Figure 3.4: The impact of initial wettability of sandpack cores on oil recovery performance

Numerical Simulation Study

In this quarter, our simulation work focuses on fitting of the recovery history and explanation of mechanism in lab experiments. Comparing polymer flooding and low salinity polymer flooding results with water flooding, we found an apparent increase in oil recovery in both clean sand and aged sand packs. However, the end point of kr_w at S_{or} for polymer shifted to a higher level than after water flooding and the S_{or} is decreased for every flooding process. This result left us three hypotheses:

1. Polymer cannot decrease S_{or} but the recovery increment comes from sweep efficiency increase (this hypothesis assumed that water flooding efficiency is ultra-low in heavy oil because of the fingering problem and the real S_{or} is not reached by the end of water flooding);
2. Polymer can decrease S_{or} and the sweep efficiency is not increased (this hypothesis assumed that the lab core flooding is rigid 1D model, so only linear flow is considered in the whole process);
3. Polymer can both decrease S_{or} and increase the sweep efficiency (this hypothesis assumed that sweep regime in lab core flooding is not rigid linear flow and the real S_{or} is not reached by the end of water flooding).

Model 1: Based on Hypothesis 1

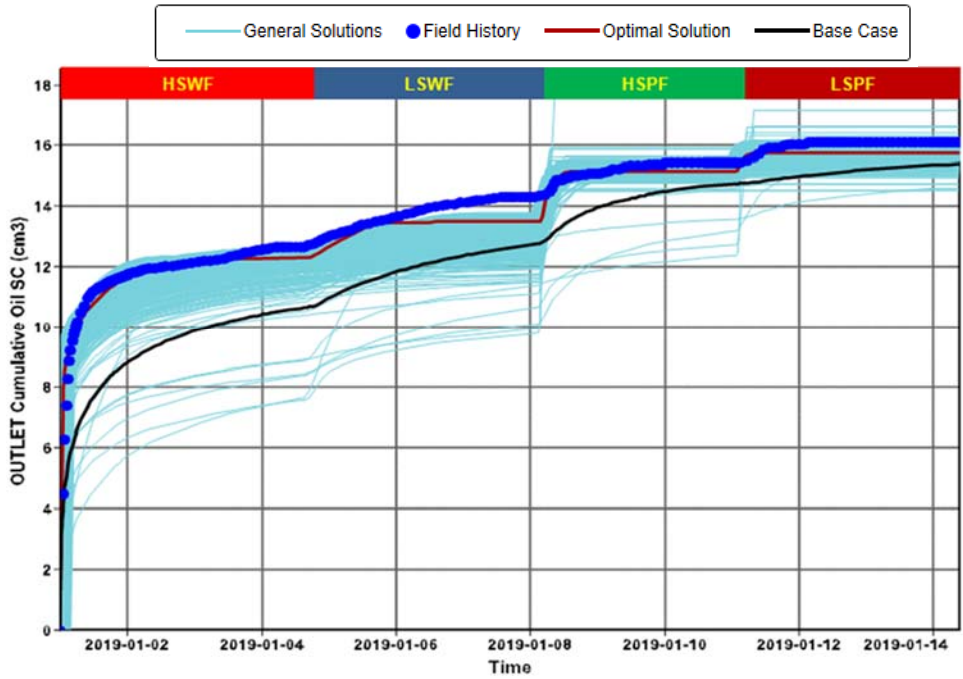


Figure 3.5: 1D Lab scale model illustration - Hypothesis 1

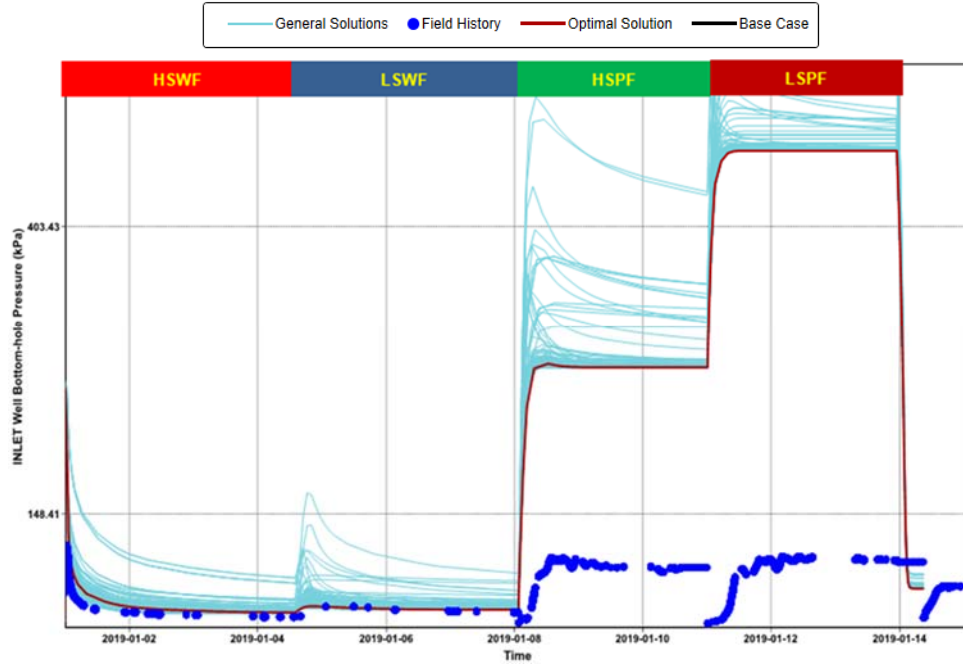
Table 3.1: Model specification– Hypothesis 1

| Length, cm | Area, cm ² | PV, cm ³ | Porosity | Swi |
|------------|-----------------------|---------------------|------------------|-----------------------|
| 20.4 | 5.067 | 29.45 | 0.285 | 0.178 |
| Grids | Oil Viscosity cp | Water Visc. cp | Absolute K md | Polymer adsorption |
| 200*1*1 | 286.3 | 1.07 | 1469 | 28 μg/g |

Results and Discussion. Based on *Hypothesis 1*, we build the 1D model illustrated in **Figure 3.5**. The model detail is listed in **Table 3.1**. The oil production and pressure history matching are shown in **Figure 3.6a** and **Figure 3.6b**. The history matching result is not very good because pressure is hard to fit with experimental data. Relative Permeability curve also indicates a fracture structure especially for oil pathways, as shown in **Figure 3.7**. Although the production can be fitted without much error, the results require a possible heterogeneous model for the core.



(a) Oil production history matching results



(a) Pressure data history matching results

Figure 3.6: Production and pressure history matching result – Hypothesis 1

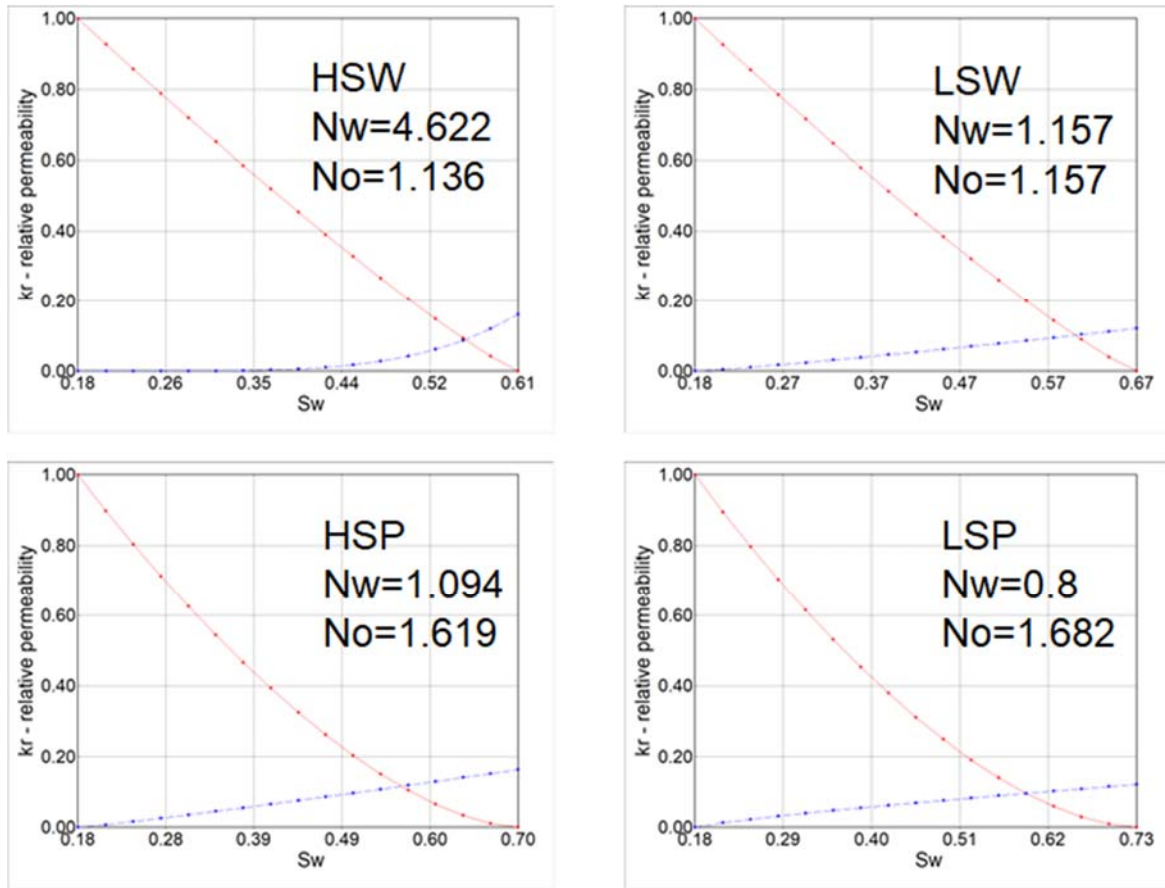


Figure 3.7: Fitting result of relative permeability curve – Hypothesis 1

Model 2: Based on *Hypothesis 2*

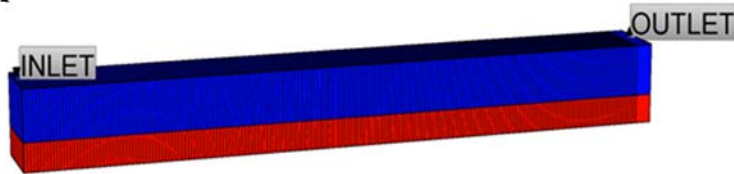


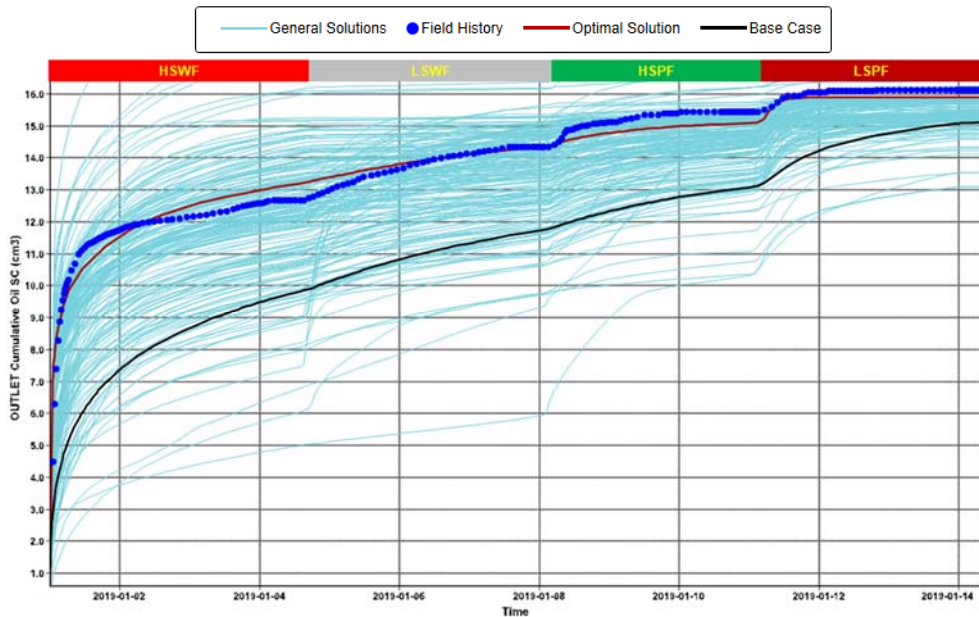
Figure 3.8: 1D Lab scale model illustration – Hypothesis 2

Table 3.2: Model specification – Hypothesis 2

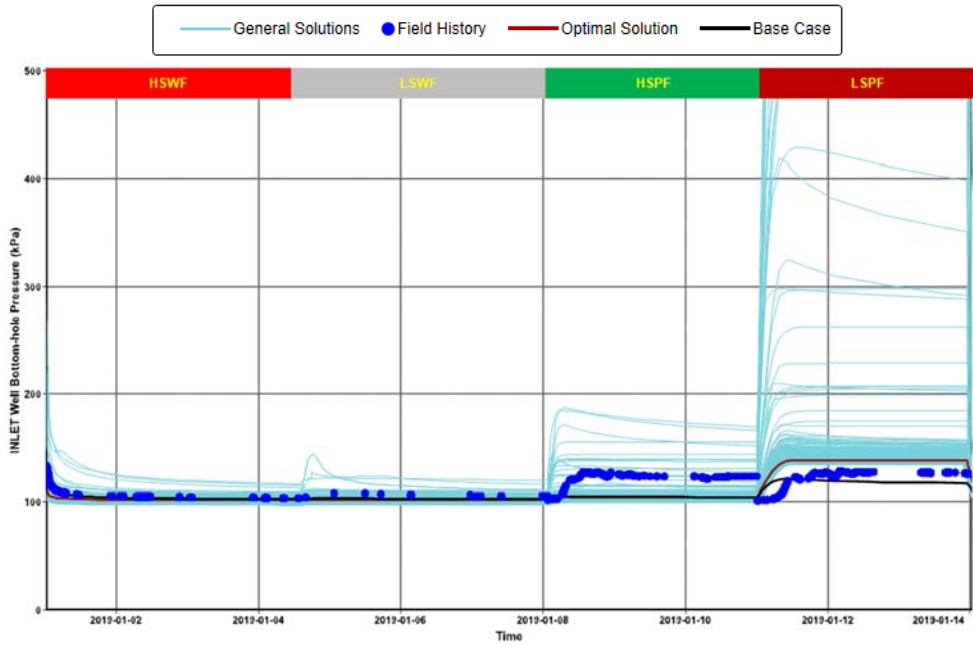
| Length, cm | Area, cm ² | PV, cm ³ | Porosity | Swi |
|------------|-----------------------|---------------------|----------|-------|
| 20.4 | 5.067 | 29.45 | 0.285 | 0.178 |

| Grids | Oil Viscosity cp | Water Visc. cp | Absolute K md | Polymer adsorption |
|---------|------------------|----------------|---------------|--------------------|
| 200*1*2 | 286.3 | 1.07 | 146~14600 | 28 $\mu\text{g/g}$ |

Results and Discussion. Based on Hypothesis 2, we built model 2 illustrated in **Figure 3.8**. The model geometry is shown in **Table 3.2**. Result shown in **Figure 3.9a** and **b** indicates that fitting of both production history and pressure profile are much better than model 1 result, especially for the pressure match. The error is decreased from 700% to 40% for PF and LSPF period. With *hypothesis 2*, we assumed that polymer cannot decrease Sor in this model. As a result, we have two fitted relative permeability curves in this model shown in **Figure 3.10**. With the best matching, the $N_w=3.803$, $N_o=1.934$ for HS flooding processes, and $N_w=1.346$, $N_o=1.724$ for LS flooding processes. The results are very similar to the K_r fitting result from field scale simulation by UAF. However, there is still large error in the pressure history matching even after further history matching by configuring the shear thinning coefficient as shown in **Figure 3.11** and **Figure 3.12**. As a result, we applied the third model based on *hypothesis 3*.



(a) Oil production history matching results



(b) Pressure data history matching results

Figure 3.9: Production and pressure history matching result – Hypothesis 2

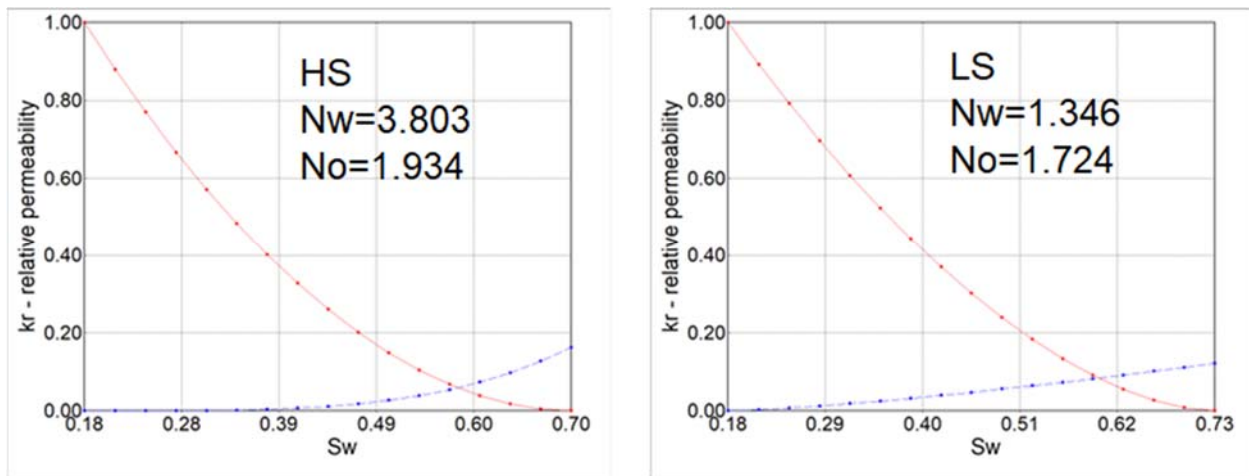


Figure 3.10: Fitting result of relative permeability curve – Hypothesis 2

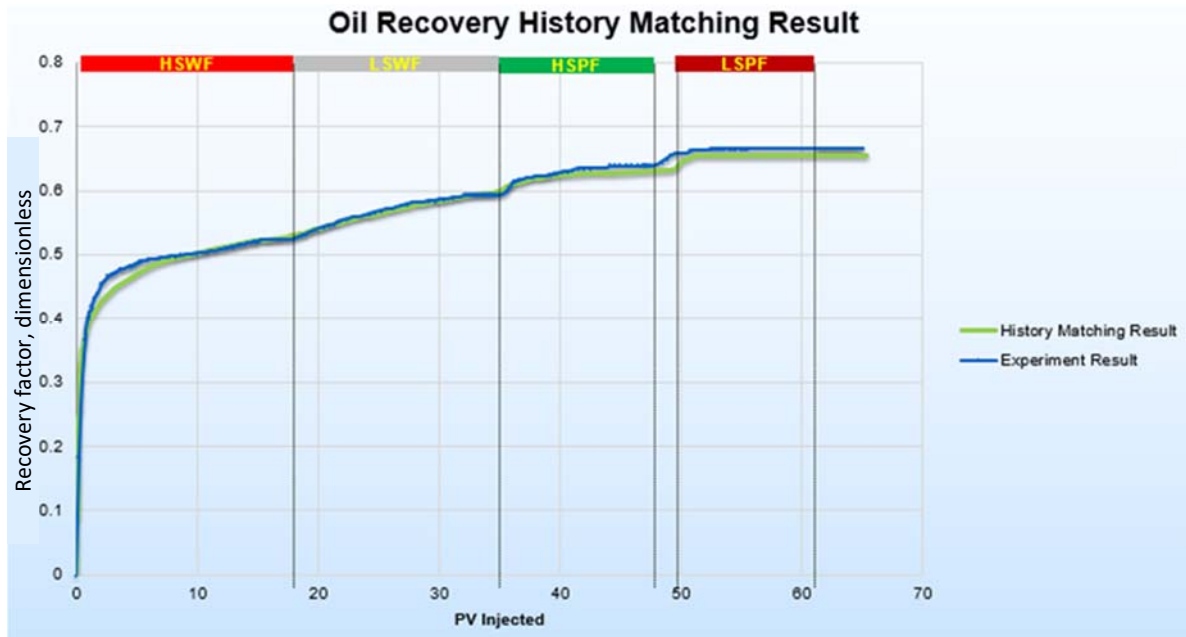


Figure 3.11: Production result of optimal case with fitting the shear thinning coefficient

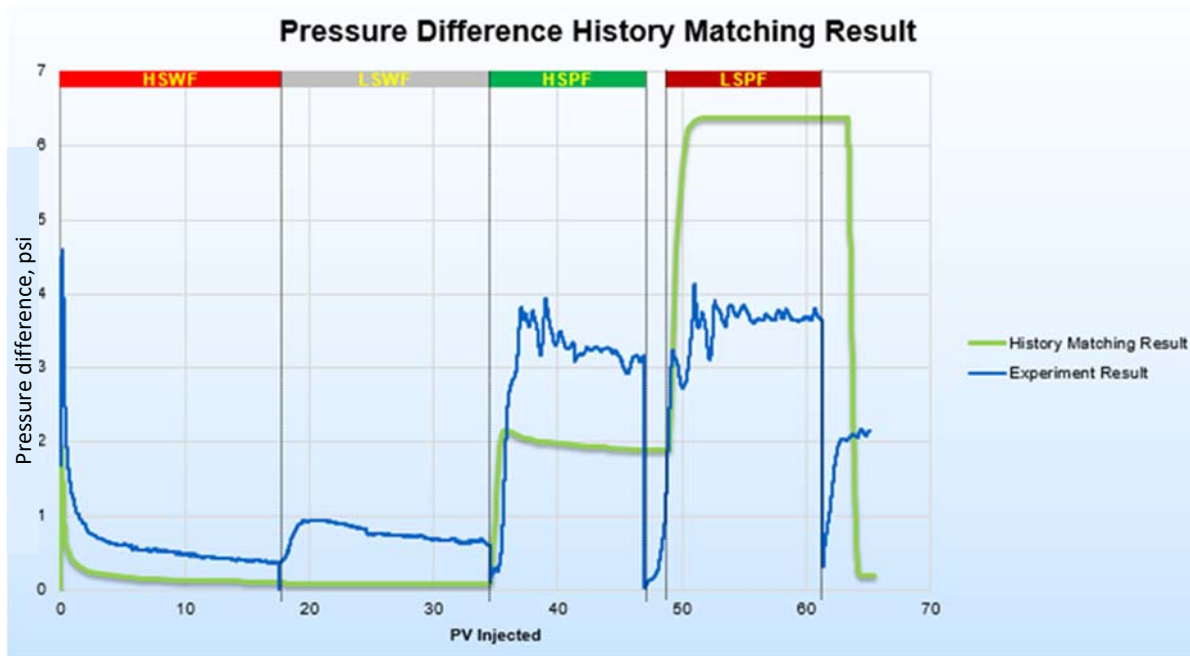
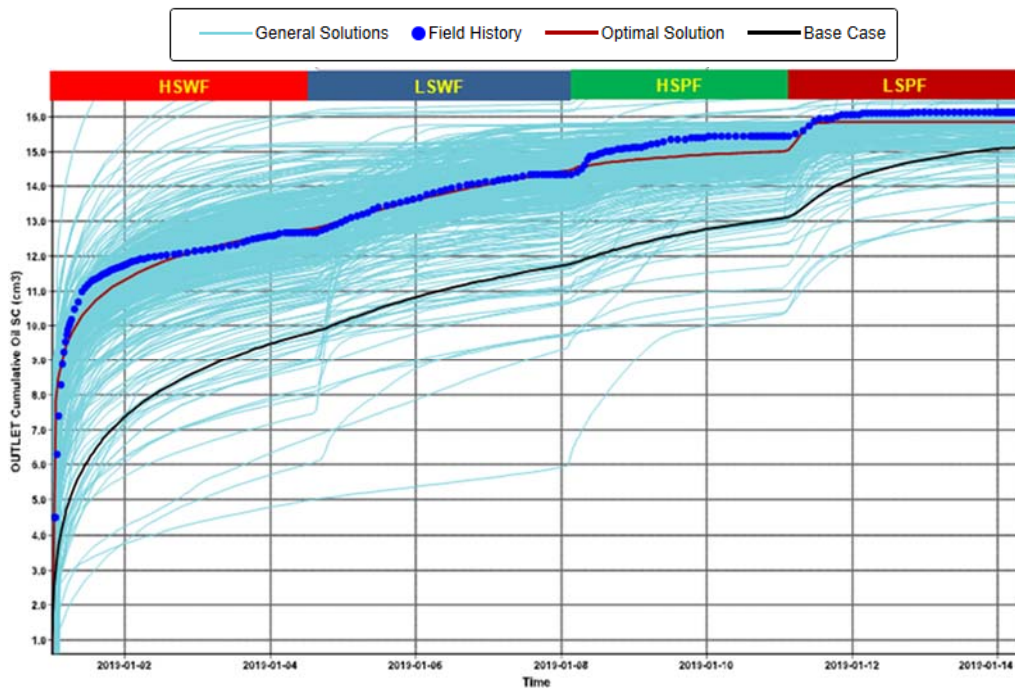


Figure 3.12: Pressure result of optimal case with fitting the shear thinning coefficient

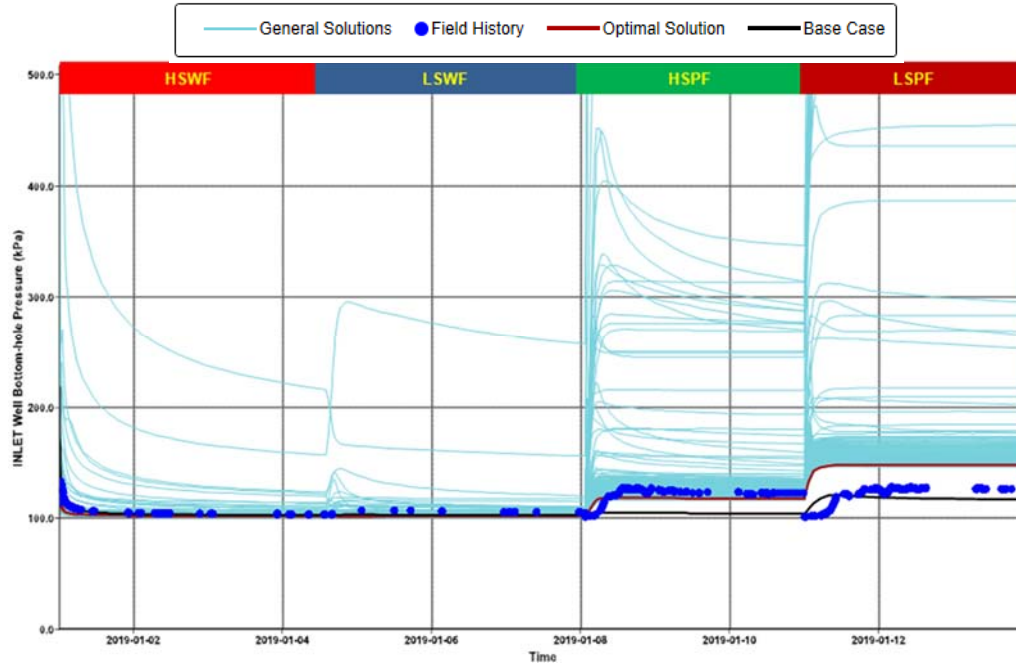
Model 3: Based on Hypothesis 3

Results and Discussion. With *Hypothesis 3*, we composed model 3 which has the same geometry with model 2 but assuming the polymer can decrease S_{or} (Considering four sets of K_r curves). The detail of

the model is listed in **Table 3.2**. Comparing model 3 with former two models, we can see that the production history matching has the highest confidence. All four period of flooding process can fit very well with experimental results. The K_r curves fitted in **Figure 3.14** also has the most reasonable result. The K_r fitted results show that ‘No’ in low salinity environment is clearly smaller than ‘No’ in high salinity environment. This result indicates that after low salinity flooding, the rock surface tends to be more water wet and the oil can flow more easily than in high salinity formation water, which coincides with our expectation for low salinity flooding mechanism. Pressure matching is still challenging though, as the error still is high as shown in **Figure 3.13b**, which is mostly the same as model 2. We will further investigate the experimental result to make sure if our pressure transducer responds correctly. **Figure 3.15** and **Figure 3.16** show a slightly better fitting result especially for the production history matching after optimization of shear coefficients. It’s clear to see the HSP and LSP may have different shear thinning behavior. As a result, for further study, we will implement two different shear coefficients for HSP and LSP separately to investigate the effect.



(a) Oil production history matching results



(b) Pressure data history matching results
Figure 3.13: Production and pressure history matching result – Hypothesis 3

Kr Curve:

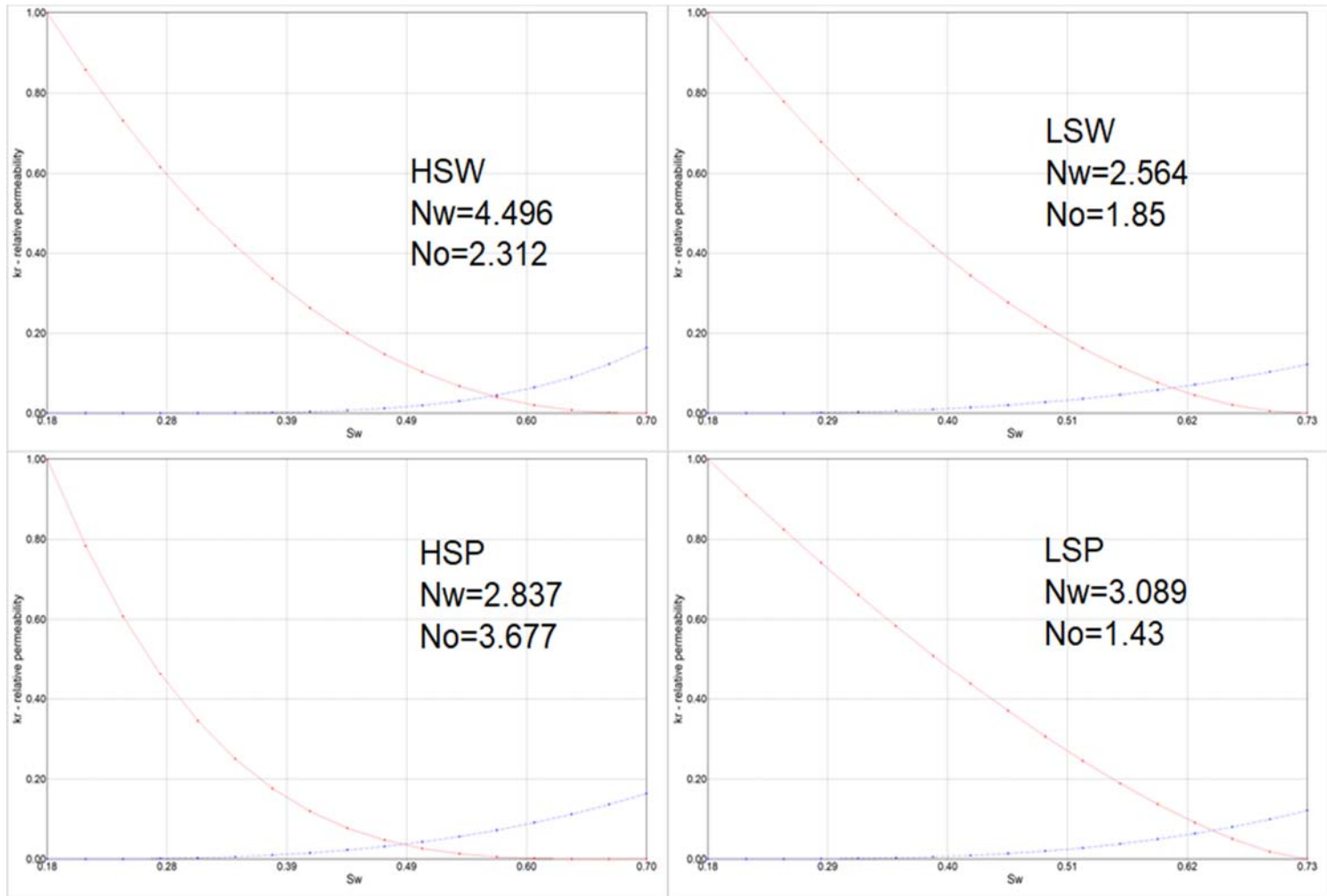


Figure 3.14: Fitting result of relative permeability curve – Hypothesis 3

Optimal Case with Fitting Shear Thinning Coefficient:

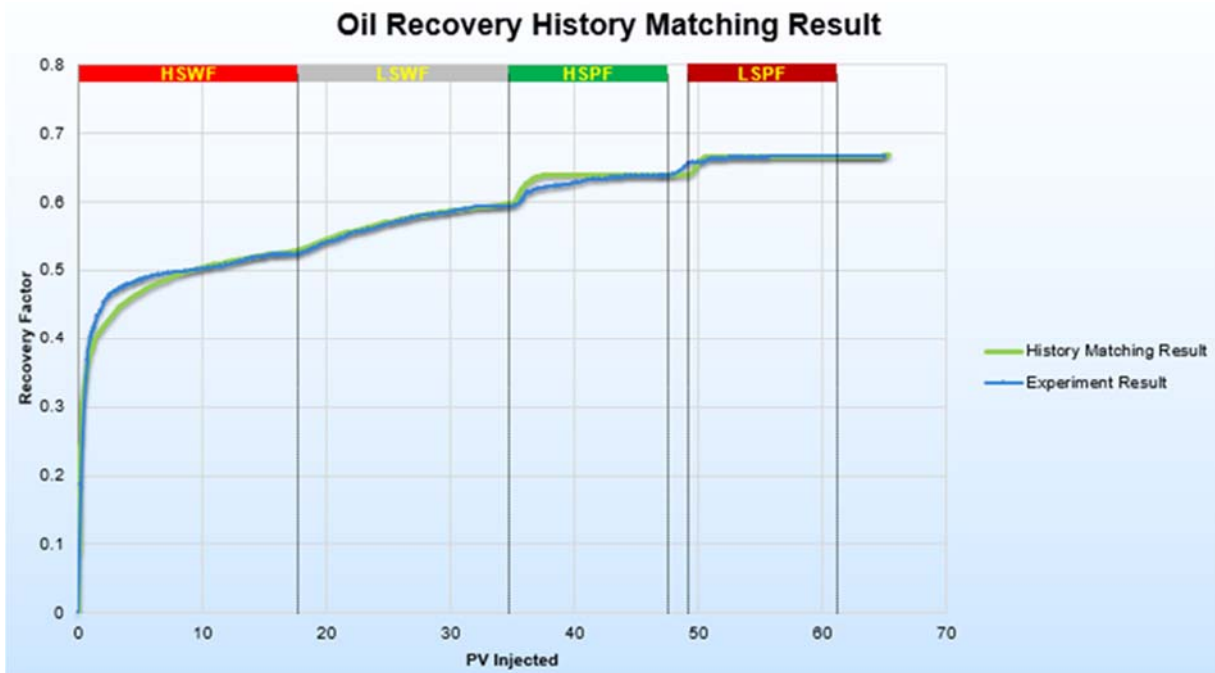


Figure 3.15: Production result of optimal case with fitting the shear thinning coefficient

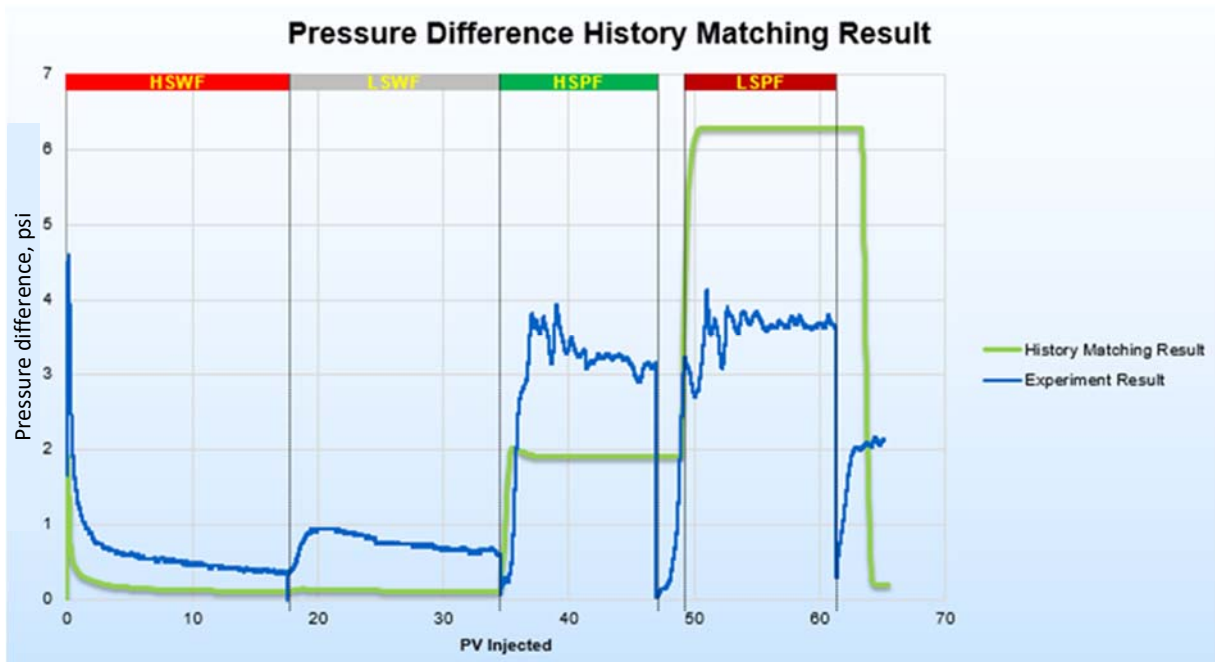


Figure 3.16: Pressure result of optimal case with fitting the shear thinning coefficient

Conclusions:

History matching results for sandpack #4 clean sand has been done with homogeneous and two kind of

heterogeneous models. The history matching results and tracer test results show that permeability of the core has increased a lot after core flooding and heterogeneity was generated during the flooding process. Based on the best matching using model 3, the K_r fitted results show that Corey’s coefficient ‘No’ in low salinity environment clearly smaller than ‘No’ in high salinity environment. This result indicates that after low salinity flooding, the rock surface tends to be more water wet and the oil can flow more easily than in high salinity formation water, which coincides with our expectation for low salinity flooding mechanism. This conclusion indicates that hypothesis 3, assuming that polymer can reduce S_{or} , has higher possibility. The model 3 considering that polymer can modify the K_r curve, can result in similar fitting confidence with model 2 for pressure matching. Different shear thinning coefficients will be considered for future work. Next step we will do history matching for sandpack #5 and discuss polymer flooding sequence effect.

Activity is ongoing.

- Task 4.0 - Reservoir Simulation Studies for Coreflooding Experiments and Optimization of Field Pilot Test Injection Strategy

Activities during June 2019, through August 2019, completed by UND include:

- Study of polymer retention effects on polymer effectiveness through simulations using a 1D homogenous model on the laboratory core flooding experiments for three NB-sand core plugs and two OA-sand core plugs.
- History matching on production index using a field-scale model and polymer effectiveness analysis using two polymers: Flopaam 3630S and 3430S.

4.1 Lab-Scale Models of Polymer Retention

4.1.1 1D homogeneous simulation models for the new polymer retention experiments

Three more polymer retention simulation attempts were designed that were similar to the previous models (as discussed in Quarterly Report 4, Section 4.1.1). All lab-scale models were established based on the actual laboratory core flooding conditions (under overburden pressure applied using a triaxial core holder). For the core plug model, length was 15.2 cm, and diameter was 2.54 cm. Injection flux (Darcy velocity) was 3.73 ft/day, and various overburden pressures were applied. **Table 4.1** summarizes the parameters. All parameters are consistent with the laboratory experimental data.

Table 4.1: Parameters used for polymer retention simulation by core flooding

| Reservoir Parameter | Case 1 | Case 2 | Case 3 |
|---------------------------|--------|--------|--------|
| Source formation | NB-1 | NB-2 | OA-1 |
| Size of X– direction, cm | 15.2 | 15.2 | 15.2 |
| Size of Y– direction, cm | 2.54 | 2.54 | 2.54 |
| Size of Z – direction, cm | 2.54 | 2.54 | 2.54 |

| | | | |
|---|-------|-------|-------|
| Pore Volume Injected, PV | 11.4 | 13.6 | 9.29 |
| Injection water salinity, ppm | 2,600 | 2,600 | 2,600 |
| Porosity, fraction | 0.250 | 0.250 | 0.250 |
| Permeability, md | 548 | 625 | 233 |
| K_{rw} at S_{or} | 0.095 | 0.116 | 0.082 |
| Overburden pressure, psi | 1,000 | 1,700 | 800 |
| *Polymer | 3630S | 3630S | 3630S |
| Polymer concentration, ppm | 1,750 | 1,750 | 1,750 |
| Polymer viscosity, cP | 40.73 | 40.73 | 40.73 |
| Resistance factor, fraction | 1 | 1 | 1 |
| Inaccessible pore volume, ft ³ | 0 | 0 | 0 |
| Initial water saturation, fraction | 0.2 | 0.2 | 0.2 |

* Polymer molecular weight, 18×10^6 Daltons

4.1.2 Discussion of results

4.1.2.1 Water relative permeability at various overburden pressures

In laboratory studies, in order to simulate actual reservoir permeability, various overburden pressures were applied to the core plugs during core flooding experiments. Therefore, the end points of relative water permeability curves were obtained due to altered water permeability at residual oil saturations. Based on the extrapolated relative water permeability curves associated with numerical simulation, we observed, for three cores floods with oil present, the relative water permeability at residual oil saturation increased with increased overburden pressure (**Figure 4.1**). This result is consistent with core flooding experimental results.

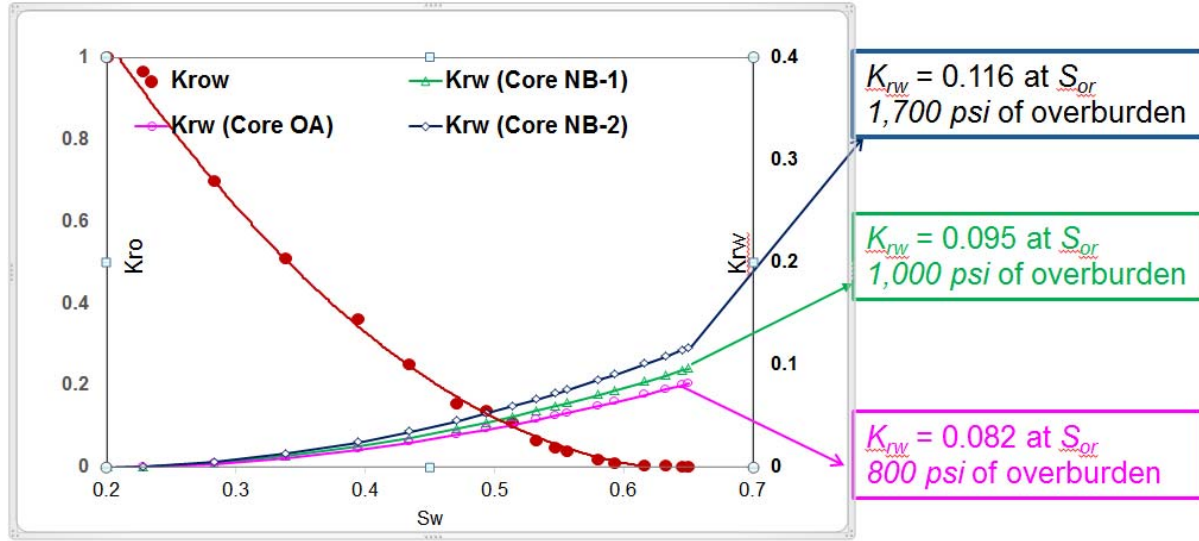


Figure 4.1: Relative water permeabilities (dimensionless) used for core flooding simulations of NB-1, NB-2, and OA-1

Here, all three core plugs were contacted by crude oil. And all three relative permeability curves were treated using identical initial water saturation, residual oil saturation, and water saturation exponent (N_w). Consequently, the relative permeability at each water saturation point was described by Eq. 4.1.

$$k_{rw} = k_{rw}(\text{endpoint at } S_{or}) [S_{wn}]^{N_w} = k_{rw}(\text{endpoint at } S_{or}) \left[\frac{S_w - S_{wi}}{1 - S_{wi} - S_{or}} \right]^{N_w} \quad (4.1)$$

Where: S_{wn} and S_w are normalized water saturation and local water saturation, respectively, N_w is Corey water-saturation exponent, k_{rw} is the relative water permeability. S_{wi} and S_{or} are initial water saturation and residual oil saturations, respectively. The k_{rw} at endpoints were obtained by the ratio of k_w at endpoints to the permeability of the core plugs.

In this study, we assumed the relative oil permeability was not affected by overburden pressure (applied based on laboratory results).

4.1.2.2 Water relative permeability effect on polymer retention

Numerical simulations of polymer retention behavior were performed using the aforementioned relative permeability curves. As shown in Figure 4.2, polymer retention increases as relative water permeability increases.

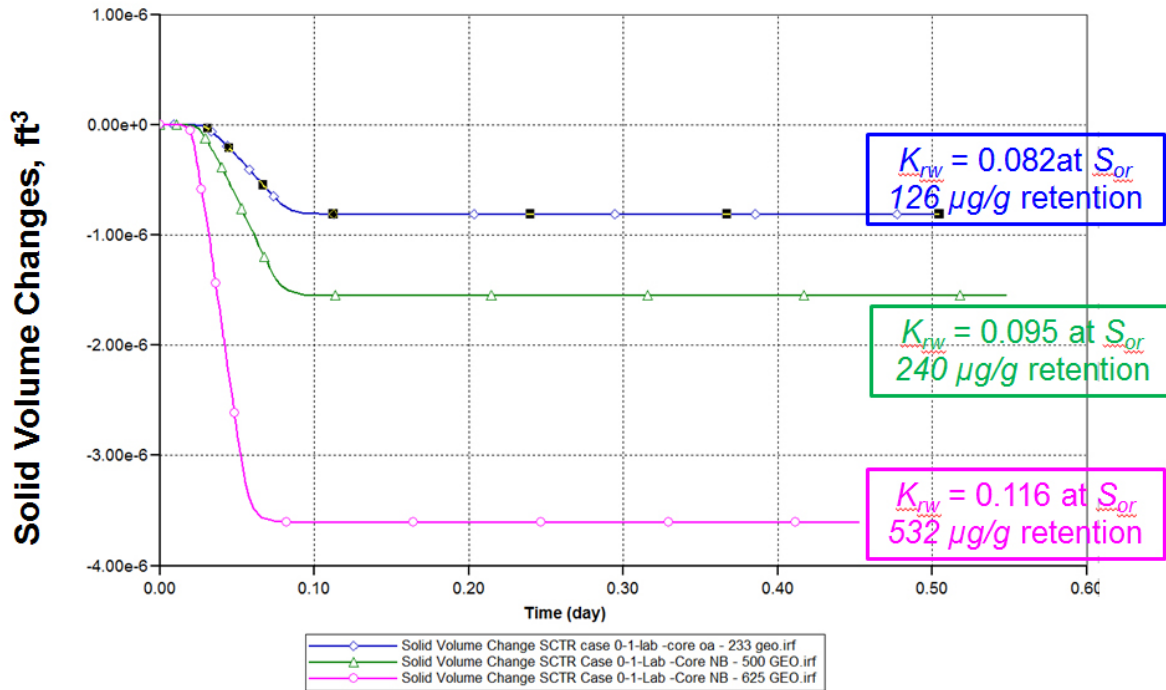


Figure 4.2: Solid volume changes for the core flooding simulations of NB-1, NB-2, and OA-1

In **Figure 4.2**, the negative values represent the difference between the volumes of polymer injected (versus produced)—corresponding to polymer retention in mass per unit volume. On the x-axis, the total time of polymer injection was 0.50 days for 10.5 PV injection for 126 µg/g (Case 3, Core OA-1); 0.60 days for 11.4 PV injection for 240 µg/g (Case 2, Core NB-2); and 0.865 days for 13.59 PV injection for 532 µg/g (Case 1 Core NB-1). The solid volume changes in **Figure 4.2** indicate: (1) as the solid volume change increases, polymer adsorption increases, and (2) relative water permeability affects polymer retention. The explanation is that polymer adsorption would increase as permeability decreases because of mechanical entrapment. On the other hand, as permeability decrease, we observed that relative water permeability ($K_{rw} = K_w/K_a$) increases under similar water permeability (K_w) conditions under the laboratory core flooding results for this circumstance.

Where, K_w , K_{rw} , and K_a are the water permeability, relative water ability, and absolute rock permeability, respectively.

4.2 History matching of field-scale model

A production-index history match was conducted for the field-scale model. Multiple water relative curves (aforementioned in the previous section) were incorporated and corresponded with the permeability distribution varied in the field-scale model.

A history match was conducted from the beginning of polymer injection (August 2018) to the end of May of 2019. **Figures 4.3 to 4.6** show history matches of water cuts and oil rates, for Wells J-27 and J-28. In these figures, the actual production data are depicted by circles, and all simulation data are depicted

by colored solid lines. The plots indicate that when incorporating the multiple relative permeability curves and permeability variances, a production history match by simulation show fairly good agreement with the actual production indices. In **Figures 4.3** and **4.4**, the solid blue and orange lines were the simulation results of different cases.

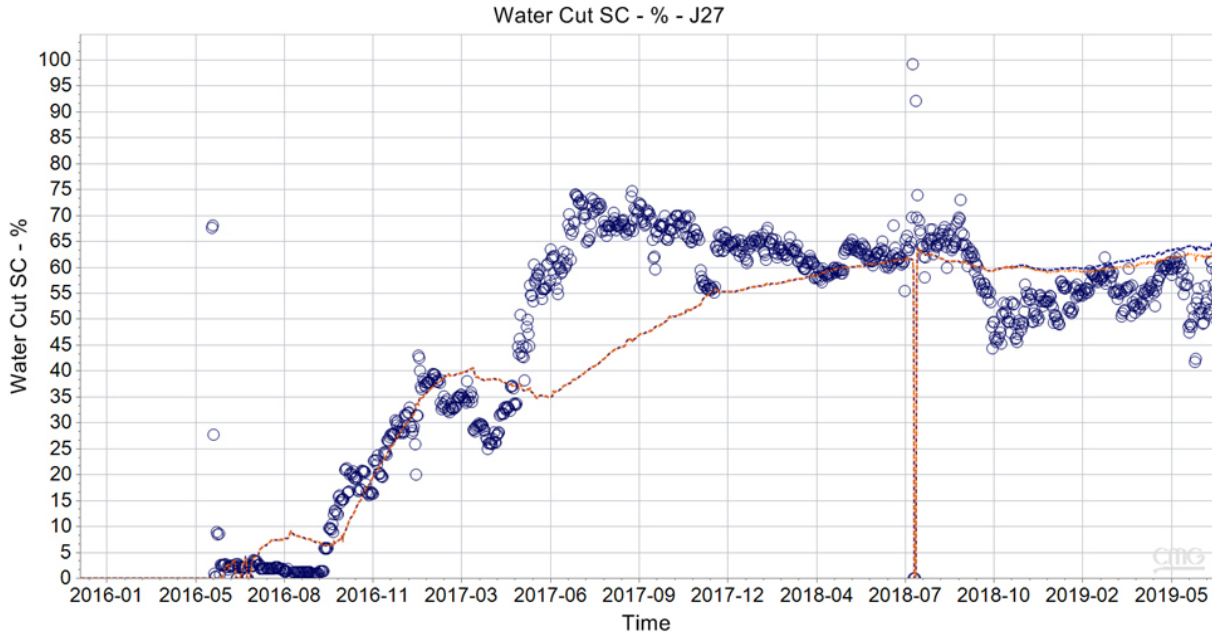


Figure 4.3: Water cut history match of Well J27

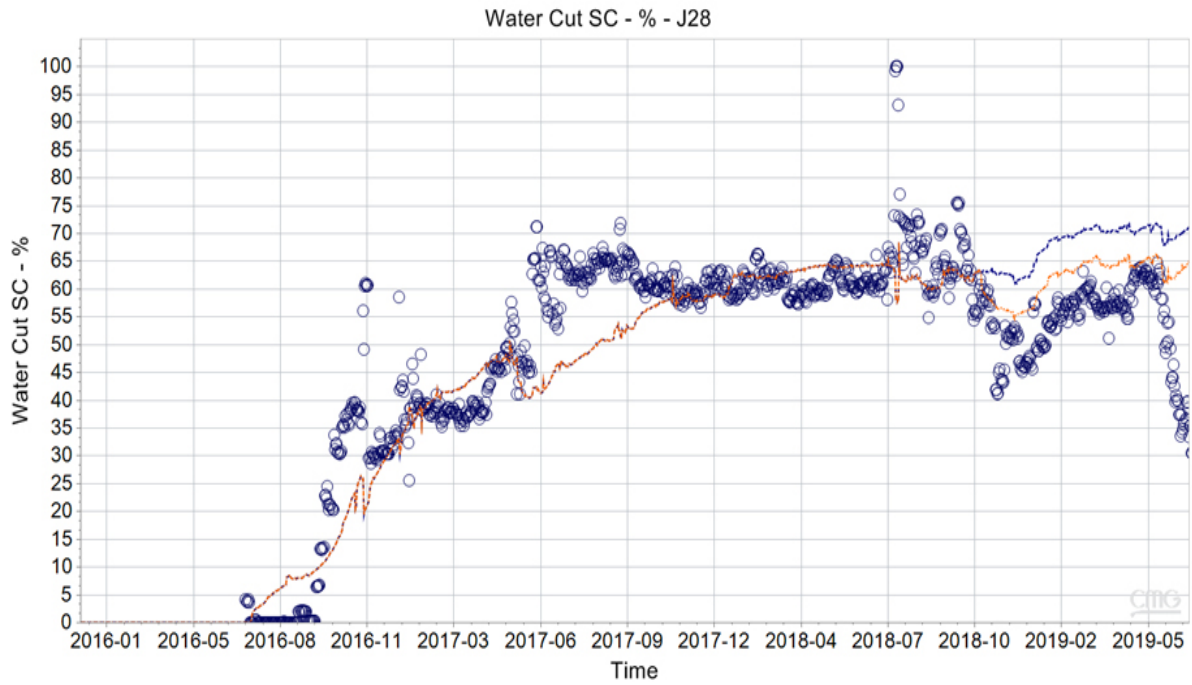


Figure 4.4: Water cut history match of Well J28

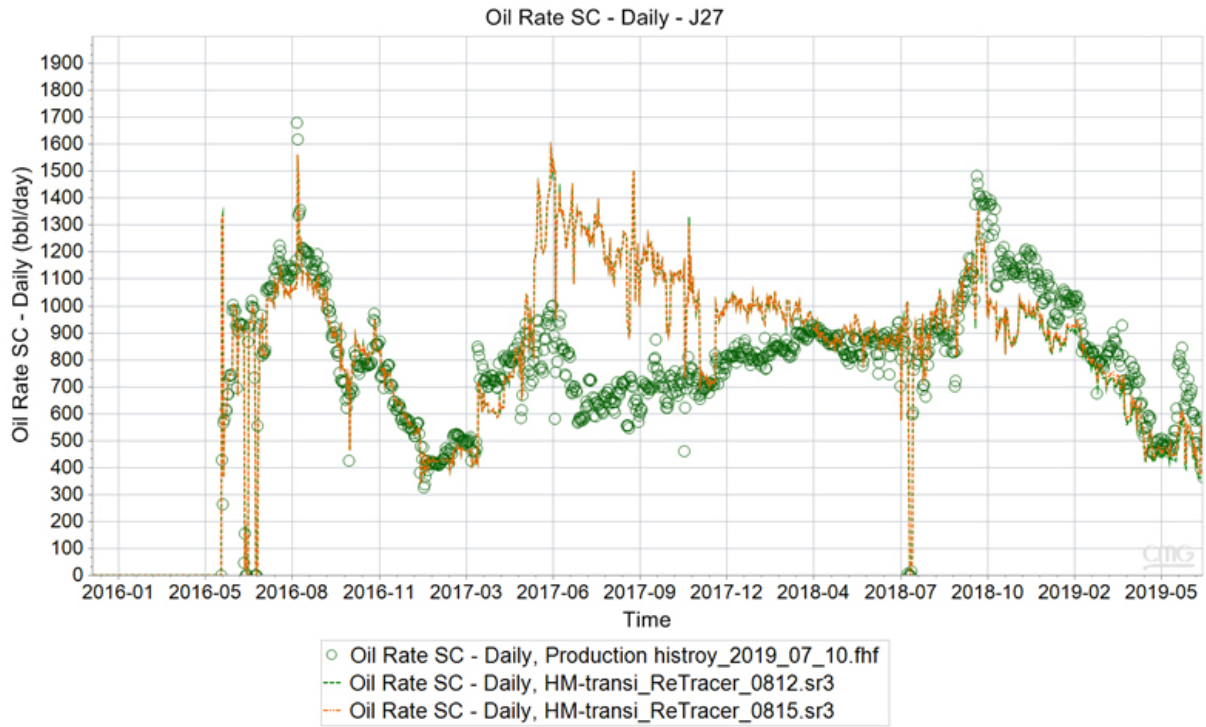


Figure 4.5: Oil rate history match of Well J27

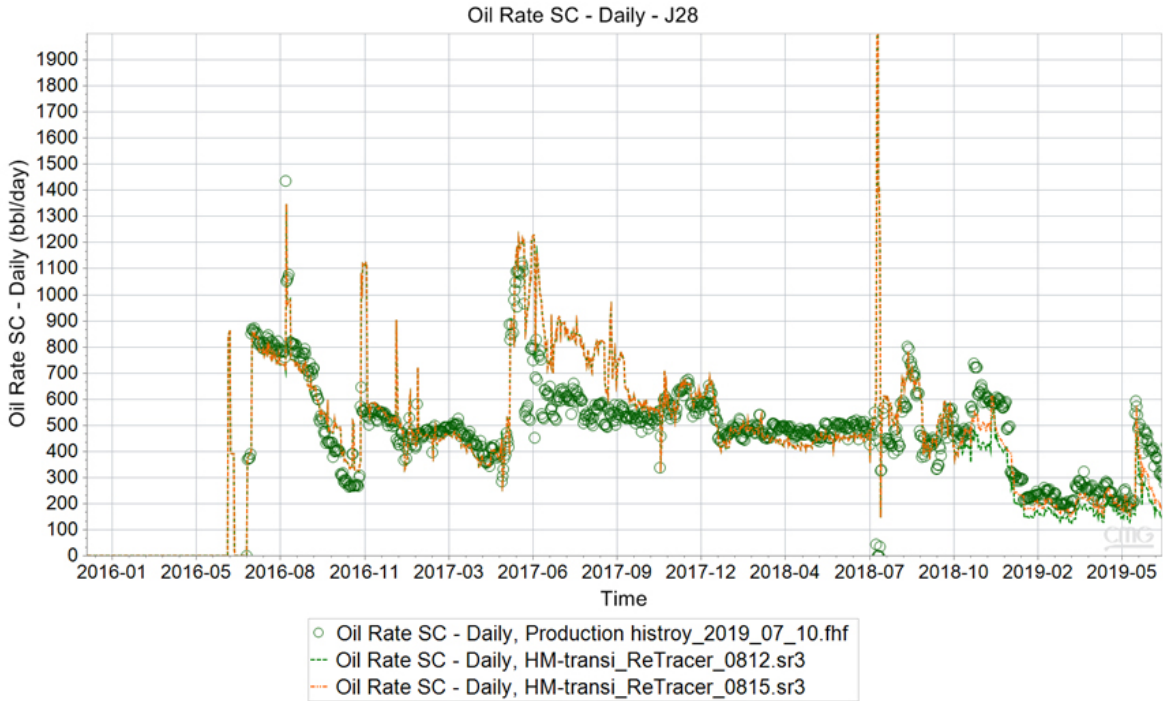


Figure 4.6: Oil rate cut history match of Well J28

4.2 Conclusions

- (1) Polymer retention is affected by relative water permeability.
- (2) With multiple relative permeability incorporation corresponding to the reservoir permeability distribution variants, the histories of oil rates and water cuts were matched well.

4.3 Future Plan

- (1) Continue to simulate polymer retention behavior using core plug experimental conditions.
- (2) Core flooding simulation for different polymer options.
- (3) Continue to history-match production history using the field-scale model and predict/optimize polymer performance and polymer injection parameters.

In this quarter, UAF’s work focused on tracer data history matching and building the new reservoir simulation model, which is reported below.

Tracer test data for history matching

Tracer test data indicates that there may exist strong communication between injector J23A and producer J27. Therefore, a block/stripe permeability field is developed, as shown in **Figure 4.7**, to identify the potential high permeable channels between injector J23A and producer J27. Twenty-six permeability blocks/stripes are assigned in each layer, resulting in 130 permeability blocks/stripes in the entire reservoir simulation model.

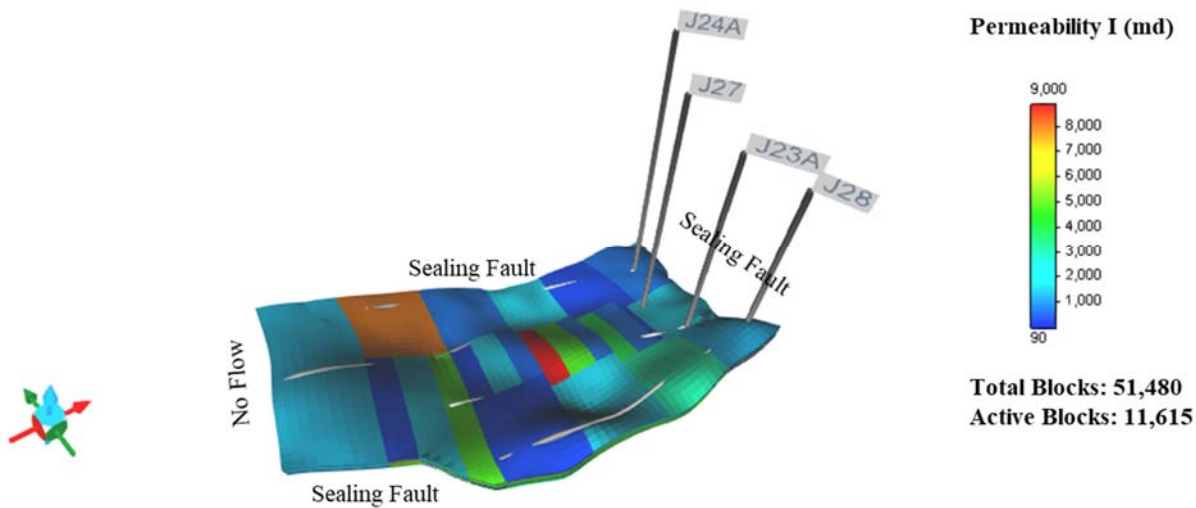


Figure 4.7: Permeability heterogeneity of block/stripe type in the simulation model

In order to obtain better history matching results, the permeabilities of the blocks/stripes in five layers and the total dispersion coefficients of tracer T140A and T140C are tuned together to match different production data in CMOST. The permeabilities of the blocks/stripes in each layer are initially assigned with the average permeability of the layer (layer 1: 1806 mD, layer 2: 1598 mD, layer 3: 2269 mD, layer 4: 1801 mD and layer 5: 1029 mD) and then tuned between 100 and 7600 mD during the history matching process. In the meantime, the total dispersion coefficients of T140A in I, J and K directions are initially

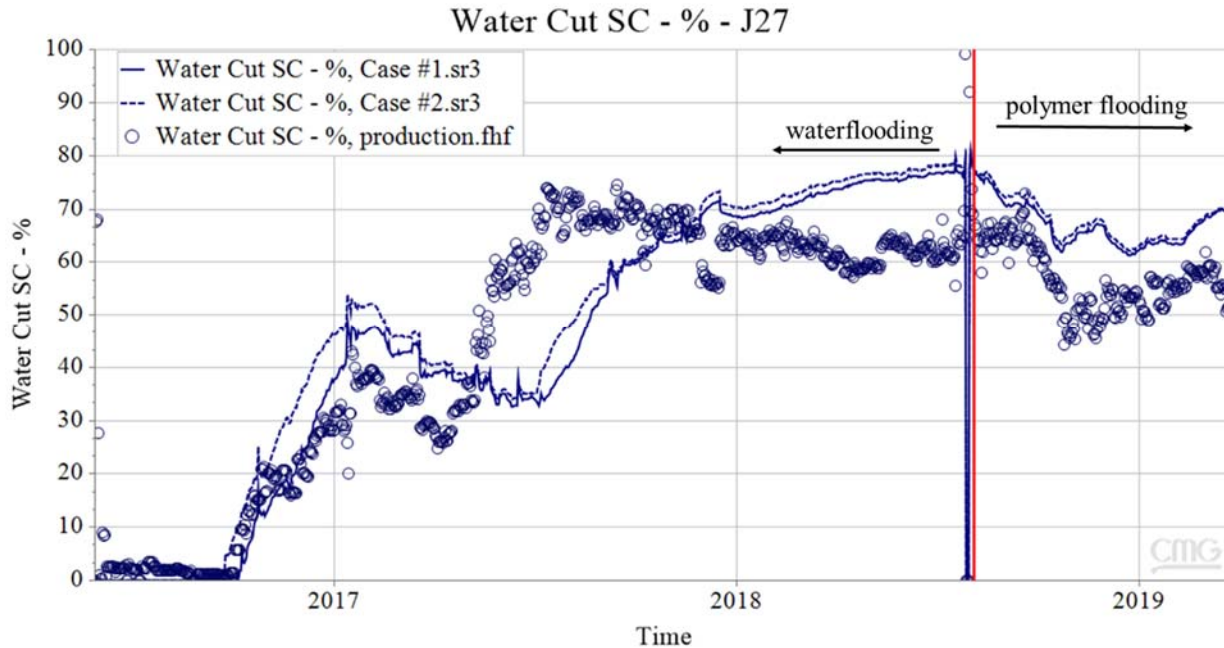
assigned to 3.52×10^{-7} , 8.24×10^{-5} and 3.63×10^{-10} , respectively, and the total dispersion coefficients of T140C in I, J and K directions are assigned to 9.51×10^{-9} , 2.70×10^{-4} and 1.82×10^{-5} , respectively. The following two case studies are conducted to investigate the influence of production data to be matched in the history matching process:

Case #1: oil production rate and water mass fraction of T140A and T140C to be matched

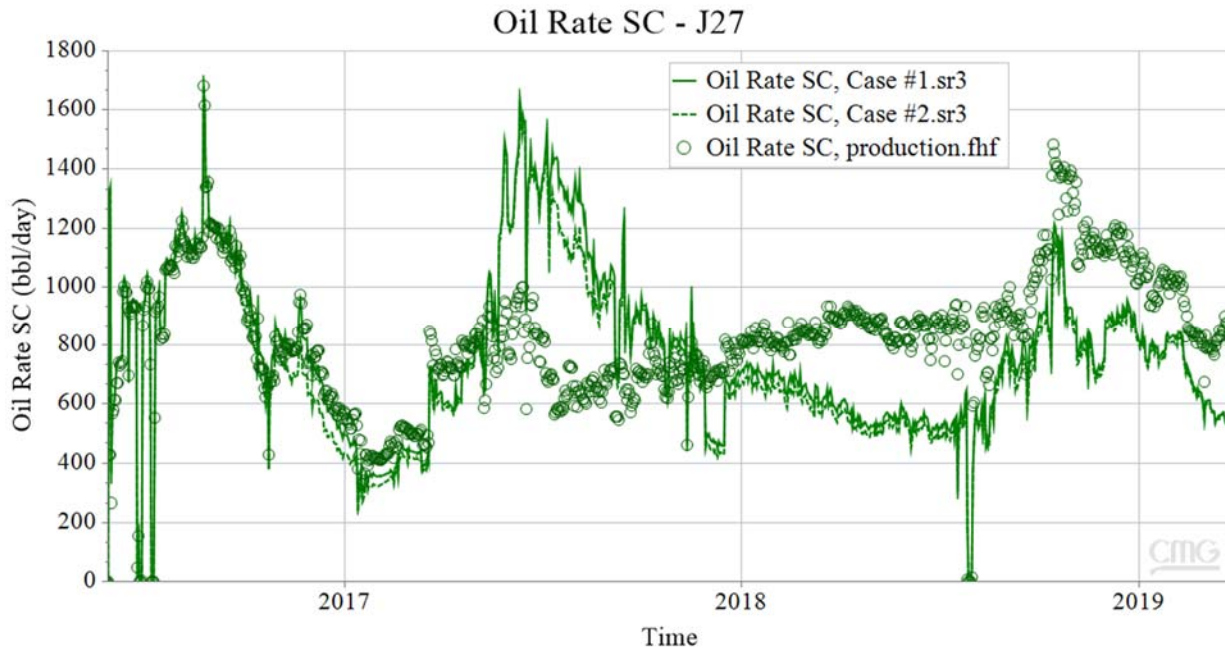
Case #2: cumulative oil production and water mass fraction of T140A and T140C to be matched

History matching results

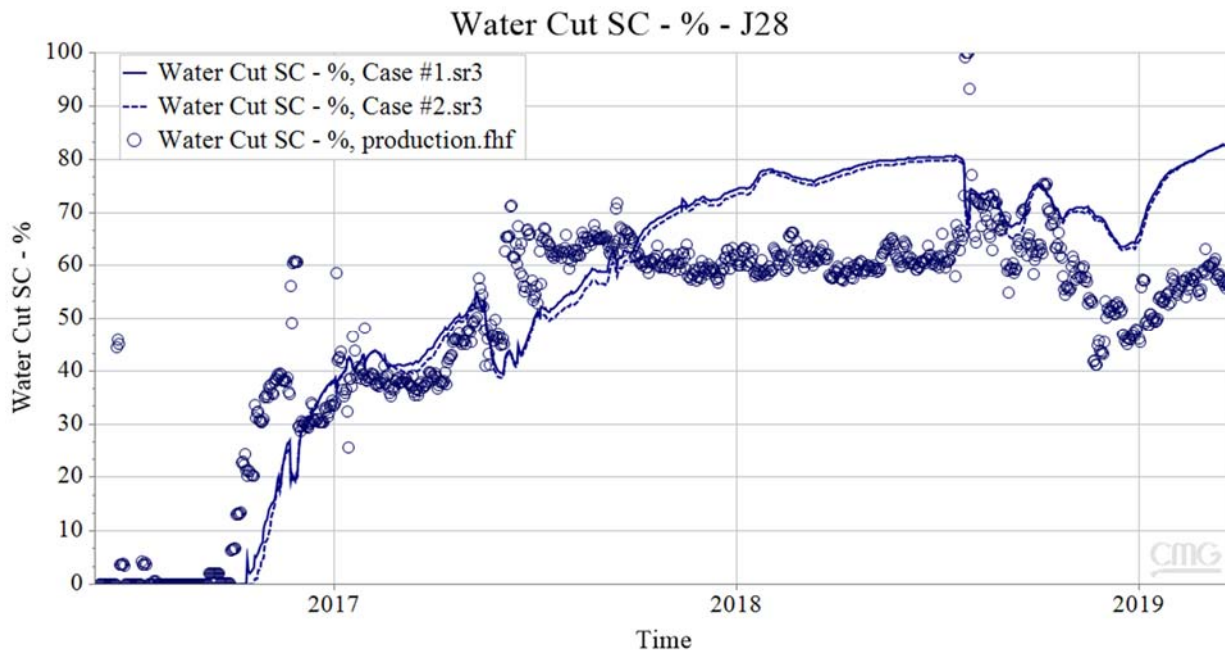
The optimal history matching results of water cut and oil production rate for two production wells are shown in **Figure 4.8**. It can be seen that the simulated production data of these two case studies have little difference whether the oil production rate or the cumulative oil production is to be history matched. The simulated oil production rate of producer J27 deviates from the actual production data from May 2017 to June 2018, which means that the estimated permeability distribution field cannot represent the heterogeneity of real oil field.



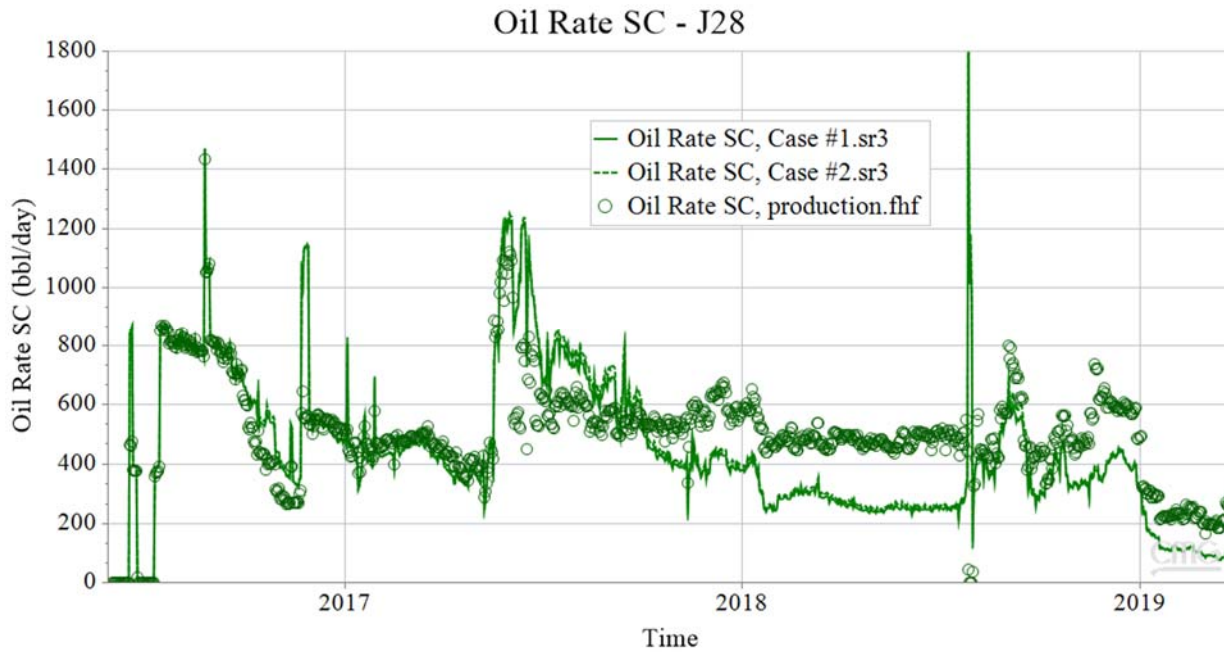
(a) Water cut of producer J27



(b) Oil production rate of producer J27



(c) Water cut of producer J28

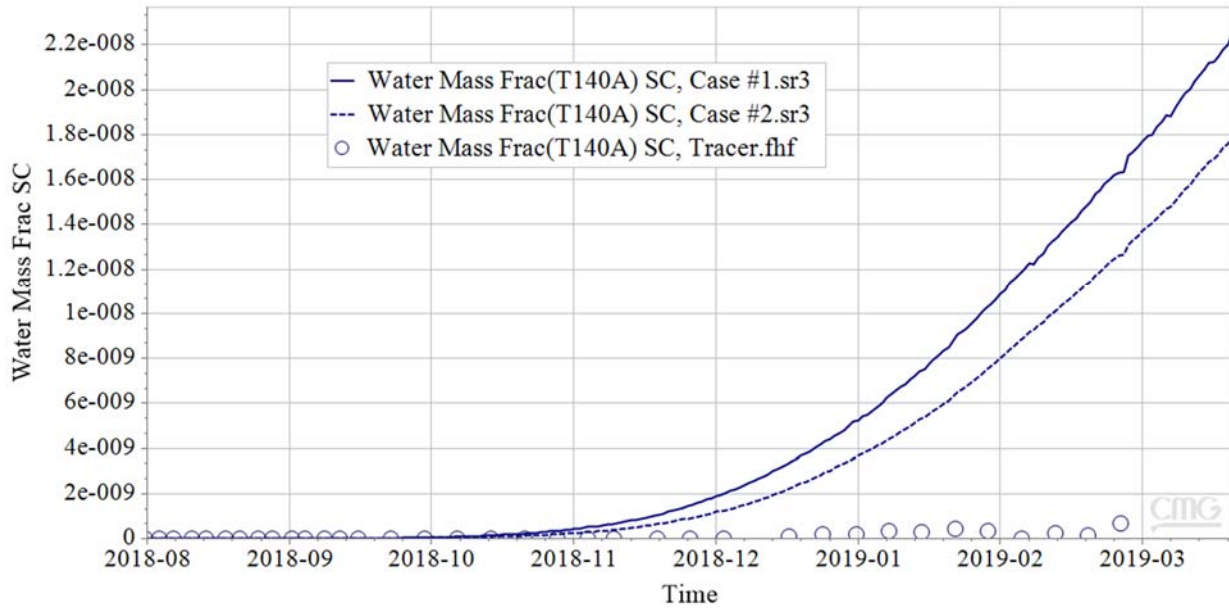


(d) Oil production rate of producer J28

Figure 4.8: History matching results of (a) water cut (b) oil production rate for producer J27 and (c) water cut (d) oil production rate for producer J28

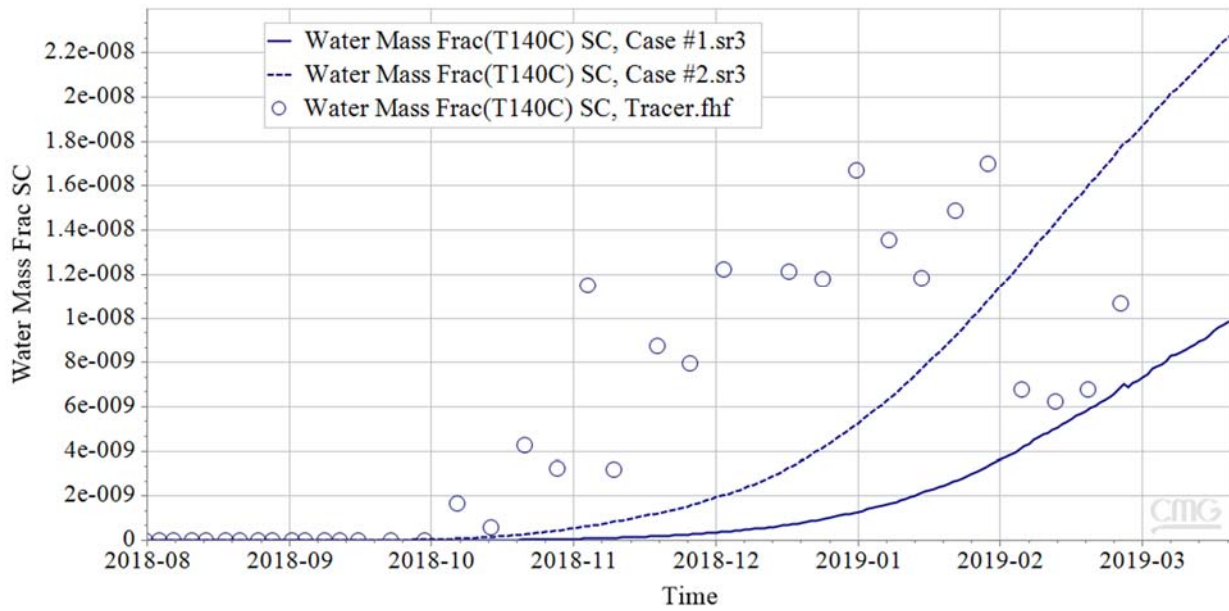
The history matching results of tracer concentration in producer J27 and J28 are presented in **Figure 4.9**. It can be seen that the simulated T140A concentration in producer J27 of these two case studies differ vastly from the observed data. However, the results of T140C concentration in two production wells are improved by history matching the cumulative oil production. Compared to matching the oil production rate, a better simulation result of tracer concentration can be obtained by matching the cumulative oil production.

Water Mass Frac SC - J27

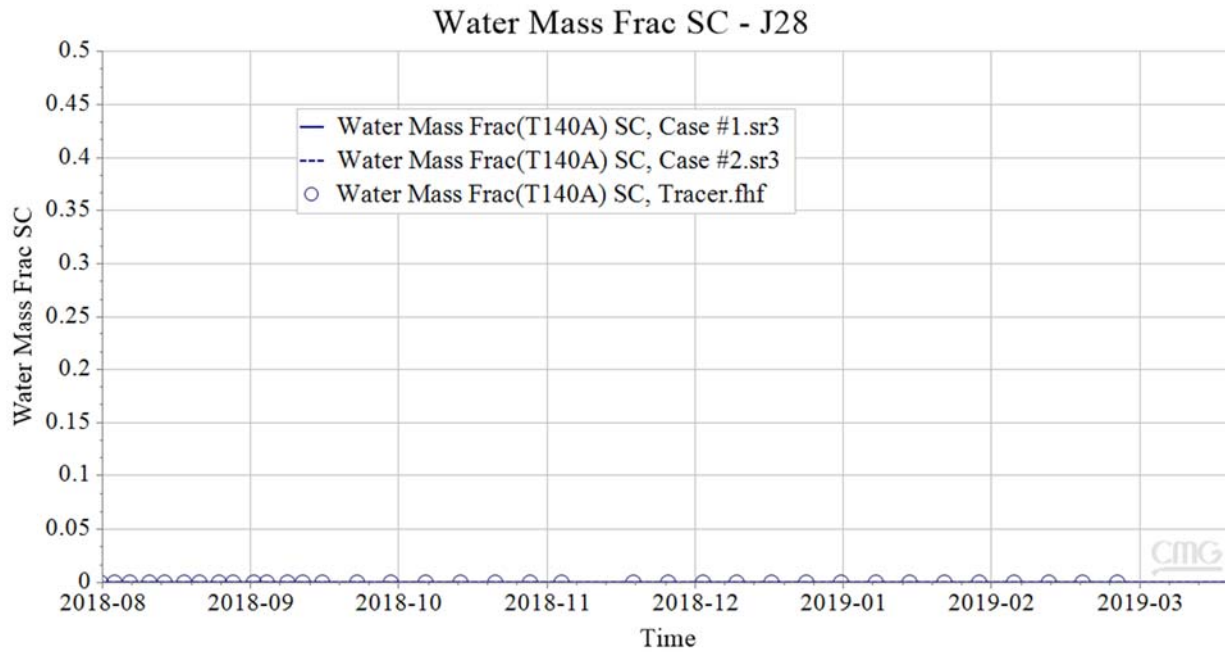


(a) History matching results of T140A in producer J27

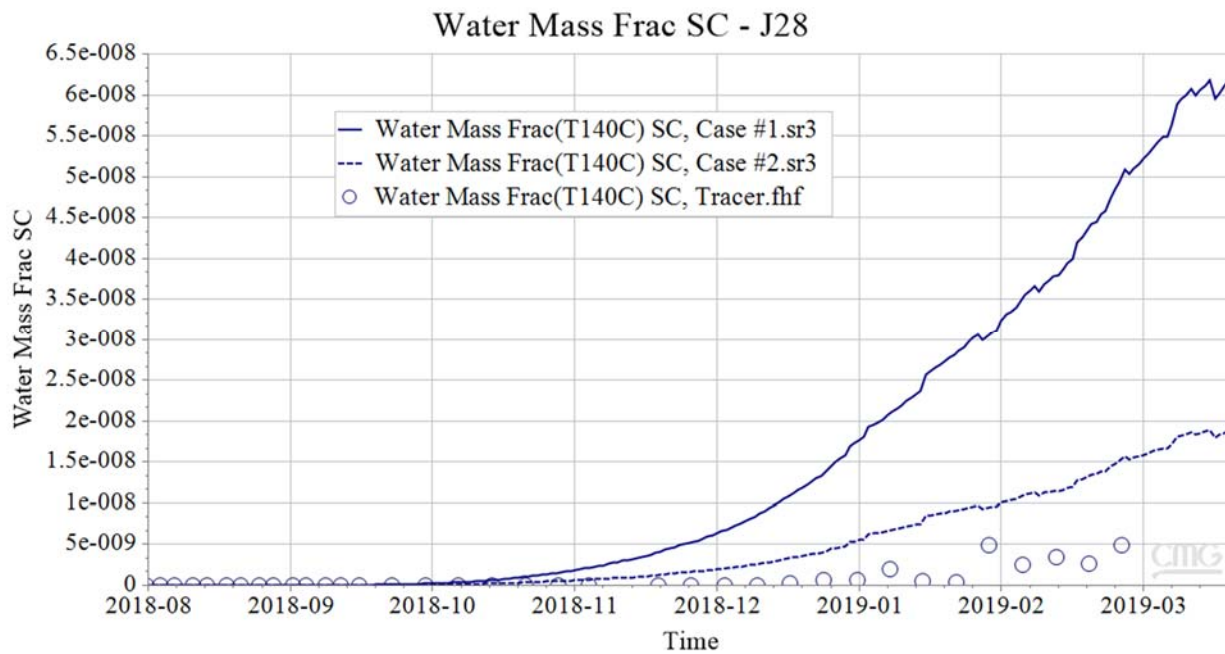
Water Mass Frac SC - J27



(b) History matching results of T140C in producer J27



(c) History matching results of T140A in producer J28



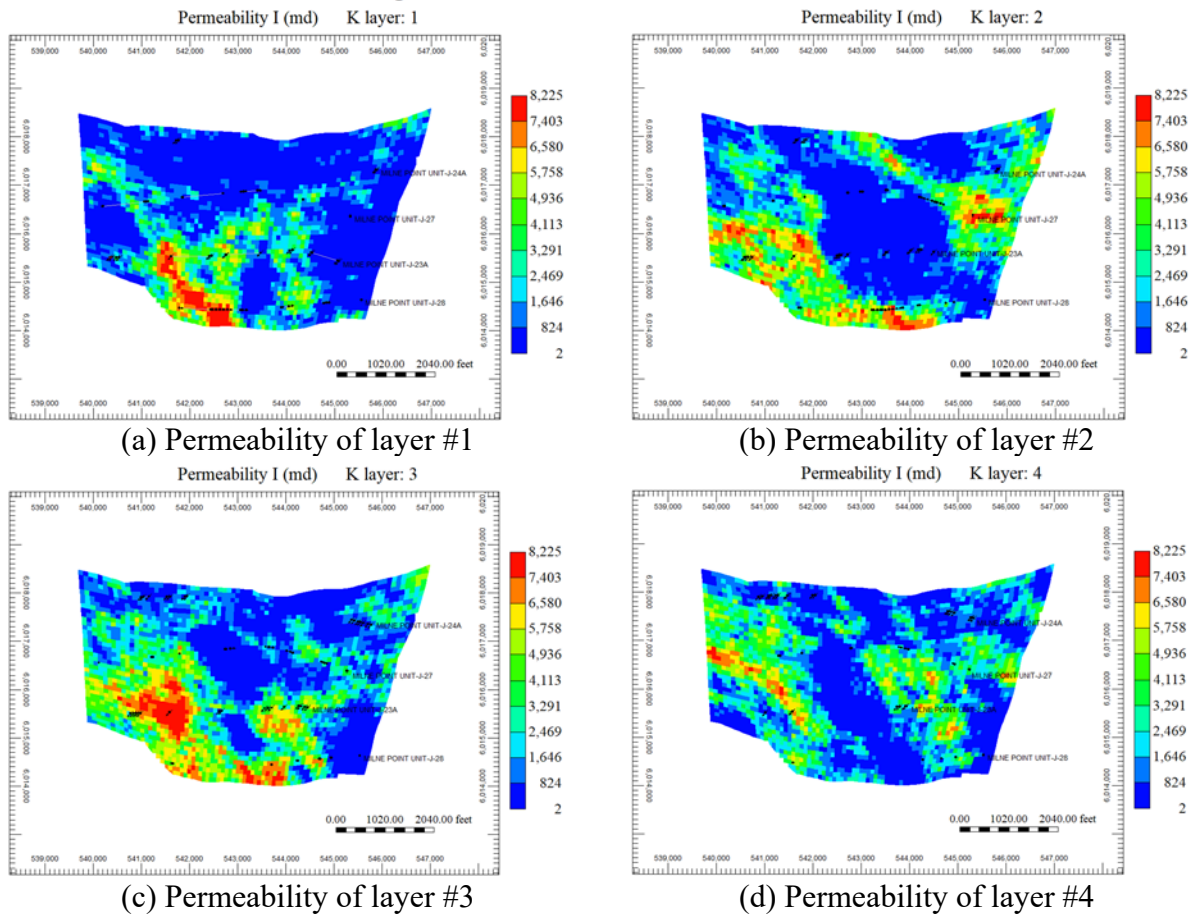
(d) History matching results of T140C in producer J28

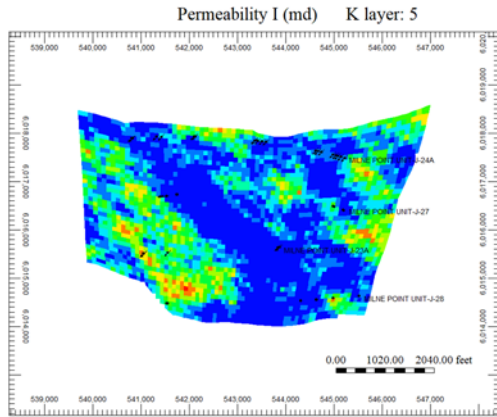
Figure 4.9: History matching results of (a) T140A concentration (b) T140C concentration in producer J27 and (c) T140A concentration (d) T140C concentration in producer J28

New reservoir simulation model

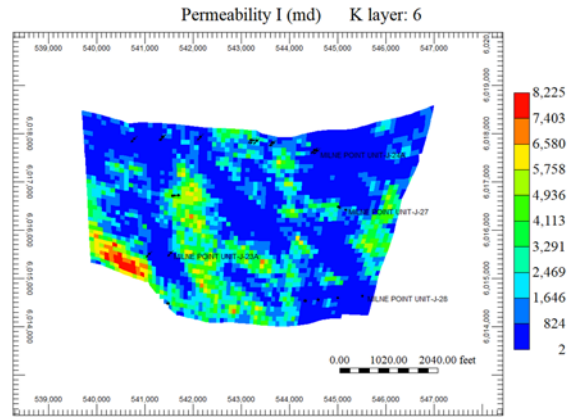
During the tracer data history matching process, the block type permeability field between injector J23A and producer J27 is subdivided to the stripe type permeability field. In this way we try to obtain more accurate permeability field, which can reflect the reservoir heterogeneity, by tuning the blocks/stripes permeability. The history matching results show that tuning the blocks/stripes permeability cannot generate representative heterogeneous reservoir simulation model, which has the same production response trend as the actual production data.

Permeability and porosity. Hilcorp geologists have developed a static reservoir model based on core data and well log interpretation. Porosity and permeability distributions have been generated using a geostatistical model as shown in **Figure 4.10** and **4.11**.

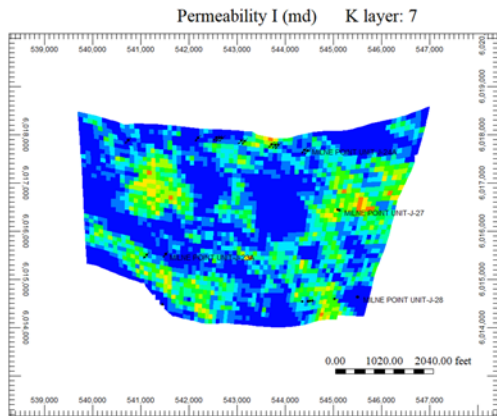




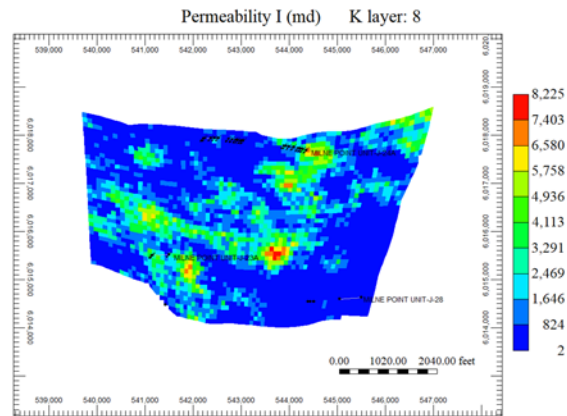
(e) Permeability of layer #5



(f) Permeability of layer #6

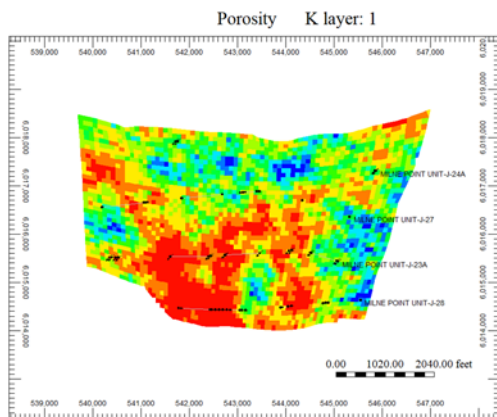


(g) Permeability of layer #7

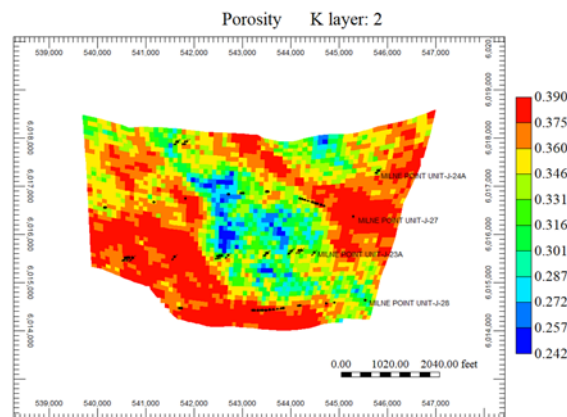


(h) Permeability of layer #8

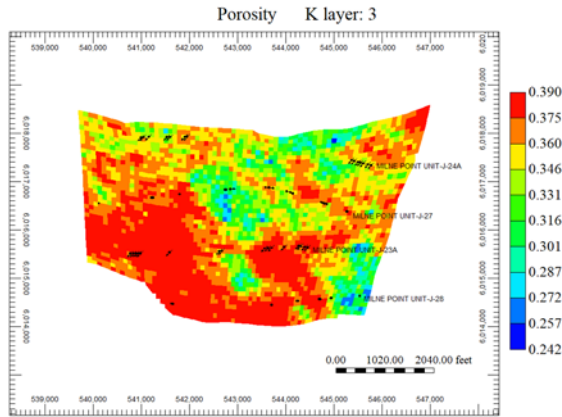
Figure 4.10: Permeability distribution of (a) layer #1, (b) layer #2, (c) layer #3, (d) layer #4, (e) layer #5, (f) layer #6, (g) layer #7 and (h) layer #8 in the reservoir simulation model



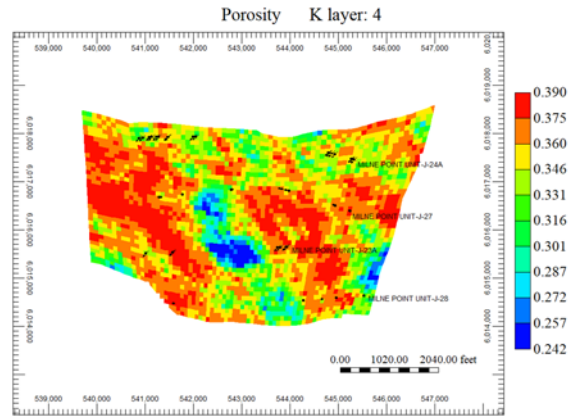
(a) Porosity of layer #1



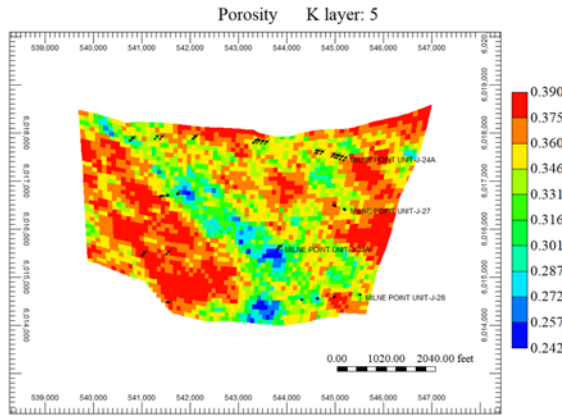
(b) Porosity of layer #2



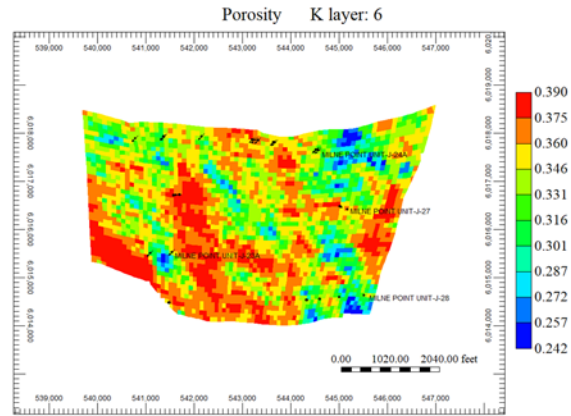
(c) Porosity of layer #3



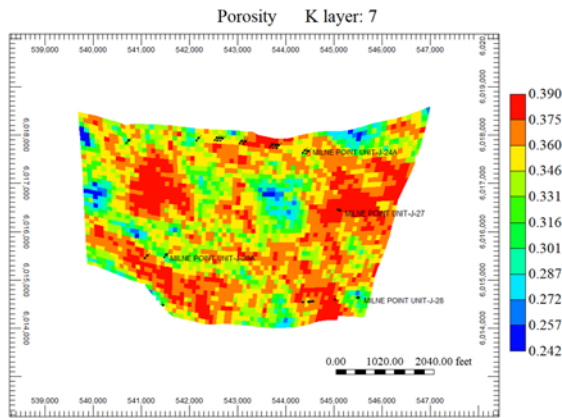
(d) Porosity of layer #4



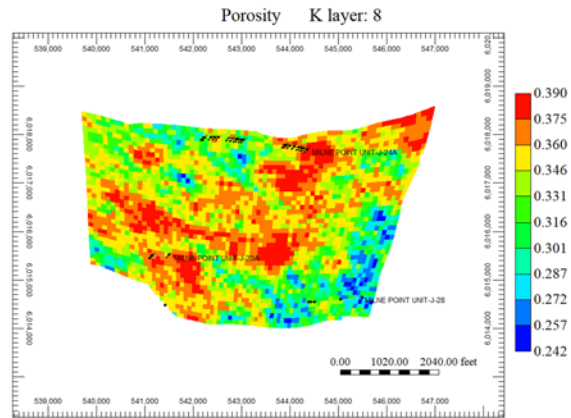
(e) Porosity of layer #5



(f) Porosity of layer #6



(g) Porosity of layer #7



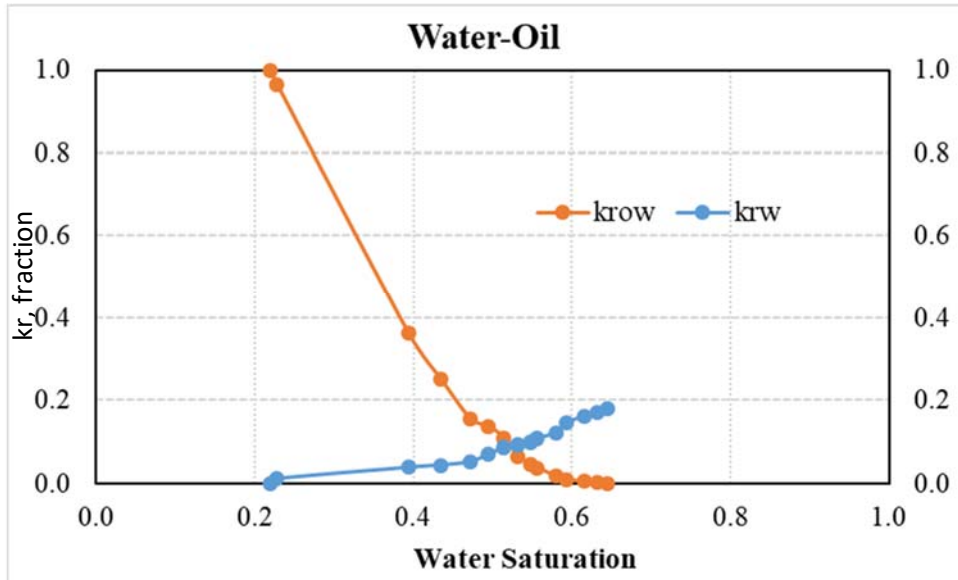
(h) Porosity of layer #8

Figure 4.11: Porosity distribution of (a) layer #1, (b) layer #2, (c) layer #3, (d) layer #4, (e) layer #5, (f) layer #6, (g) layer #7 and (h) layer #8 in the reservoir simulation model

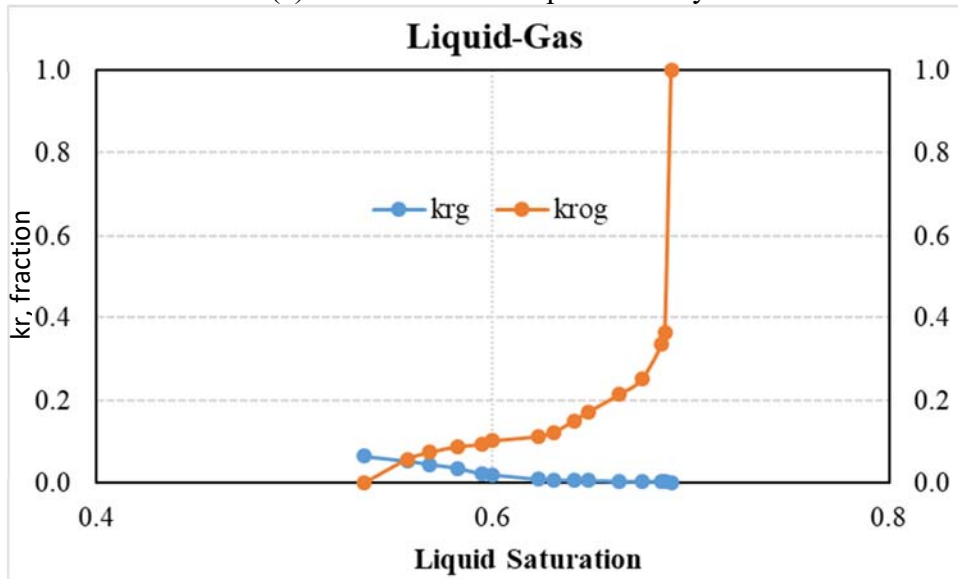
Relative permeability. The relative permeability data are sourced from the NB sand at 4186.6 ft (water-oil relative permeability) and 4184.9 ft (gas-oil relative permeability). The curves are shown in **Figure**

4.12.

In the following reservoir simulation process, the relative permeability curves are fixed while the permeability of each grid in the reservoir simulation model is the only parameter that needs to be tuned.



(a) Oil/water relative permeability



(b) Gas/oil relative permeability

Figure 4.12: The relative permeability curves of (a) oil/water and (b) gas/oil

UAF's future work will focus on building the reservoir simulation model in IMEX and comparing the simulation results obtained from STARS and IMEX. The permeability of each grid will be tuned to history

matching the cumulative oil production and water cut. Then sensitivity analysis will be conducted using the updated reservoir simulation model.

Both UND and UAF activities are ongoing.

- Task 5.0 - Implementation of Polymer Flood Field Pilot in Milne Point

Polymer has been injected continuously since startup on August 28th 2018 except 2 short shutdowns due to necessary equipment modifications and repairs in September and November 2018 respectively, and more recently a much prolonged disruption due to polymer hydration issues which will be discussed below. However, after 2 months of hard work by the Milne Point team assisted by SNF staff, the polymer hydration problem has been resolved and normal polymer injection has been resumed since August 29th, 2019. Ultimately as a team we have learned a lot about polymers, polymer facilities and onsite QC required.

Polymer Injection Status Timeline

- 8/23 polymer skid (PSU) online with water
- 8/28 polymer injection starts
- 9/25 PSU shutdown
 - More HC gas found in source water
 - Need to modify and reclassify PSU to Class I Div. II
- 10/15 Resume polymer injection
 - Ran downhole gauge
 - Performed post polymer step rate test
- 11/9 J-23A shut in for PFO while waiting for pump repair
- 11/16 J-24A shut in for PFO while repairing augur
- 12/3 Resume polymer injection
- 1/17/19 Attempted IPROF for J-23A, but tool covered by black goo
- 3/28/19 Pumped 8 kg Tracer T-801 into J-24A
- 3/29/19 Pumped 8 kg Tracer T-803 into J-23A
- 3/29/19 Coil tubing clean out J-23A, repeat IPROF
 - Tool did not go all the way down, got partial results
 - ICD#1=5.6%, ICD#2=27.8%, ICD#3=40.7%
 - 74% polymer injecting into first segment (heel-2766')
- 6/7/19-6/14/19 J-28 false polymer positive by flocculation test
- 6/19/19 shut down PSU due to polymer hydration issues
- 6/22/19 PSU back online, J-23A rate decreased by 400 bpd, J-24A by 200 bpd
- 7/6/19 J-23A PFO test, no damage identified
- 7/8/19 Treat injectors with hot KCL water to remove damage – not effective
- 7/15/19 J-23A and J-24A step rate test
- 7/18-8/28/19 straight water or low concentration polymer while diagnosing
- 8/29/19 polymer hydration problems resolved, resume polymer injection
- 9/2/19 J-23A and J-24A step rate test

Polymer Hydration Problem

Starting from mid-June, Milne Point operations experienced polymer hydration problems, i.e. fish eyes were observed in mixing tanks. In addition, the units would not hold a setpoint injection viscosity, and filter ratio tests often failed. Polymer injection was interrupted to diagnose and remediate the causes. The Milne Point team assisted by SNF staff made a tremendous amount of effort examining the quality of polymer, source water, the functions of the PSU, and the polymer mixing process. The main causes have been identified as

1. Methane and fines content in the source water. Both of these elements are detrimental to proper polymer hydration and neither were considered in the mixing equipment (PSU) design.
2. The stirrers of the maturation tanks at J-pad were turned off about half of the time due to issues with the logic of the PSU program.
3. Inappropriate mixing funnel configuration leading to intermittent excessive polymer rates into the funnel.

We have made or planning to implement the following changes to the PSU:

1. Keep stirrers on 100% of the time by changing the program logic.
2. Optimize the polymer auger and polymer valve timing by changing the program logic.
3. Remove the downcomer in the water tank to effectively release the methane in the source water.
4. Change the set points of the pressure release valve (PRV) and the vacuum release valve (VRV) to further remove methane.
5. Close a slit in the PSU funnel overflow to address funnel water flow. (SNF operates their units in the USA/Canada with the slit welded closed, and elsewhere with the slit open).
6. Tuning ratio of water to funnel and funnel mix port by logic change to address funnel water flow.
7. Relocating PSV and N2 line directly to funnel to maintain positive pressure in the funnel during the entire cycle.
8. Adding filter pods to the mix water. We have passed the filter ratio (FR) test without the filter pods, but the fines seem to pop up intermittently, and we do know they affect the FR test.

These are the additional QC measures we are implementing:

1. For every lot number, test particle size distributions using sieve shaker.
2. For every lot number, test moisture content using moisture balance.
3. Every day, test wellhead injection fluid from every unit using the FR method recommended by the University of Texas. The UT method and SNF method ended up giving us closer matched results than expected. However, there is more empirical evidence that supports the UT method.
4. For the FR test, an automated system will be implemented, saving time, and adding to measurement accuracy.

Ultimately as a team we learned a lot about polymer properties, polymer facilities and onsite QC required. Here are the main lessons we learned in the process:

1. QC is more important for polymer flooding compared to standard oilfield practices.
2. Injecting poorly hydrated polymer, or bad polymer quality will have a direct impact on the reservoir.
3. Make sure polymer units can handle fines and gas in the source water and have sufficient residence time.
4. Do not rely on a single sample for unit design. The source water samples we submitted did not tell the full story in terms of methane and fines.

Polymer Injection Performance

The injectivity of J-23A and J-24A apparently decreased after a 5-day shut in mid-June. A short pressure falloff (PFO) test was performed on J-23A early July to assess the apparent formation damage. However, the PFO results did not indicate severe skin damage.

Step rate tests were also performed in early September on both injectors to assess the injectivity and fracture pressure. **Figures 5.1** and **5.2** show the step rate test results for J-23A and J-24A respectively.

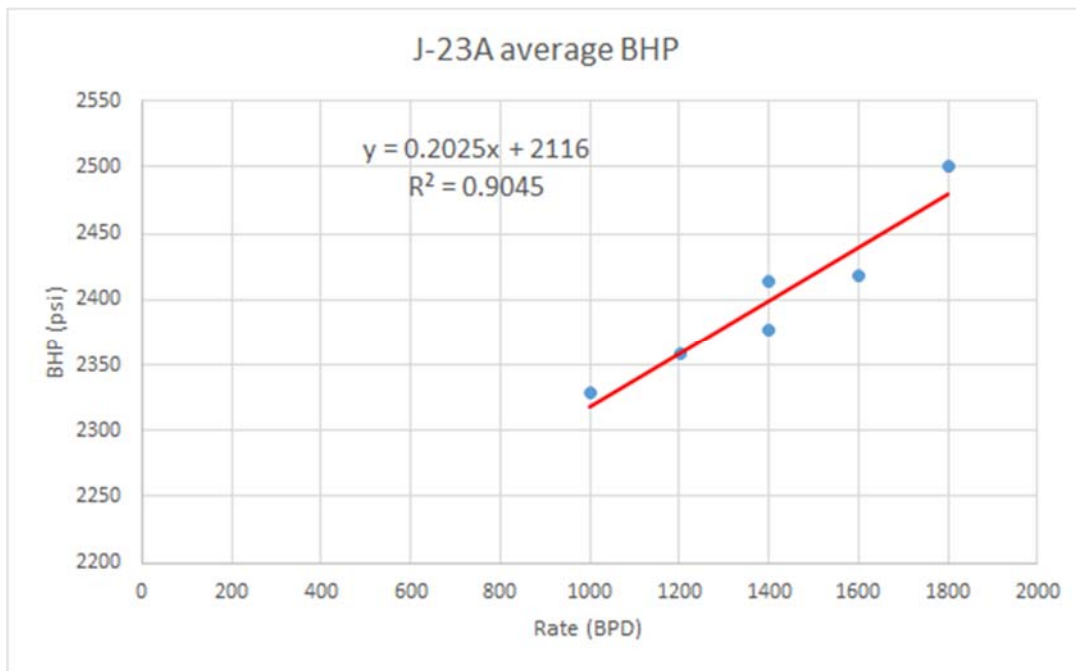


Figure 5.1: J-23A step rate test

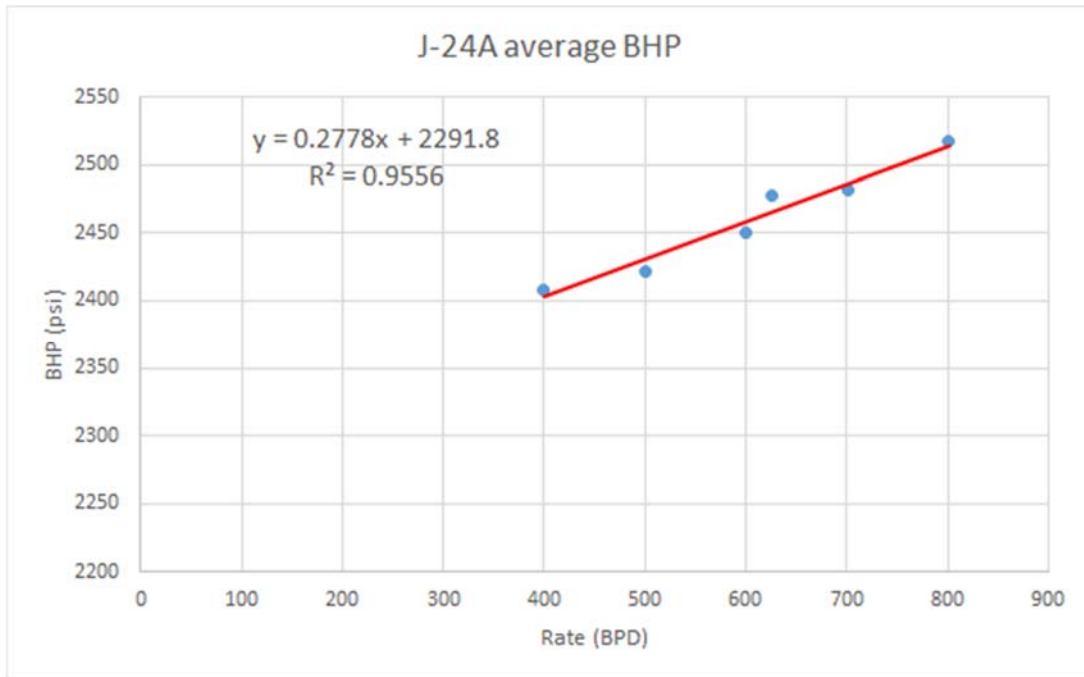


Figure 5.2: J-24A step rate test

Here are the main observations from the step rate test data:

1. All data fall on a straight line for both wells, indicating no formation break down during the test.
2. Injectivity index is fairly high in both wells (5 bpd/psi for J-23A and 3.6 for J-24A) indicating that the sand is already fractured/parted at the lowest injection rate.
3. Would need higher wellhead pressure to achieve target injection rate. This means that higher pressure limit is needed in future pump design.
4. Based on the results of the step rate test and the earlier PFO test, there seems to be no severe skin damage to the injectors. The reduced injectivity may have been caused by the high viscosity of the polymer solution which means that we just have to increase injection pressure to achieve target injection rate.
5. In the long run, we should still plan IPROFS to see how the polymer injection is distributed along the wellbore.

As of August 31, 2019, cumulative polymer injected was 288,000 lbs into J-23A and 121,000 lbs into J-24A. Polymer concentration was between 1200 to 2000 ppm to achieve a target viscosity of 45 cP as shown in **Figure 5.3**.

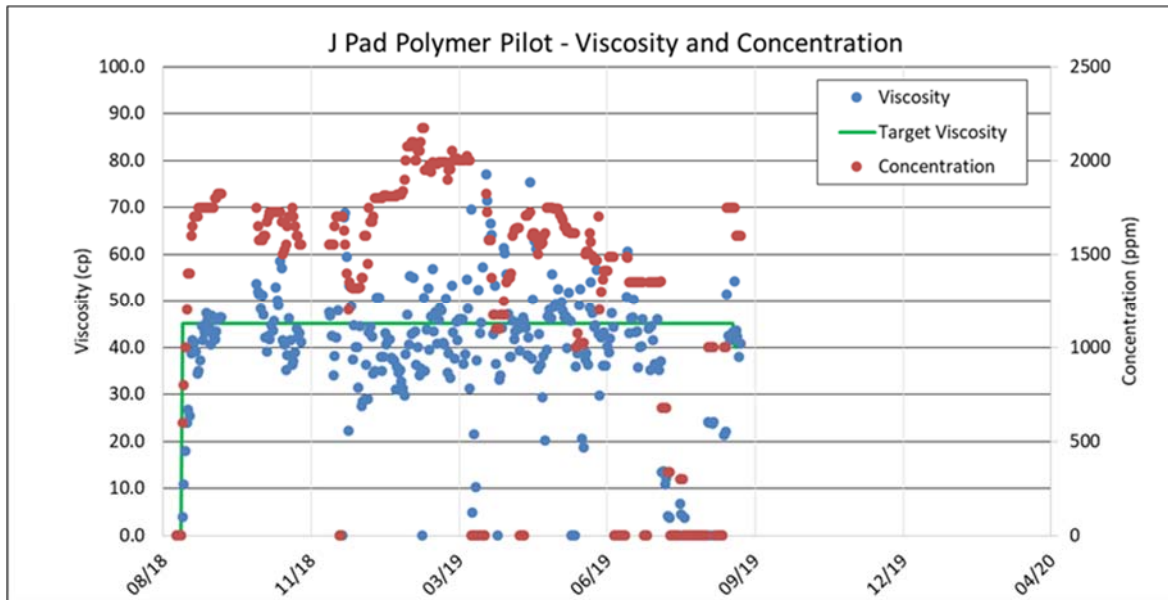


Figure 5.3: Polymer concentration and viscosity

Figure 5.4 shows daily injection rate and pressure for J-23A. The injection rate was originally kept at approximately 2200 barrels per day (bpd) while the wellhead pressure stayed at or below 500 psi for the first 4 months and then started to creep up, indicating that the injectivity was decreasing as the reservoir was filled with polymer. Maximum wellhead injection pressure was initially set at 700 psi to prevent fracturing the formation. Injection rate had to be reduced gradually since March 2019 to keep the wellhead injection pressure below 700 psi. In July 2019, we raised the maximum injection pressure to 1000 psi to achieve reasonable injection rate. Current injection pressure is approximately 980 psi and the injection rate is about 1800 bpd.

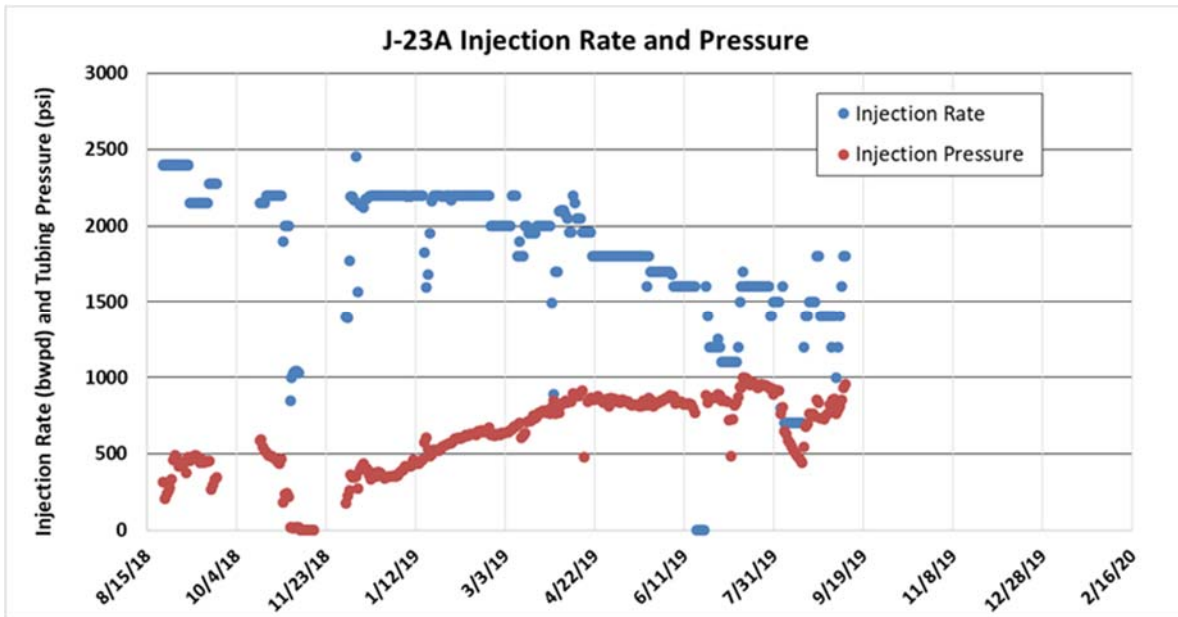


Figure 5.4: Injection rate and pressure for J-23A

Figure 5.5 shows daily injection rate and pressure for J-24A. The injection rate was originally kept at approximately 1200 barrels per day (bpd) while the wellhead pressure stayed at or below 700 psi for the first 2 months. Then the wellhead pressure started to increase and the injection rate decreased to 600-800 bpd, indicating that the injectivity was decreasing as the reservoir is filled with polymer. Current injection pressure is approximately 950 psi and the injection rate is about 650 bpd.

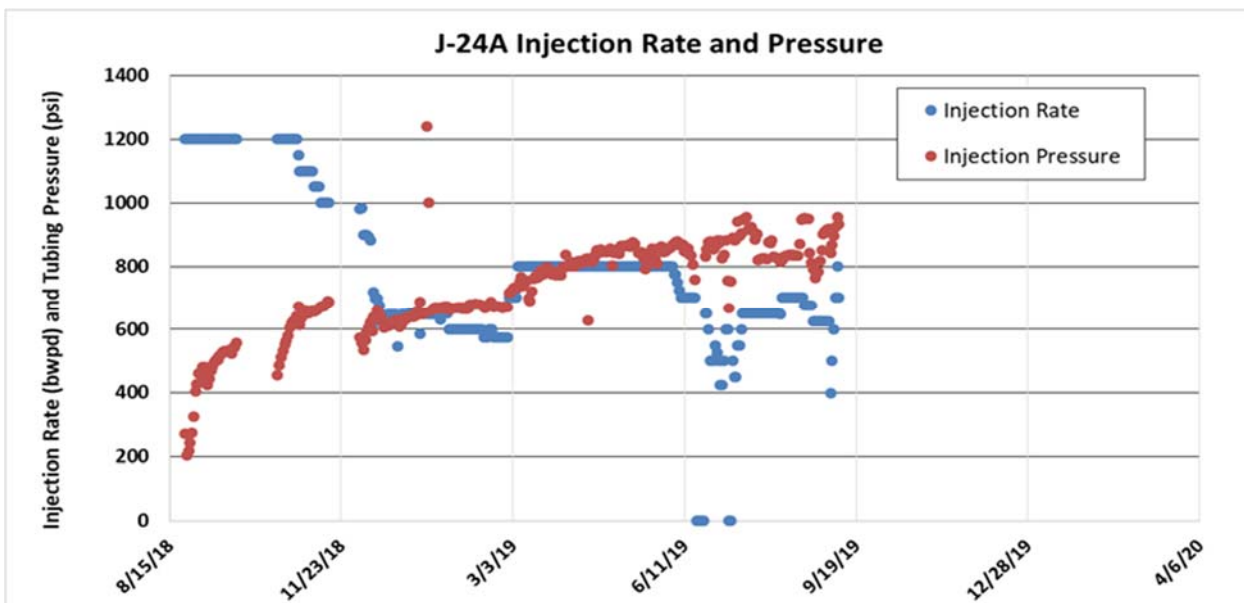


Figure 5.5: Injection rate and pressure for J-24A

Figure 5.6 is a Hall Plot for both J-23A and J-24A, which plots the integration of the differential pressure between the injector and the reservoir versus cumulative water injection. The data would form a straight line if the injectivity stays constant over time, curve up if the injectivity decreases and vice versa. **Figure 5.6** clearly shows that injectivity in both injectors has been decreasing as the reservoir is filled with polymer.

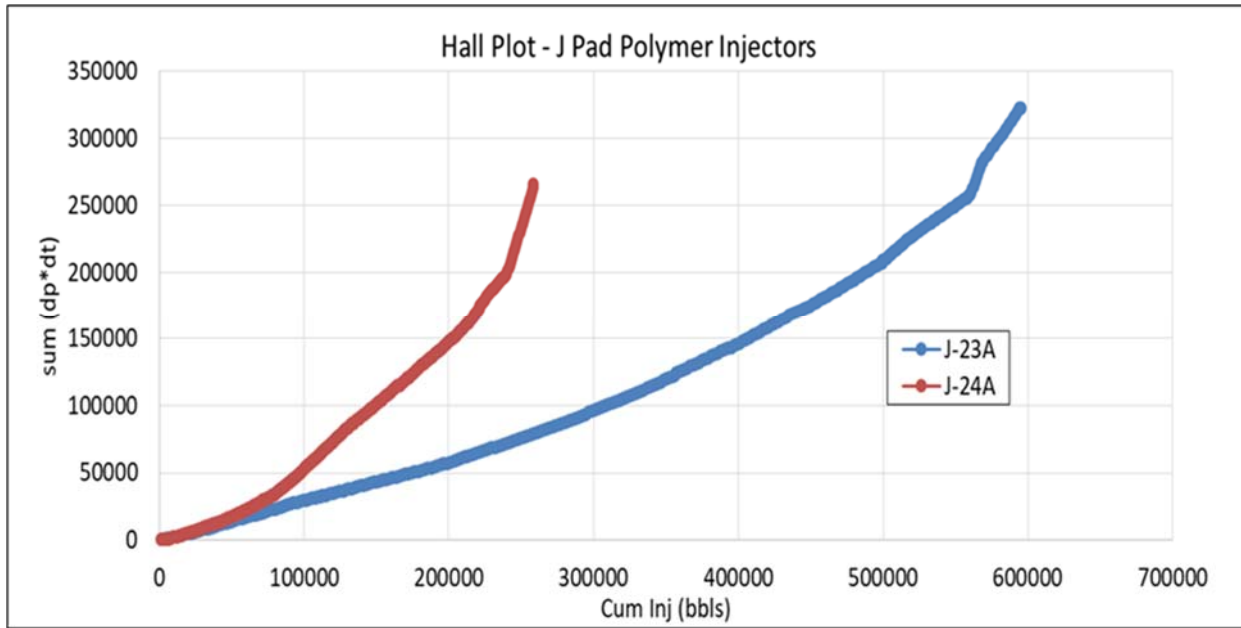


Figure 5.6: Hall plot for J-23A and J-24A

Figure 5.7 shows that the total pore volume of polymer injected is approximately 6% into J-23A and 4% into J-24A, which is considered very low since a typical polymer flood would require 0.5 to 1.0 pore volume.

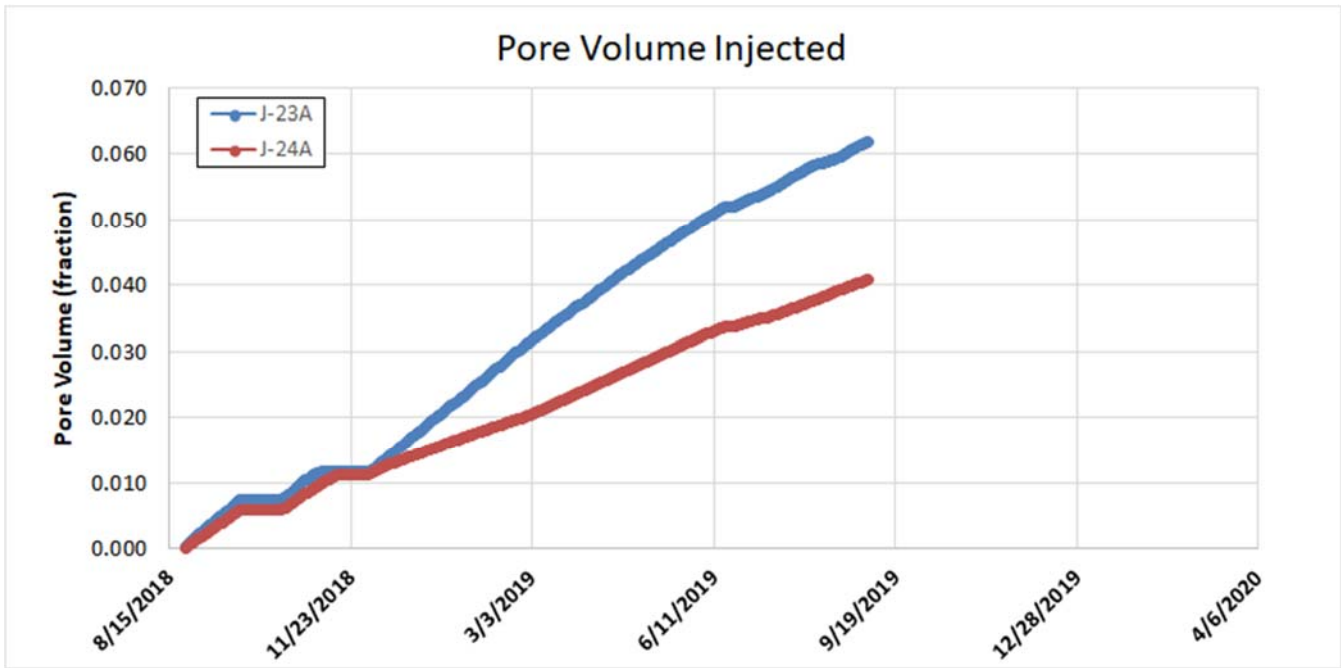


Figure 5.7: Pore volume of polymer injected

Production Performance

Figure 5.8 depicts the production performance of producer J-27 which is supported by both injectors, J-23A from the south side and J-24A from the North. Production data show that the total liquid rate has stabilized, the oil rate is increasing and the water cut has decreased from approximately 65% prior to polymer injection to about 40% one year after.

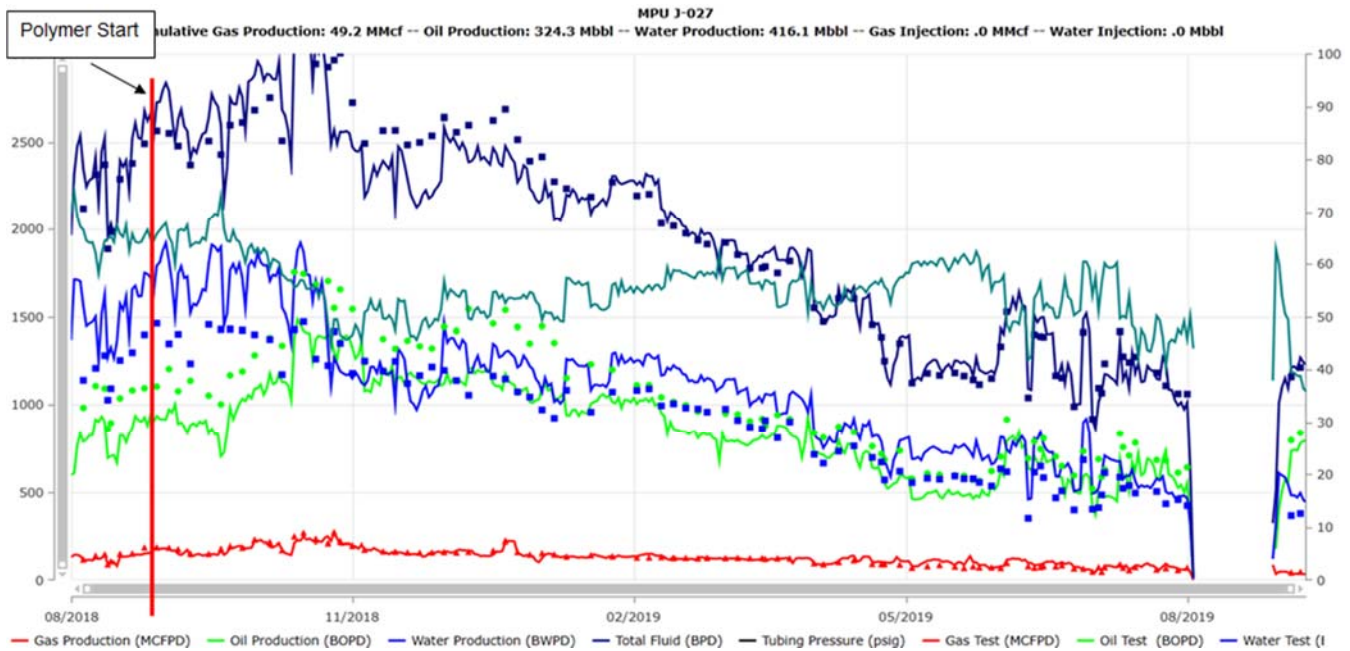


Figure 5.8: J-27 Production performance

Figure 5.9 depicts the production performance of J-28 which is supported only by J-23A from the north. The oil rate has recently increased to pre polymer level and the water cut has decreased from 70% before polymer start up to about 20% one year after.

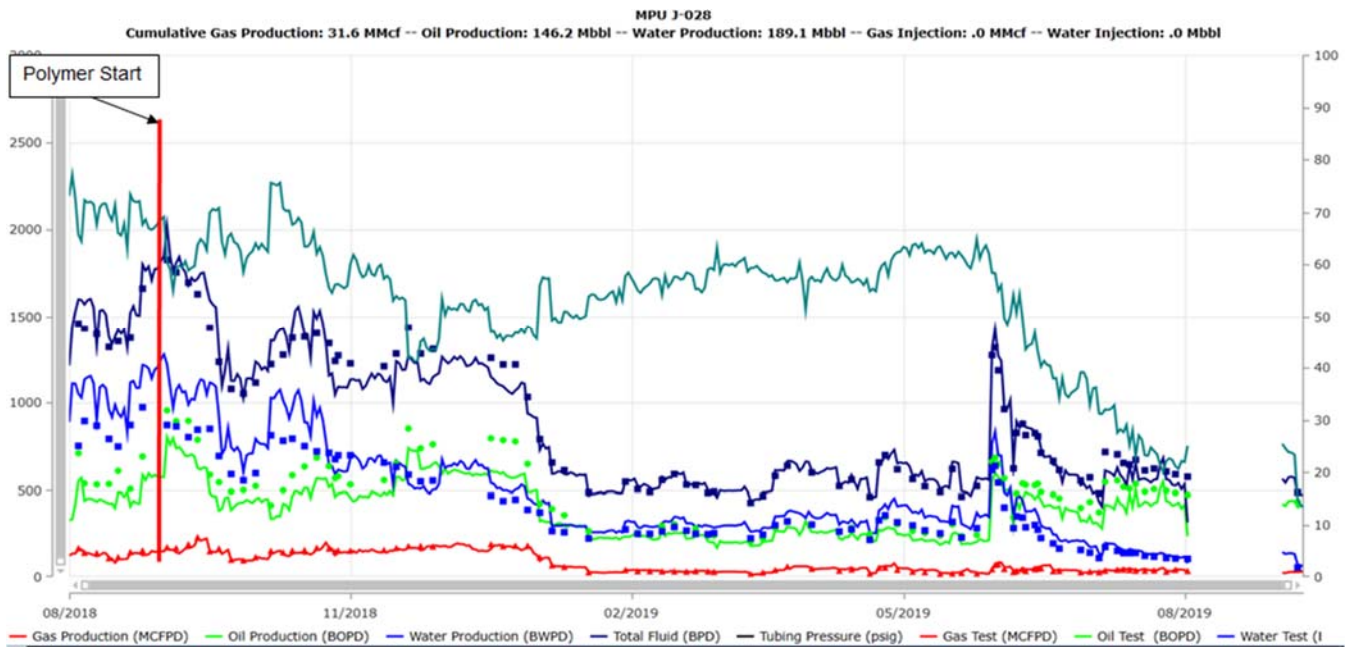


Figure 5.9: J-28 Production performance

Water/Oil Ratio versus Oil Recovery Factor

Figure 5.10 compares the actual and predicted water/oil ratio (WOR) versus oil recovery factor in the project area. The green dots are actual production data, the blue line is the predicted WOR trend for waterflooding and the red line represents the predicted WOR trend for polymer flooding by numerical simulation. As can be seen, the actual data closely follow the predicted WOR trend for polymer flooding. The fast decrease in WOR recently as well as shortly after the start of polymer injection is possibly caused by improvement in injection conformance due to high viscosity polymer plugging up high permeability channels that might have existed between the injectors and the producers but not included in the simulation model.

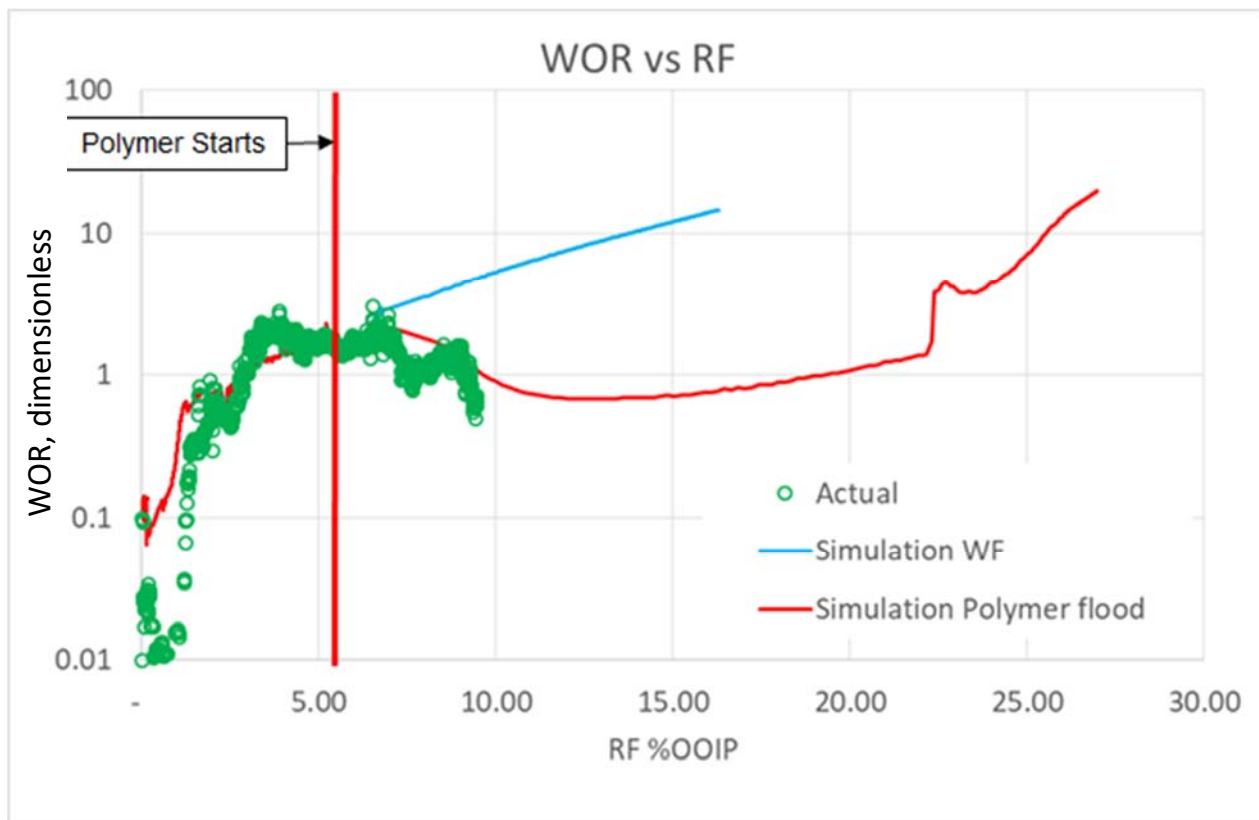


Figure 5.10: Water/Oil ratio versus oil recovery factor trend

Pre-Polymer and Post-Polymer Tracer Tests

A pre-polymer tracer test was conducted 25 days prior to the start of polymer injection to assess the waterflood breakthrough timing. Two different tracers named T-140C and T-140A were pumped into injectors J-23A and J-24A, respectively, on August 3, 2018. Produced water samples were taken weekly from producers J-27 and J-28 and analyzed in the laboratory to detect tracer concentration and the results are shown in **Figure 5.11**. Tracer T-140C was first observed in J-27, 70 days after injection and the tracer

concentration reached the first peak at 155 days indicating that communication between injector J-23A and producer J-27 was strong. The T-140C concentration from producer J-27 exhibits multiple peaks in the first 300 days after injection indicating that there might be multiple breakthrough points along the horizontal wellbore. Tracer T-140C from injector J-23A first appeared in producer J-28 103 days after injection and the concentration first peaked at 239 days and then peaked again 300 days after injection. Tracer T-140A from injector J-24A first appeared in producer J-27 140 days after injection and the concentration slowly increased to 5 parts per billion in 259 days, indicating poor communication between the well pair.

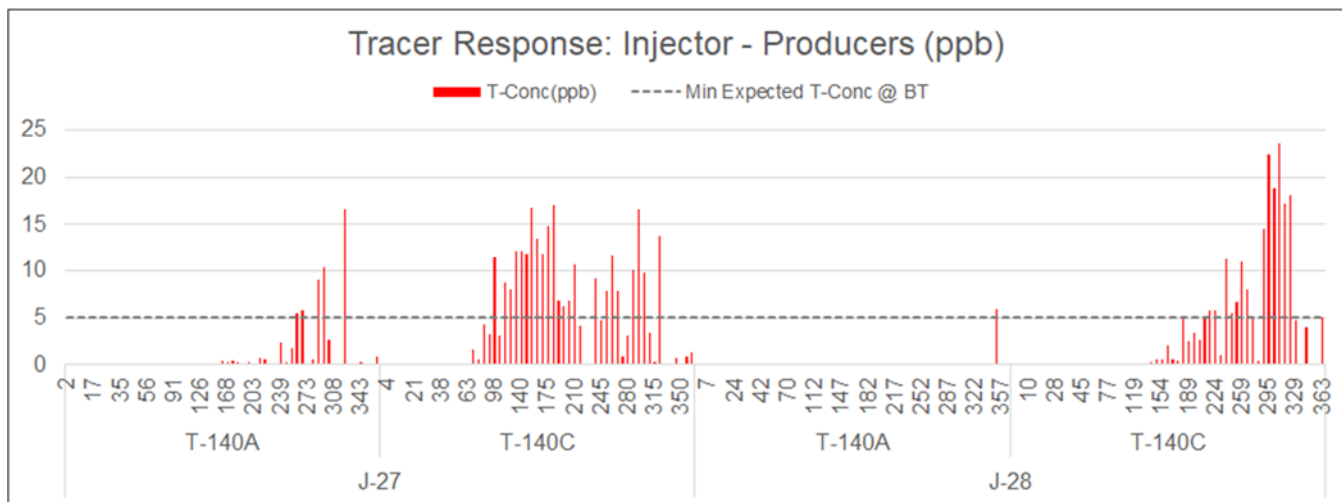


Figure 5.11: Pre-polymer tracer concentration in produced water samples

A post-polymer tracer test was also pumped 7 months after the start of polymer injection to assess the polymer breakthrough timing. Tracer T-803 was pumped into injector J-23A on March 29th, 2019 and Tracer T-801 was pumped into injector J-24A on March 28th, 2019. None of these tracers higher than 1 part per billion has yet been observed in the produced water samples 5 months after the tracers have been pumped.

Monitoring Polymer Breakthrough

Since the start of polymer injection, produced water samples have been collected weekly and analyzed onsite using the clay flocculation test, as well as in the laboratory via nitrogen-fluorescence water composition analyses to detect the presence of produced polymer in the production stream. As of the end of August 2019, 1 year after the start of polymer injection, no polymer has been confirmed by both methods although there are a few positive results recently by the clay flocculation test.

Activity is ongoing.

- Task 6.0 -Analysis of Effective Ways to Treat Produced Water that Contains Polymer

Experimental details

In the reporting quarter, oil water separation studies have continued for actual oilfield emulsions and synthetic emulsions at 50% water cut (WC) prepared in the lab. The newly received crude oil from J-28 well was in the form of emulsion with a measured water cut of 10% and was used directly for the demulsification tests which were conducted by both bottle test method and multiple scattering light method. Experiments with synthetic emulsions at 50% WC were simply carried out with bottle test method since the instability of the generated emulsion limited the application of Turbiscan. The detailed bottle test procedures have been described in previous report, thus they are not repeated here. To be noted, the un-sheared polymer solution was used in order to test the worst case condition. To prepare the compound emulsion breaker, two kinds of emulsion breaker are well premixed before adding to the emulsion.

The tested emulsion was placed into cylindrical glass cells and kept in the chamber of Turbiscan Lab analyzer (Formulation Inc., Toulouse, France) for multiple scattering light measurement which was performed at 130°F for 2 hours with 1 scan per five minutes. Turbiscan is equipped with a pulsed near infrared light source ($\lambda=880\text{nm}$) and synchronous optical detectors which determine the intensity of transmission light (T) and backscattering light (BS). The obtained curves of transmission light as a function of the height of the sample reflect the demulsification performance. The amount of water produced, the quality of the oil/water interface, the quality of the water produced and the separation kinetics can be obtained from the transmission light curves, as shown in **Figure 6.1**. The volume of produced water is directly linked to the thickness of the transmission peak obtained. The clarity of water produced can also be evaluated by assessing the transmission level of the water phase at the end of the measurement (the transmission light for deionized water is 88.1%). Interface neatness can be assessed by calculating the slope of the last transmission scan at the oil/water interface. The sharper the slope, the better the interface quality. Separation kinetics refers to the time required to complete demulsification.

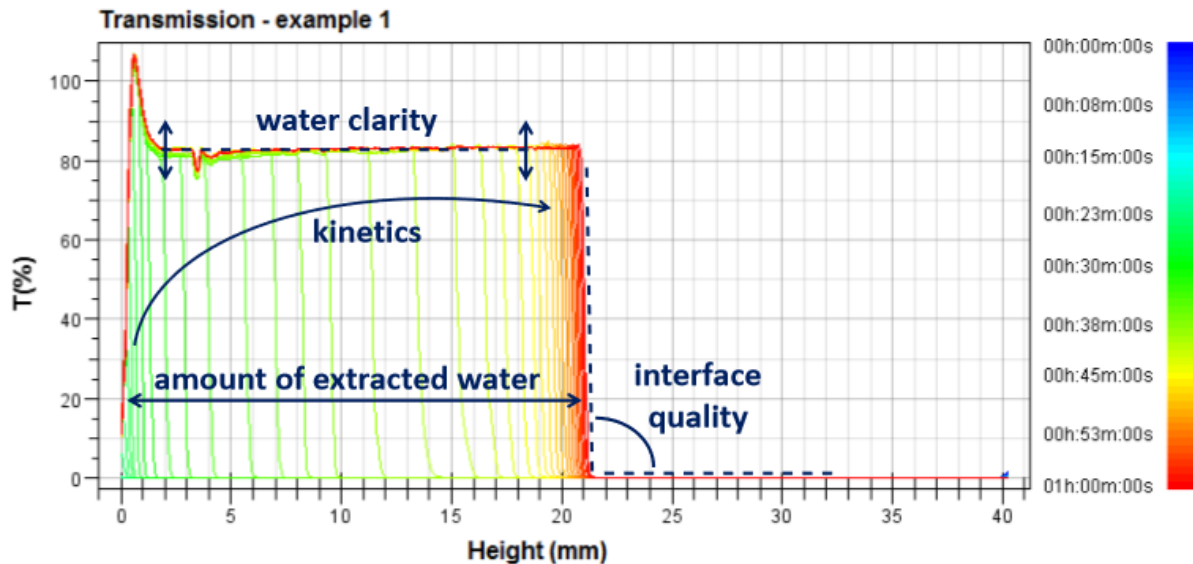


Figure 6.1: Typical transmission light profile for demulsifier.

Results and Discussion

Emulsion breaker performance on actual oilfield emulsions. The received oil sample was found to be w/o emulsion with a measured water content of 10%. This emulsified oil sample was directly used to evaluate the performance of four types of emulsion breakers (E12085A, E18276A, N1691 and R01319) both by visual observation (e.g., bottle test) and Turbiscan Lab analyzer.

Bottle test. Water separation of four emulsion breakers from the bottle test at a dosage rate of 100ppm and 1200ppm are shown in **Figure 6.2**. At 100ppm dosage, the separation efficiency (fraction) of emulsion breakers in the order from the highest to the lowest is E18276A > E12085A > R01319 > N1691. All the separated water is clear and the interface is sharp. It is just the oilfield emulsion is rather stable which takes approximately 4 days to reach the separation equilibrium. To overcome this shortage, the separation rate was significantly increased by increasing the dosage to 1200ppm, as shown in **Figure 6.2b**. The separation efficiency of four emulsion breakers at 1200ppm was in the same order. However, the separated water quality qualified by the color of the separated water is remarkably different. The separated water color for E12085A, E18276A, N1691 and R01319 is described as dark yellow, light yellow, dark, and clear, respectively. Taking all the factors into account, E18276A is considered as the most appropriate emulsion breaker.

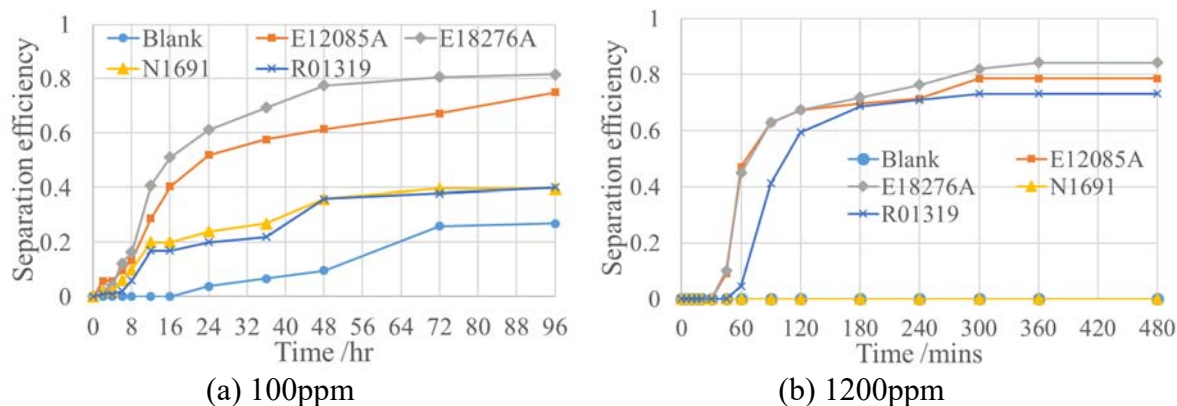


Figure 6.2: The performance of four emulsion breakers for oilfield emulsion.

Turbiscan Lab analysis. The same experiment was also conducted with Turbiscan Lab, which is faster, more accurate and objective, to confirm the demulsification performance of four emulsion breakers. Comparing with the bottle test method, the separated water volume, the quality of the oil/water interface, the water quality and the separation kinetics can be quantified by analyzing the transmission light profiles which are presented in **Figure 6.3**. Three oil-soluble demulsifiers (E12085A, E18276A and R01319) perform better than the water-soluble demulsifier N1691 which barely works as indicated by the little transmission variation. For the three oil-soluble emulsion breakers, the four parameters mentioned above are compared in the radar chart shown in **Figure 6.4**. Consistent with the bottle test results, E18276A is the most applicable emulsion breaker for the oilfield emulsion.

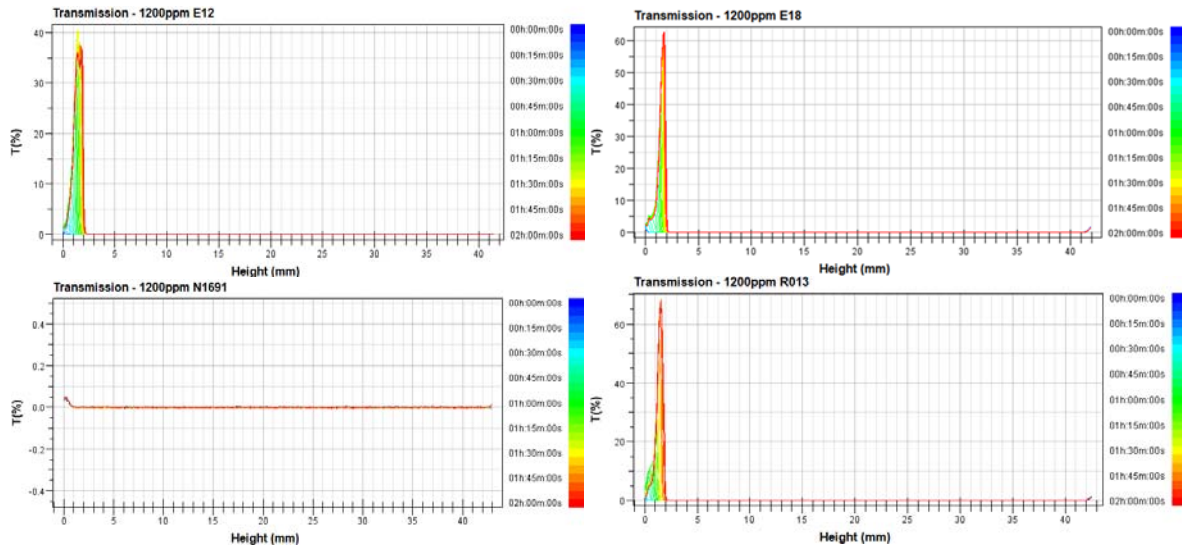


Figure 6.3: The transmission light intensity of the oilfield emulsion with four demulsifiers

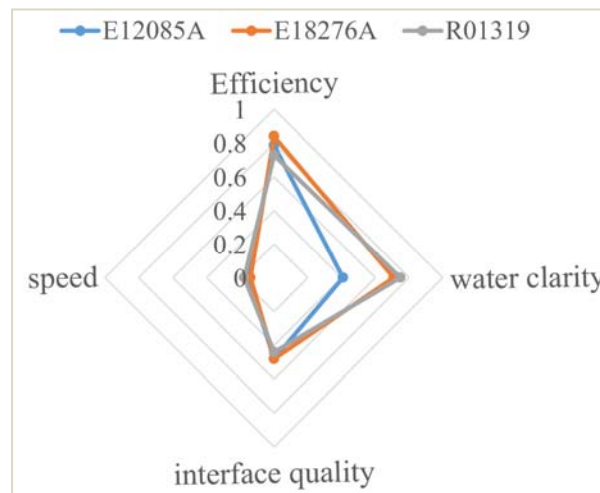


Figure 6.4: Demulsification performance comparison for three oil-soluble demulsifiers

The effect of polymer on separation behaviors of synthetic emulsions. For the emulsion prepared at 50% WC, the task to investigate the influence of polymer was challenging because the emulsion was subjected to heterogeneous transferring due to the immediate free water separation. To continue this unfinished task, the emulsion was prepared in small quantity (50mL) and fully transferred to the test tubes. Besides, the water separation was observed in seconds to capture the early separation.

The water separation as a function of time is shown in **Figure 6.5** at varying polymer concentration. Without polymer, the emulsion rapidly separated into two layers which contain w/o emulsion on the top and o/w emulsion at the bottom. The decreasing slope of the separation curve reflects the separation rate of the emulsion decreased with increasing polymer concentration, which could be attributed to the increased viscosity of the continuous phase. To be clear, polymer drastically impedes the water separation

at the short residence time. Take 5mins for example, the water separation efficiency is decreased from 97% to 55% as polymer concentration increased to 800ppm. Whereas, there is not much difference in separation efficiency as the residence time extends to 30mins, implying extending settlement time is one potential method to minimize the stabilization effect of polymer. To be noted, the separation efficiency in the presence of polymer is slightly above that of the emulsion without polymer. It could be due to the massive amount of oil droplets in the separated water which could pose great challenge to water treatment process. The oil content in the separated water (OIW) measured after 24hrs is displayed in **Figure 6.6**. The OIW value increases with increasing polymer and the OIW in the presence of polymer is two to six times higher than the environmental specification which is 50ppm. Furthermore, seen from **Figure 6.7**, the polymer contributes to the formation of the middle layer and the middle layer thickness slightly increases with the residence time, resulting in the difficulty of further water treatment.

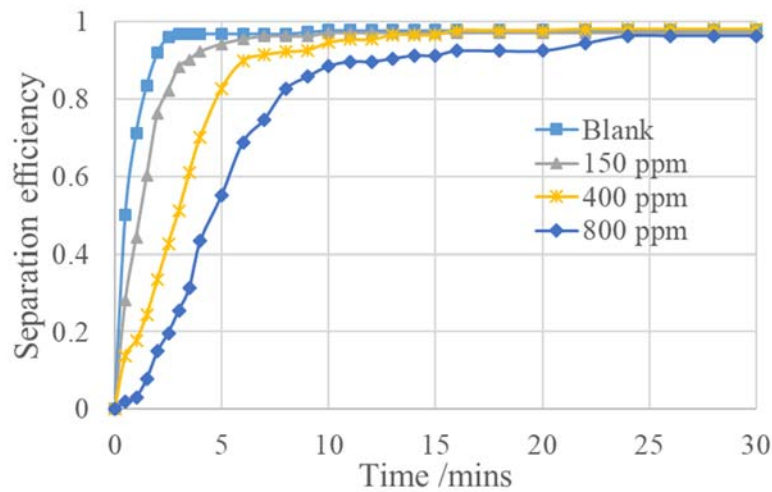


Figure 6.5: The effect of polymer on emulsion stability at 50% WC

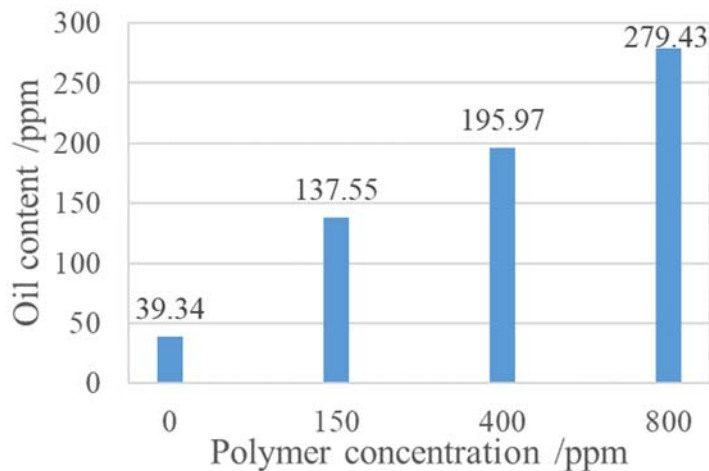


Figure 6.6: The oil content in the separated water at varying polymer concentration

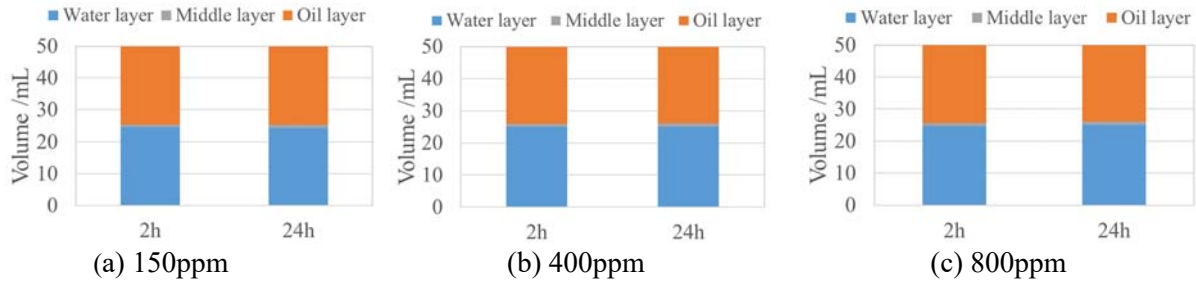


Figure 6.7: Volume of phases in the presence of polymer

Emulsion breaker performance for synthetic emulsions without polymer. The performance of four types of emulsion breaker and multiple compound emulsion breakers at different dosage rate are investigated by bottle test method.

Performance of individual emulsion breaker. The performance of four demulsifiers with a dosage of 100ppm for emulsions without polymer at 50% WC is shown in **Figure 6.8**. It is found all four emulsion breakers could produce a satisfactory water phase with OIW lower than 50ppm. In spite of the water quality, water-soluble emulsion breaker N1691 exhibited the highest separation efficiency, which makes N1691 the best emulsion breaker in this case. In comparison with the separation of blank sample shown in **Figure 6.5**, the addition of three oil-soluble emulsion breakers inhibits the water separation severely since the oil-soluble EBs tend to convert the unstable water continuous emulsion into stable oil continuous emulsion. However, this unfavorable condition is improved by increasing the residence time. As shown in **Figure 6.9**, the separation efficiency of two oil-soluble emulsion breakers E12085A and E18276A is higher than that of N1691 at 4 hours.

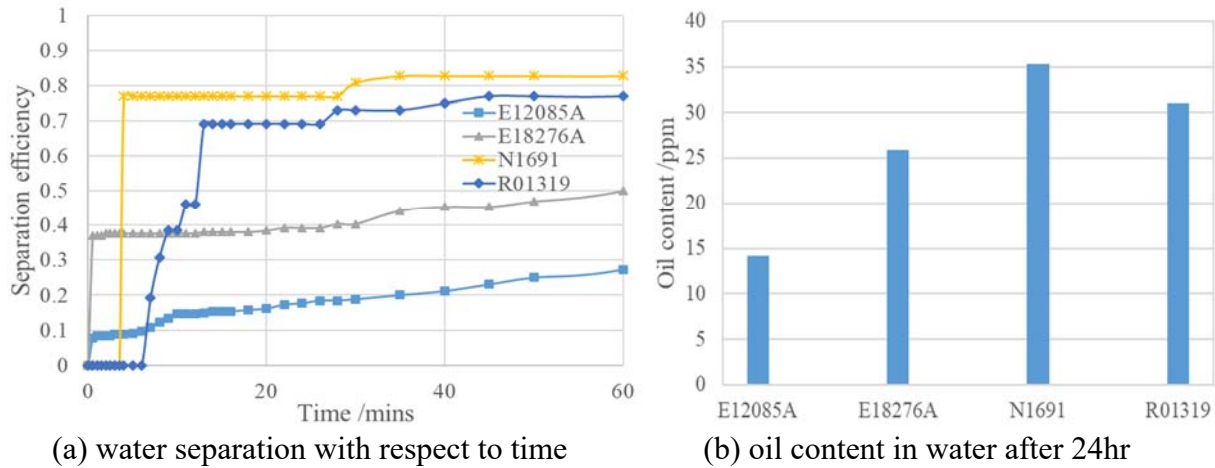


Figure 6.8: The performance of four demulsifiers for emulsions without polymer at 50% WC

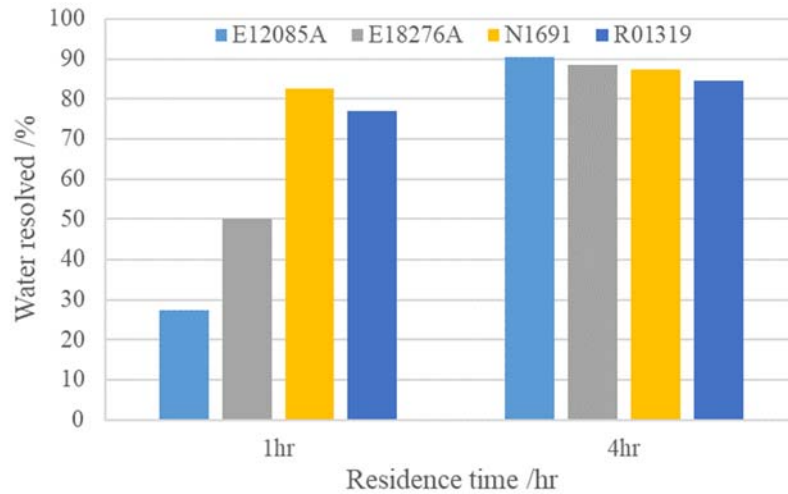


Figure 6.9: The performance of four demulsifiers at different residence time

The performance of individual emulsion breaker at different dosage rate. Increasing the emulsion breaker dosage is one typical way to improve the separation and the optimized dosage is of great importance for the field application due to the side effects of over-dosage, such as decreased separation efficiency, poor water quality, massive oil adhesion and so on. Three oil-soluble emulsion breakers are selected because of their low separation efficiency at short residence time. **Figure 6.10** shows the performance of E12085A at different dosage. The increasing dosage contributes to a remarkable increase of the separation rate to ensure a higher separation at a shorter residence time. And the OIW values at all three concentrations are below 50ppm even though the OIW value is increasing as the concentration increases. Similarly, **Figure 6.11** presents the performance of E18276A at different dosage. The increasing dosage could also effectively increase the separation rate and the optimized dosage for E18276A is suggested to be 300ppm to achieve high separation efficiency and low OIW. **Figure 6.12** shows increasing dosage of R01319 can slightly increase the separation efficiency and drastically reduce the OIW. However, the minor improvement on separation rate and the blunt interface caused by massive oil adhesion could limit its application in oilfield.

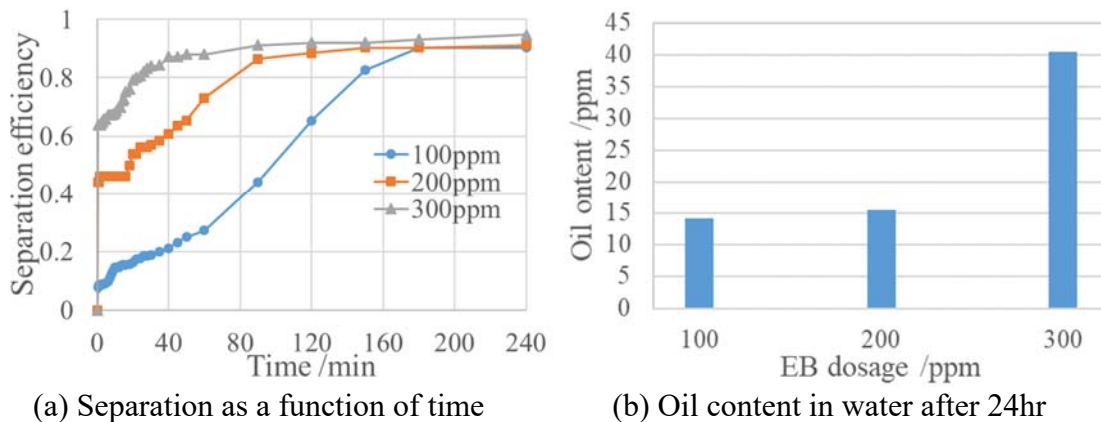
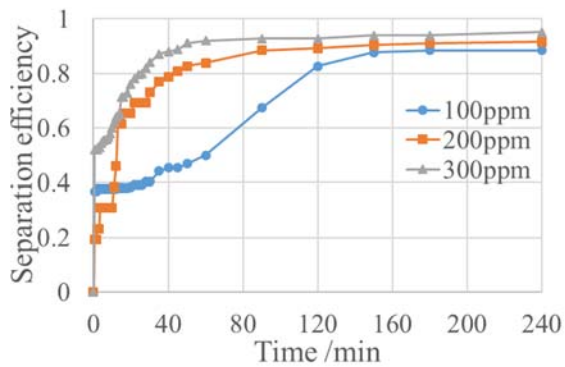
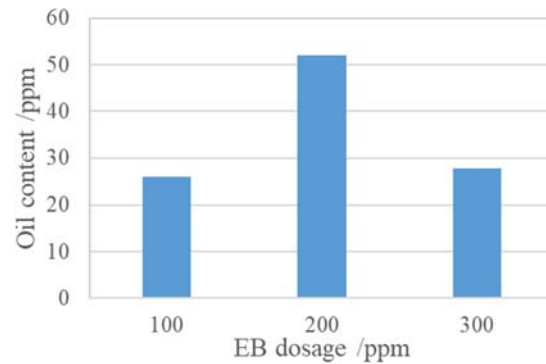


Figure 6.10: The effect of dosage on the performance of E12085A

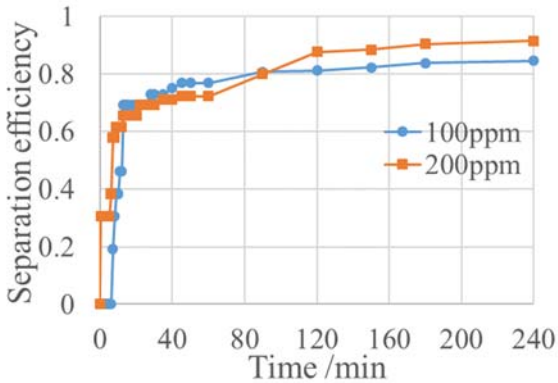


(a) Separation as a function of time

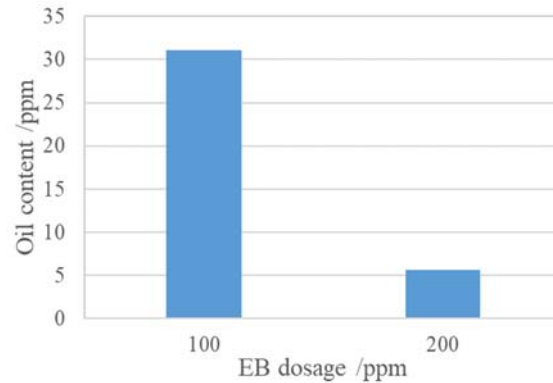


(b) Oil content in water after 24hr

Figure 6.11: The effect of dosage on the performance of E18276A



(a) Separation as a function of time



(b) Oil content in water after 24hr

Figure 6.12: The effect of dosage on the performance of R01319

Performance of compound emulsion breaker. Multiple compound emulsion breakers are proposed and evaluated to find the best combination which can make use of the advantage of individual emulsion breakers to a maximum extent. Based on the analysis for each individual emulsion breaker, E12085A produces the best water quality and the highest separation efficiency if the residence time is long enough; E18276A has the best performance for w/o emulsion; N1691 is capable to resolve the emulsion at 50% WC at a relatively low dosage; R01319 has good ability to break the emulsion with polymer which will be mentioned in the next part. Thus, the compound emulsion breakers E12+N16, E12+R13 and E12+E18 are proposed and their performance at 100ppm is demonstrated in **Figure 6.13**. E12+E18 is the most promising compound emulsion breaker which can achieve a fast and efficient separation. Comparing with E12, E12+N16 can also increase the separation efficiency from 65% to 80% at 2hrs and yield a clearer water phase. The combination of E12+R13 is undesired because it lowers the final separation efficiency.

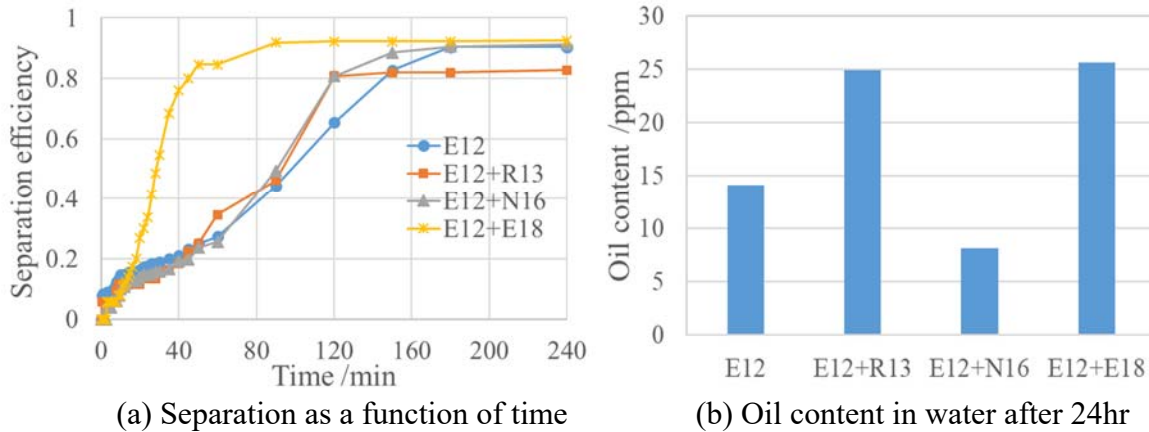


Figure 6.13: The performance of compound emulsion breaker for emulsions at 50% WC

Performance of compound emulsion breaker at different dosage rate. For the same reason, the efficiency of compound emulsion breaker E12+E18 and E12+N16 is also measured at different dosage. The results are shown in **Figure 6.14** and **Figure 6.15** respectively. For E12+E18, the separation efficiency is slightly declined as the dosage increases to 200ppm even though the separated water phase becomes clearer, which makes 100ppm the optimized dosage. For E12+N16, the increasing dosage does improve the final separation efficiency and the separated water quality. However, slow separation rate is a concern.

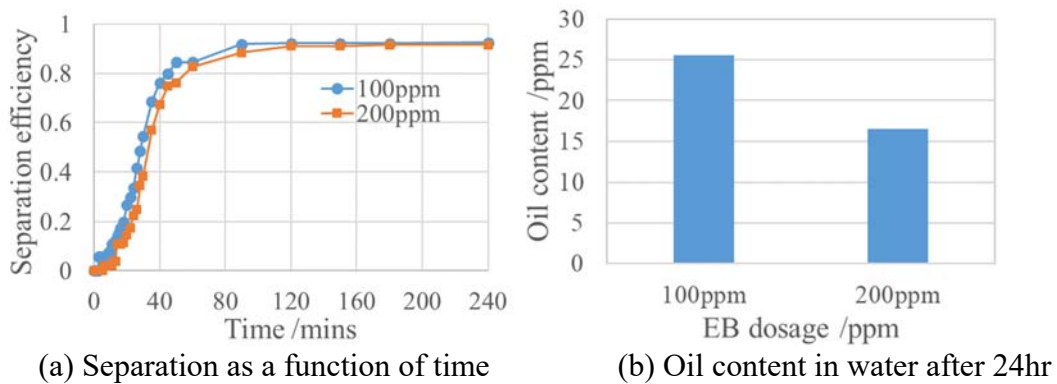


Figure 6.14: The performance of E12+E18 at two different dosages

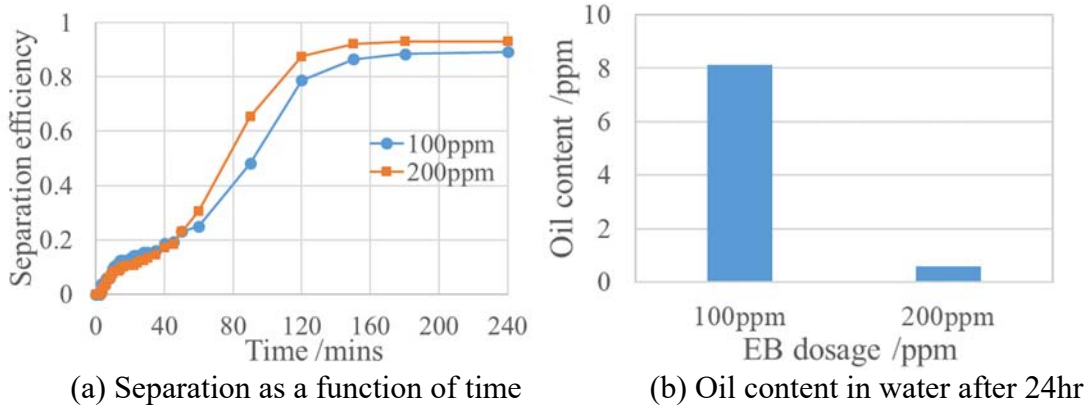


Figure 6.15: The performance of E12+N16 at two different dosages

In order to conduct a comprehensive analysis, the performance of all the qualified emulsion breakers for emulsion at 50% WC without polymer were compared in terms of separation efficiency, water clarity, separation speed and dosage, as shown in **Figure 6.16**. Those four parameters are defined as follows:

$$Efficiency = \frac{V_s}{V_t} \quad (6.1)$$

$$Water\ clarity = \frac{C_a - C_m}{C_a} \quad (6.2)$$

$$Separation\ speed = \frac{T_m - T_e}{T_m} \quad (6.3)$$

$$Dosage = \frac{C_{max} - C}{C_{max}} \quad (6.4)$$

Where, V_s is the separated water volume at 4 hrs;

V_t is the total water volume;

C_a is the allowed oil content in water, typically it is 50ppm;

C_m is the measured oil content in water after 24 hrs;

T_m is the measurement time for separation.;

T_e is the time required to reach the separation equilibrium;

C_{max} is the maximum dosage of emulsion breaker used in the experiment;

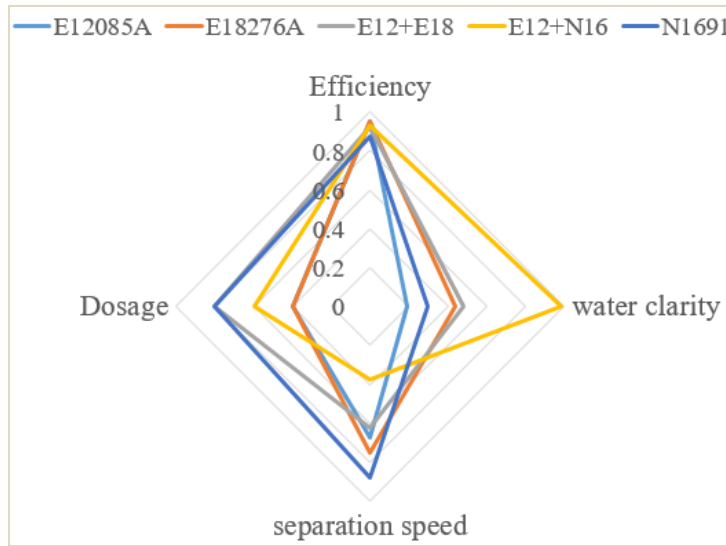
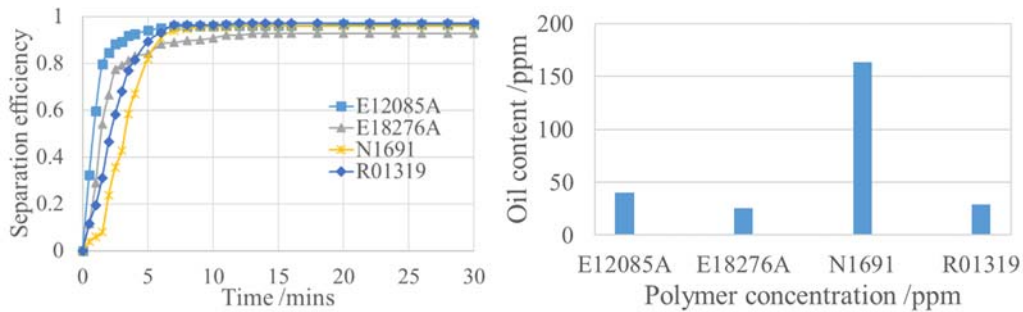


Figure 6.16: Performance comparison for all qualified demulsifiers

As seen from **Figure 6.16**, the three most efficient emulsion breakers for emulsion without polymer at 50% WC are E12+N16, N1691 and E12+E18, respectively.

Emulsion breaker performance for synthetic emulsion with polymer. Considering the effect of polymer on the separation behavior of emulsion at 50% WC, the qualified emulsion breaker should be able to boost the separation speed, eliminate the middle layer and recover the oil droplets from the separated water as much as possible. The performance of four individual emulsion breakers is evaluated to select the best emulsion breaker for emulsions with polymer at 50% WC. The effect of polymer concentration on the selected best emulsion breaker is also investigated. Moreover, the suitability of two compound emulsion breakers mentioned above for the emulsion with polymer is also tested.

Performance of individual emulsion breaker. The performance of emulsion breaker at a dosage of 50ppm for the emulsion with 800ppm polymer, which is the most stable emulsion at 50% WC, is shown in **Figure 6.17**. Generally speaking, the addition of emulsion breaker can reduce the oil content and shorten the residence time from 25mins to 7mins. The difference is three oil-soluble emulsion breakers can achieve a separation efficiency of over 93% and an OIW lower than 50ppm while water-soluble emulsion breaker yields an unsatisfactory OIW of 160ppm which surpasses the environmental regulation limit. To clarify, the separation efficiency of three oil-soluble emulsion breakers in the order from highest to lowest is R01319 > E12085A > E18276A and the separation speed in a decreasing order is E12085A > R01319 > E18276A. Based on the analysis, R01319 and E12085 are highly competent for emulsions with polymer.

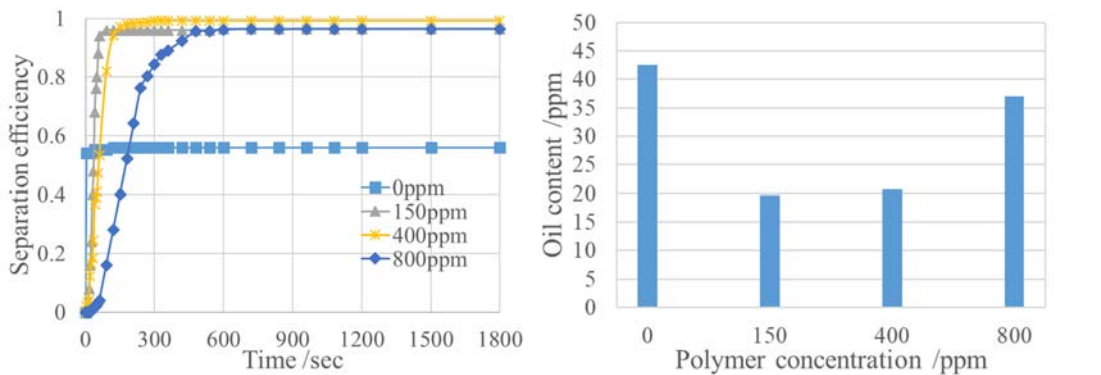


(a) Separation as a function of time

(b) Oil content in water after 24hrs

Figure 6.17: The performance of four emulsion breakers at presence of 800ppm polymer

The effect of polymer concentration on emulsion breaker performance. In this study, R01319 is selected and its performance at different polymer concentration is shown in **Figure 6.18**. As can be seen, with presence of emulsion breaker, the emulsion without polymer has the lowest separation efficiency and the addition of polymer favors the separation, which means the treatment of emulsion without polymer is challenging for the application of R01319. It is because at the absence of polymer, R01319 tends to convert the unstable water continuous emulsion into stable oil continuous emulsion as mentioned above and the presence of polymer prevents this conversion during the demulsification process. This difficulty necessitates further investigation of a more suitable emulsion breaker.

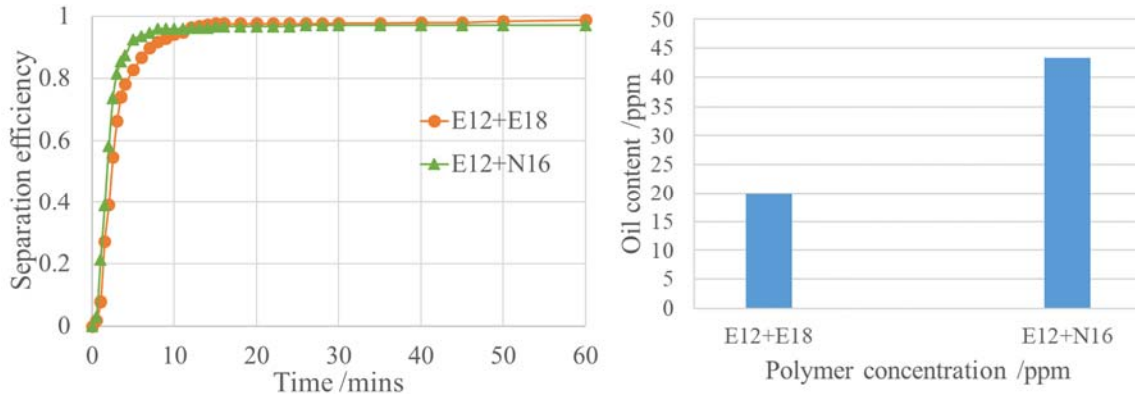


(a) Separation as a function of time

(b) Oil content in water after 24hrs

Figure 6.18: The performance of R01319 at varying polymer concentration

Performance of compound emulsion breaker. The compound emulsion breaker which works efficiently for emulsion without polymer (e.g. E12+E18 and E12+N16) is also applied to the emulsion with polymer to check their compatibility. E12+E18 performs better than E12+N16 in terms of separation efficiency and water quality as shown in **Figure 6.19**. Similarly, by applying the same method, the performance of compound emulsion breaker is also compared with that of individual emulsion breaker as seen in **Figure 6.20**. Conclusion can be easily drawn that E12+E18 is the most satisfactory emulsion breaker that can be employed for emulsions with polymer and without polymer at 50% WC.



(a) Separation as a function of time (b) Oil content in water after 24hrs
Figure 6.19: The performance of compound emulsion breaker at 800ppm polymer

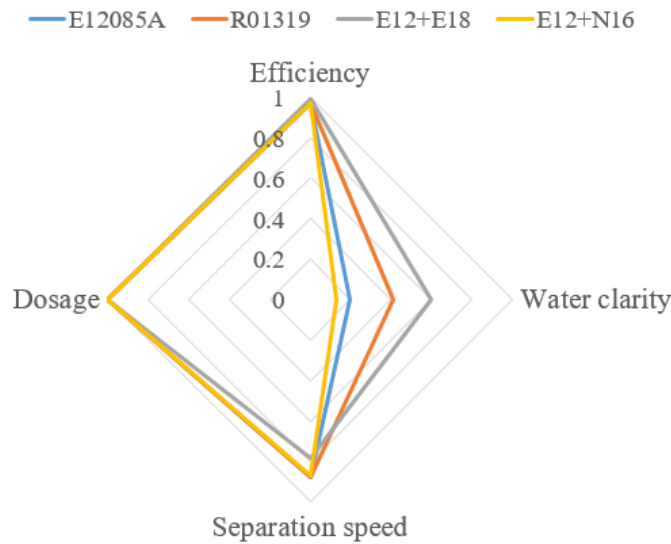


Figure 6.20: Performance comparison for all qualified demulsifiers at presence of polymer

Future Work

This will focus on studying the separation behavior of emulsion in the presence of un-sheared polymer at 20% WC, as well as the evaluation of performance of emulsion breakers (especially compound emulsion breaker E12+E18).

- Task 6.0a –Polymer Fouling of Heater Tubes

Experimental details

In the reporting quarter, fouling experiments on copper tubes heated by circulating hot oil inside them, were carried out at different temperatures – 165 °F, 250 °F, 350 °F and polymer concentrations – 160ppm, 400ppm, 800ppm to see their influence on scaling and fouling on tubes, other tube materials – Stainless Steel was also investigated for fouling to see the effect of different materials. The procedure involved

heating produced water and produced water with polymer from 77°F to 122°F. The increase in weight of tubes was noted to measure amount of deposit formed. This was done 5 times with a fresh batch of solution in each run and the time to heat the solution was recorded to get the decrease in heating efficiency of the tubes. Scanning Electron Microscopy (SEM) were carried out to observe the morphology difference between deposits formed with and without polymer. For SEM the deposit was directly scraped off the surface of the tubes. Pictures were taken at 400 and 3000 magnifications.

Results and Discussion

The effect of polymer. The amount of deposit formed in a particular amount of time increased as the concentration increased from 0ppm to 800ppm. The deposit on the surface of tubes when polymer was present can be seen to be sticking more to the surface than the deposit without the polymer as it can be seen in **Figure 6.21**. The deposit without polymer falls off easily and this could mean the calcium forms a complex with polymer as suggested in literature.

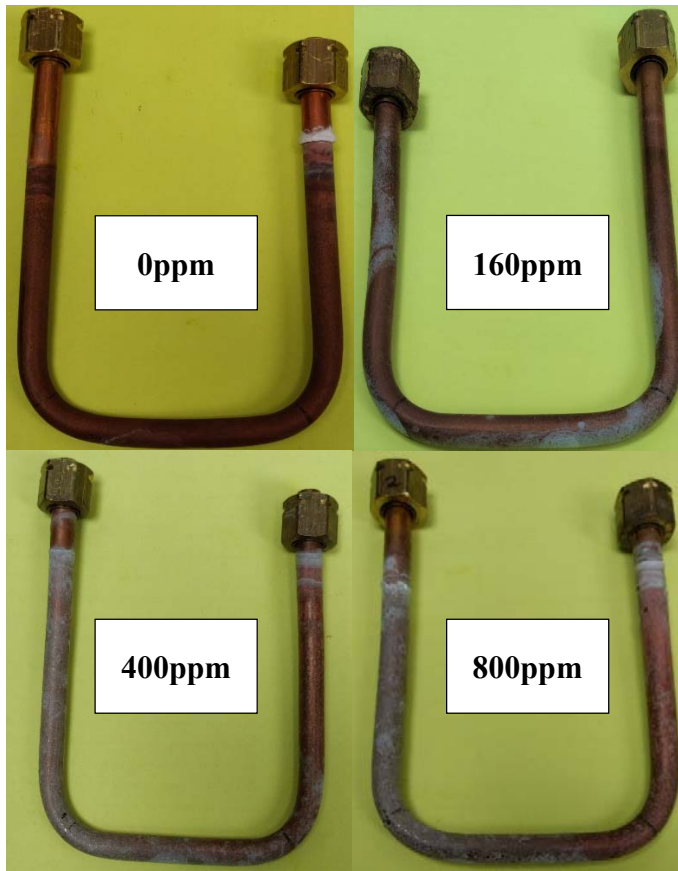


Figure 6.21: Copper tubes after experiment at 350 °F

The effect of temperature. At a fixed polymer concentration, increasing the temperature from 165 °F to

350 °F increased the amount of deposit formed in a particular amount of time as it can be seen in **Table 6.1**. The deposit rates given consider the deposit at the end of each runs and the amount of deposit formed in that run, then an average of those 5 rates is taken.

Table 6.1: Deposit rates on copper tube at 800ppm polymer concentration

| Temperature (°F) | Deposit Rate (mg/min) |
|------------------|-----------------------|
| 165 | 0.1056 |
| 250 | 2.1523 |
| 350 | 2.9010 |

The effect of tube material – Stainless-Steel. Stainless Steel was tested at 165 °F at two polymer concentrations – 0ppm and 800ppm. The amount of cumulative deposit formed in 5 runs has been compared with copper in **Figure 6.22**.

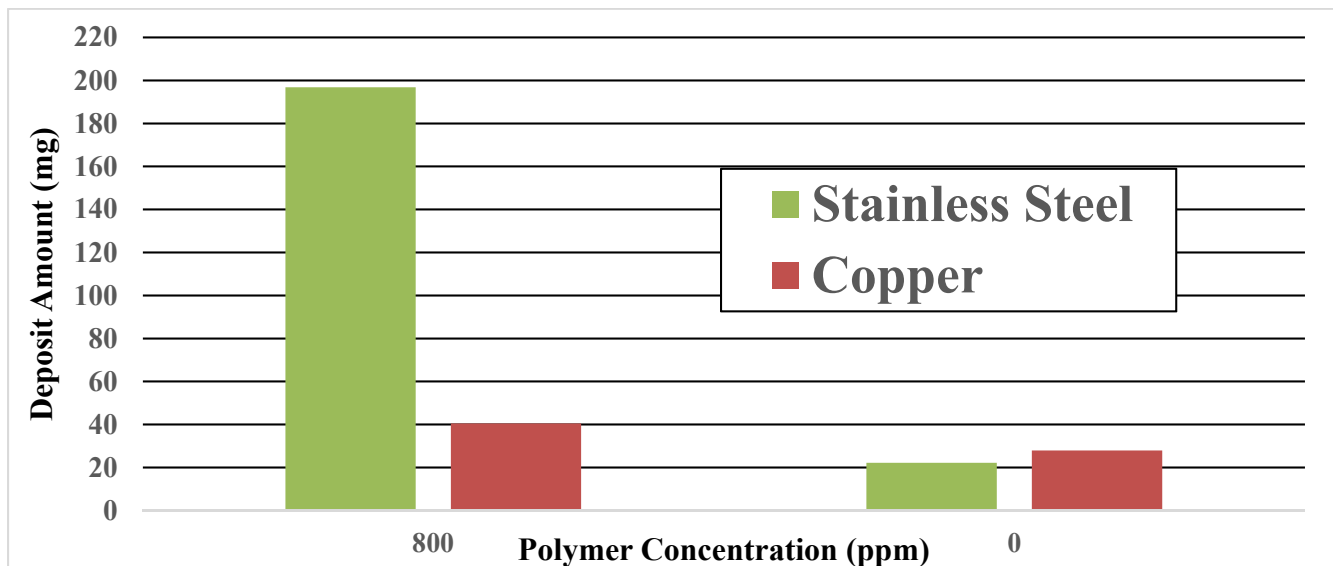


Figure 6.22: Comparison of deposit amount on stainless-steel and copper

The amount of deposit formed at 0ppm polymer is almost same in both tubes but at 800ppm the stainless-steel tube is fouled much more. Another observation was that stainless steel took significantly more time than copper tube to heat the solution with 800ppm polymer which perhaps contributed to more fouling. **Table 6.2** shows the difference in heating times for Stainless-Steel and Copper at 165 °F at 800ppm polymer concentration.

Table 6.2: Comparison of heating times for Stainless-Steel and Copper at 165 °F and 800ppm polymer concentration

| Stainless-Steel | | Copper | |
|-----------------|--|------------|--|
| Run Number | Time to heat solution from 77 °F to 122 °F (minutes) | Run Number | Time to heat solution from 77 °F to 122 °F (minutes) |
| 1 | 98 | 1 | 57.5 |
| 2 | 99.25 | 2 | 77.5 |
| 3 | 107.5 | 3 | 77 |
| 4 | 106.5 | 4 | 75.25 |
| 5 | 106.5 | 5 | 78 |

Scanning Electron Microscopy (SEM). The results for the copper tube at 350 °F are shown in **Figure 6.23**, which indicate the difference in structure of deposit at different polymer concentrations as a more compact – honeycomb like structure can be seen in higher concentrations of 400ppm and 800ppm. Also, at 3000x, magnification crystals can be seen at 800ppm concentration.

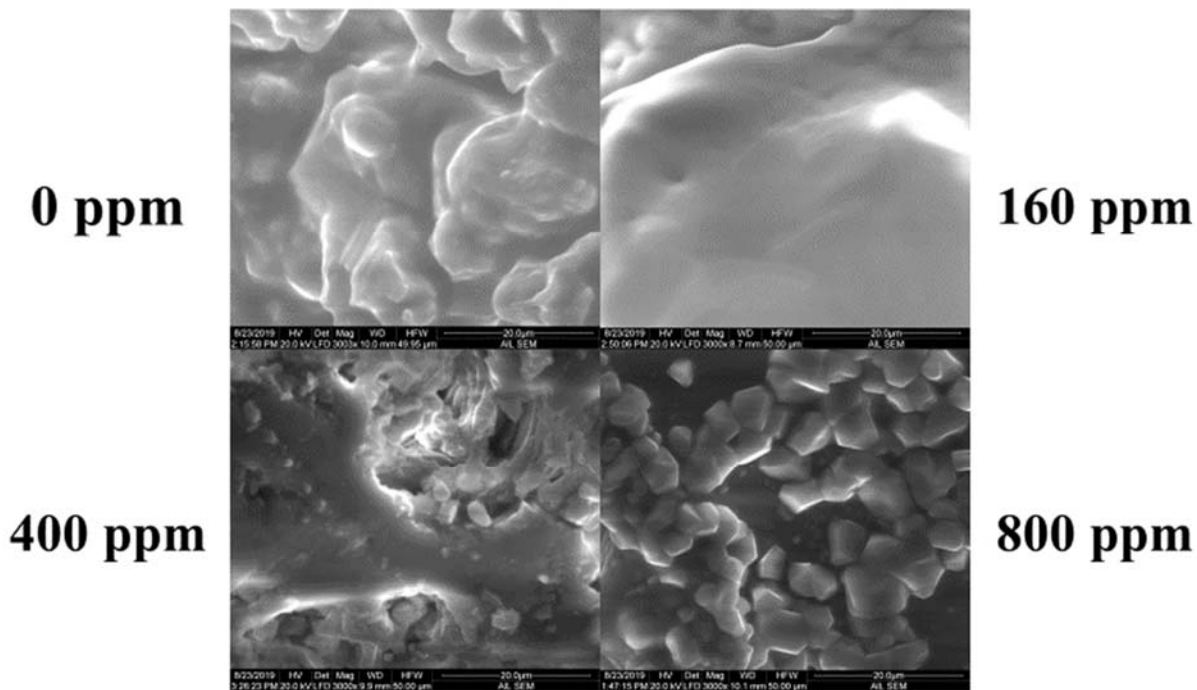


Figure 6.23: SEM images of deposit at different polymer concentrations at 350 °F at 3000 magnification on copper tubes

Future Work

Carbon-Steel tubes will be tested to identify which material is the best and fouls least. XRD analysis will be carried on the samples to identify the difference in crystals with and without polymers and SEM

imaging will also be done on different materials of tubes to get a comparative analysis of the deposit structure. The Dynamic Scale Loop will be completed, and experimental results are expected.

Both activities are ongoing.

- Task 7.0 - Feasibility of Commercial Application of the Proposed Advanced Polymer Flooding in ANS Heavy Oil Reservoirs

Activity has not yet started.

c. Opportunities for Training and Professional Development

All the graduate students working on the project are obvious recipients of training and professional development in petroleum engineering.

d. Dissemination of Results to Communities of Interest

Engineers from ConocoPhillips and Hilcorp continue to communicate about the project on a regular basis.

e. Plan for Next Quarter

Building on the current progress achieved by the research team, work planned for the next quarter will include steadily progressing toward the planned completion dates outlined in **Table A** below.

Table A: Summary of milestone status.

| Milestones | Task No. | Planned Completion Date | Actual Completion Date | Verification Method | Comments |
|--|----------|-------------------------|---|---------------------------|----------|
| Project Management Plan | 1a | o 9/30/2022 | o Ongoing (latest revision 4/30/2019) | Report/Bi-weekly meetings | None |
| Data Management Plan | 1b | o 8/31/2018 | o 7/20/2018 (latest revision 4/30/2019) | Report/Bi-weekly meetings | None |
| <ul style="list-style-type: none"> • Quantify polymer retention | 2 | o 3/31/2019 | o Some tests completed but is ongoing due to consistently high values | Report/Bi-weekly meetings | None |

University of Alaska Fairbanks

| | | | | | |
|--|---|---|---|---------------------------|------|
| <ul style="list-style-type: none"> ● Effect of water salinity on S_{or} ● Screening of gel products for conformance control | 3 | <ul style="list-style-type: none"> ○ 4/30/2019 ○ 6/30/2019 | <ul style="list-style-type: none"> ○ Some tests completed per the planned date; however, August 16th marks the true completion. ○ Initiated; design of sandpack and experimental protocol discussed in August 30th project review meeting | Report/Bi-weekly meetings | None |
| <ul style="list-style-type: none"> ● Pilot area model waterflooding history match ● Coreflooding model history match ● Updated area model for polymer flood prediction ● Reservoir modeling report | 4 | <ul style="list-style-type: none"> ○ 12/31/2018 ○ 4/30/2019 ○ 5/31/2019 ○ 5/31/2019 | <ul style="list-style-type: none"> ○ 2/1/2019 ○ Some completed but is ongoing ○ Completed but is also ongoing refinement ○ Extensively reported in Quarterlies, but a formal report was submitted on July 11, 2019 as special status report | Report/Bi-weekly meetings | None |
| <ul style="list-style-type: none"> ● Injection profile with polymer inj. ● PFO (post-polymer) ● Tracer tests (post-polymer) | 5 | <ul style="list-style-type: none"> ○ 12/31/2018 ○ 12/31/2018 ○ 12/31/2018 | <ul style="list-style-type: none"> ○ Ongoing ○ Ongoing ○ Ongoing <p><i>Note – all have been completed from the reporting standpoint, but given the dynamic nature of the pilot these are also ongoing</i></p> | Report/Bi-weekly meetings | None |

University of Alaska Fairbanks

| | | | | | |
|---|---|--|--|---------------------------|------|
| <ul style="list-style-type: none"> ● Initial treatment plan recommendation based upon literature survey ● Static polymer deposition quantification and analyses ● Finalization of the fouling flow loop design | 6 | <ul style="list-style-type: none"> ○ 12/31/2018 ○ 09/30/2019 ○ 06/30/2019 | <ul style="list-style-type: none"> ○ Ongoing However, recent tests have been used to identify/screen an effective emulsion breaker. ○ Ongoing; some tests on copper and carbon steel already completed and the deposit imaged ○ Ongoing | Report/Bi-weekly meetings | None |
|---|---|--|--|---------------------------|------|

2. PRODUCTS

Both conference publications cited below are now cataloged in www.onepetro.org, SPE's online library.

Samson Ning, John Barnes, Reid Edwards, Kyler Dunford, Abhijit Dandekar, Yin Zhang, Dave Cercone, Jared Ciferno: First Ever Polymer Flood Field Pilot to Enhance the Recovery of Heavy Oils on Alaska North Slope – Polymer Injection Performance. Selected for presentation at the Unconventional Resources Technology Conference Denver, CO July 22-24, 2019. URTeC 643.

A.Y. Dandekar, University of Alaska - Fairbanks; B. Bai, Missouri University of Science & Tech; J.A. Barnes, Hilcorp Alaska LLC; D.P. Cercone, J. Ciferno, National Energy Technology Laboratory; S.X. Ning, Reservoir Experts LLC; R.S. Seright, New Mexico Inst-Mining & Tech; B. Sheets, University of Alaska Fairbanks; D. Wang, University of North Dakota; Y. Zhang, University of Alaska – Fairbanks: "First Ever Polymer Flood Field Pilot - A Game Changer to Enhance the Recovery of Heavy Oils on Alaska's North Slope". SPE-195257-MS.

3. PARTICIPANTS & OTHER COLLABORATING ORGANIZATIONS

Hilcorp hired two operators dedicated to the project operations. Two reservoir engineers are in charge of the test design and analysis; one facilities engineer is in charge of polymer skid design and installation; and one operations engineer is in charge of downhole well work.

All the listed project personnel identified on the second page, and graduate students working on different tasks formally contribute 2 hours every other Friday in a project working meeting. Additionally, sub-group working meetings, typically lasting for 2-4 hours in a month are also held to discuss specific tasks such as reservoir simulation. For graduate students, the typical formal working hours per week are 20. Besides these, additional hours are typical in preparing reports, presentations for meetings, and potential publications.

4. IMPACT

The project continues to be an outreach tool since it is actually showcased (relevant parts of it) in the petroleum engineering curriculum. On July 23rd the project PI gave a seminar on this project at the University of Alberta, during his visit as an external examiner for a PhD student.

5. CHANGES/PROBLEMS

- a) Polymer retention experiments in both the NB and OA sands have consistently resulted in significantly high values, which constitutes a major challenge for the project.
- b) The heterogeneity of the reservoir rock in the flood pattern has posed a challenge in obtaining a "perfect" or "complete" history match, which has necessitated a new geomodel, based on the reinterpretation of seismic and log data.
- c) PSU problems that have already been discussed in Task 5.0

6. SPECIAL REPORTING REQUIREMENTS

Nothing to Report.

7. BUDGETARY INFORMATION

A summary of the budgetary information for the first budget period of the project is provided in **Table B**. This table shows the planned costs, reported costs, and the variance between the two. Reported costs is the sum of UAF's incurred expenses and the sum of the invoices received from our project partners.

Table B: Budgetary information for Budget Period 2, Q1.

| Baseline Reporting Quarter | Budget Period 2 | |
|-----------------------------|------------------------------|------------------|
| | June 1 2019 – August 31 2019 | |
| | Q1 | Cumulative Total |
| Baseline Cost Plan | | |
| Federal Share | 1,673,080 | 3,913,227 |
| Non-Federal Share | 203,923 | 961,687 |
| Total Planned | 1,877,003 | 4,874,914 |
| Actual Incurred Cost | | |
| Federal Share | 618,122 | 1,754,642 |
| Non-Federal Share | 166,025 | 1,276,808 |
| Total Incurred Cost | 784,147 | 3,031,450 |
| Variance | | |
| Federal Share | 1,054,958 | 2,158,585 |
| Non-Federal Share | 37,898 | -315,121 |
| Total Variance | 1,092,856 | 1,843,464 |

Please note that the PMP also has a spending plan that is based on calendar quarters.

8. PROJECT OUTCOMES

Nothing to Report.